AD-A018 518

PREDICTION OF THE PRESSURE OSCILLATIONS IN CAVITIES EXPOSED TO AERODYNAMIC FLOW

D. L. Smith, et al

Air Force Flight Dynamics Laboratory
Wright-Patterson Air Force Base, Ohio

October 1975

DISTRIBUTED BY:

NTIS
National Technical Information Service
U. S. DEPARTMENT OF COMMERCE

357085

AFFDL-TR-75-34

ADA018518

PREDICTION OF THE PRESSURE OSCILLATIONS IN CAVITIES EXPOSED TO AERODYNAMIC FLOW

AERO-ACOUSTICS BRANCH
VEHICLE DYNAMICS DIVISION

OCTOBER 1975

TECHNICAL REPORT AFFDL-TR-75-34
FINAL REPORT FOR PERIOD SEPTEMBER 1971 – APRIL 1975

DDC
RECEIVED
DEC 18 1975
A

Approved for public release; distribution unlimited

Reproduced by
NATIONAL TECHNICAL
INFORMATION SERVICE
US Department of Commerce
Springfield, VA. 22151

AIR FORCE FLIGHT DYNAMICS LABORATORY
AIR FORCE WRIGHT AERONAUTICAL LABORATORIES
Air Force Systems Command
Wright-Patterson Air Force Base, Ohio 45433

NOTICE

When Government drawings, specifications, or other data are used for any purpose other than in connection with a definitely related Government procurement operation, the United States Government thereby incurs no responsibility nor any obligation whatsoever; and the fact that the Government may have formulated, furnished, or in any way supplied the said drawings, specifications, or other data, is not to be regarded by implication or other wise as in any manner licensing the holder or any other person or corporation, or conveying any rights or permission to manufacture, use, or sell any patented invention that may in any way be related thereto.

This report has been reviewed by the Information Office (OI) and is releasable to the National Technical Information Service (NTIS). At NTIS, it will be available to the general public, including foreign nations.

This technical report has been reviewed and is approved for publication.

DAVEY L. SMITH
Project Engineer

FOR THE COMMANDER

HOWARD A. MAGRATH
Director
Vehicle Dynamics Division

ACCESSION for
NTIS White Section
DDC Buff Section
UNANNOUNCED
JUSTIFICATION
BY
DISTRIBUTION/AVAILABILITY CODES
Dist. AVAIL. and/or SPECIAL

Copies of this report should not be returned unless return is required by security considerations, contractual obligations, or notice on a specified document.

AIR FORCE - 17-11-75 - 150

UNCLASSIFIED
SECURITY CLASSIFICATION OF THIS PAGE (When Data Entered)

REPORT DOCUMENTATION PAGE

READ INSTRUCTIONS BEFORE COMPLETING FORM

1. REPORT NUMBER
AFFDL-TR-75-34

2. GOVT ACCESSION NO.

3. RECIPIENT'S CATALOG NUMBER

4. TITLE (and Subtitle)
PREDICTION OF THE PRESSURE OSCILLATIONS IN CAVITIES EXPOSED TO AERODYNAMIC FLOW

5. TYPE OF REPORT & PERIOD COVERED
Final Report
Sep 1971 to Apr 1975

6. PERFORMING ORG. REPORT NUMBER

7. AUTHOR(s)
D. L. SMITH
L. L. SHAW

8. CONTRACT OR GRANT NUMBER(s)

9. PERFORMING ORGANIZATION NAME AND ADDRESS
Aero-Acoustics Branch, Vehicle Dynamics Div.
Air Force Flight Dynamics Laboratory
Wright-Patterson AFB, Ohio 45433

10. PROGRAM ELEMENT, PROJECT, TASK AREA & WORK UNIT NUMBERS
62201F, 14710220

11. CONTROLLING OFFICE NAME AND ADDRESS
Aero-Acoustics Branch, Vehicle Dynamics Div.
Air Force Flight Dynamics Laboratory
Wright-Patterson AFB, Ohio 45433

12. REPORT DATE
October 1975

13. NUMBER OF PAGES
79

14. MONITORING AGENCY NAME & ADDRESS (if different from Controlling Office)

15. SECURITY CLASS. (of this report)
UNCLASSIFIED

15a. DECLASSIFICATION/DOWNGRADING SCHEDULE

16. DISTRIBUTION STATEMENT (of this Report)
Approved for public release; distribution unlimited.

17. DISTRIBUTION STATEMENT (of the abstract entered in Block 20, if different from Report)

18. SUPPLEMENTARY NOTES

19. KEY WORDS (Continue on reverse side if necessary and identify by block number)
Cavity Flow
Cavity Oscillations
Pressure Oscillations
Flight Tests
Prediction Methods

20. ABSTRACT (Continue on reverse side if necessary and identify by block number)
Cavities, or rectangular cutouts, exposed to fluid flow can produce an intense aero-acoustic environment. Past experience has shown that severe fluctuating pressures exist in open aircraft weapon bays under certain flight conditions. The aircraft designer must be able to predict the fluctuating pressure environment of cavities in order to assess the effects on the internally carried stores or near-by structure. Prediction methods were formulated based primarily on data from flight tests on cavities with length-to-depth-ratios of 4, 5 and 7

DD FORM 1 JAN 73 1473 EDITION OF 1 NOV 65 IS OBSOLETE

UNCLASSIFIED
SECURITY CLASSIFICATION OF THIS PAGE (When Data Entered)

over a Mach number range of 0.6 to 1.30. Available data in the literature were then used to extend the range of application of the prediction method to cavities with length to depth ratios from 2 to 7 and for Mach numbers from 0.5 to 3.0.

The prediction method enables designers to estimate the (1) modal frequencies, (2) modal frequency amplitudes, (3) broadband amplitudes, (4) length-to-depth effect, (5) Mach number effect, and (6) the longitudinal distribution of the fluctuating pressures in the cavity.

FOREWORD

This report was prepared by the Acoustics Development Group, Aero-Acoustics Branch, Vehicle Dynamics Division, Air Force Flight Dynamics Laboratory, Wright-Patterson Air Force Base, Ohio. The work described herein was conducted as Air Force Systems Command's exploratory development program. It establishes prediction methods for pressure fluctuations in bomb bay cavities. This program was directed under Project 1471, "Aero-Acoustic Problems in Flight Vehicles," Task 147102, "Aero-Acoustics" and Work Unit 14710220 "Aero-Acoustic Environment of Weapons Bays in Air Force Bomber Aircraft." Mr. D. L. Smith was the engineer in charge of the work.

This report concludes the work on Work Unit 14710220 which covered the period from September 1971 to April 1975.

This report was submitted for publication by the authors in March 1975.

TABLE OF CONTENTS

Section		PAGE
I.	INTRODUCTION AND BACKGROUND	1
II.	TEST RESULTS	11
	1. Boundary Layer Characteristics	11
	2. Static Pressures	14
	3. Cavity Temperatures	16
	4. Vibration Levels	19
	5. Resonant Frequencies	23
	6. Fluctuating Pressures	28
	7. Effect of Store Insertion	57
III.	SUMMARY AND EVALUATION OF PREDICTION SCHEME	63
IV.	SUMMARY AND RECOMMENDATION	73
	APPENDIX	74
	REFERENCES	79

Preceding page blank

LIST OF ILLUSTRATIONS

		PAGE NR
Figure 1	Cavity Configurations Tested	3
Figure 2	Modifications to the Standard SUU-41 Dispenser Pod	5
Figure 3	Ten Inch Deep Cavity (L/D = 4) Mounted in Modified SUU-41 Pod	6
Figure 4	Modified SUU-41 Pod Mounted on RF-4C Test Aircraft	7
Figure 5	Cavity Instrumentation Location	8
Figure 6	Closed Cavity Instrumentation Location	9
Figure 7	Boundary Layer Profiles from the Modified SUU-41 Pod	12
Figure 8	One-Third Octave Band Normalized Pressure Level Spectra from Microphone A of the Flat Plate Configuration for 20,000 Foot Altitude	13
Figure 9	One-Third Octave Band Sound Pressure Level Spectra from the Flat Plate and L/D = 5 Cavity at 3,000 Foot Altitude and Mach 0.82	15
Figure 10	Longitudinal Variation of Static Pressure along the L/D = 4 Cavity Floor	17
Figure 11	Comparison of the Recovery Factors for the Flight Data to Wind Tunnel Results from Reference 4	18
Figure 12	Thermal Recovery Factors as a Function of Mach Number for L/D = 7 with Ogive Store at an Altitude of 20,000 Feet	20
Figure 13	Acceleration Spectra from Accelerometer J at an Altitude of 3000 Feet and Mach Number of 0.82	21
Figure 14	Comparison of Actual and Vibration Induced SPL for the L/D = 7 Configuration at a Mach Number of 0.82 and Altitude of 3,000 Feet	22
Figure 15	Narrowband (2 Hz) Spectrum from the Front of the L/D = 4 Cavity for an Altitude of 20,000 Feet at Mach Number 1.30	24
Figure 16	Narrowband (2 Hz) Spectrum from the Front of the L/D = 5 Cavity for an Altitude of 20,000 Feet at Mach Number 1.30	25

PAGE NR

Figure 17	Narrowband (2 Hz) Spectrum from the Front of the L/D = 7 Cavity for an Altitude of 20,000 Feet at Mach Number 1.30	26
Figure 18	Nondimensional Resonant Frequencies as a Function of Mach Number	27
Figure 19	Overall Fluctuating Pressure Levels from the Front of the Cavities	30
Figure 20	One-Third Octave Band Sound Pressure Level Spectra from the Front of the Cavity for a Mach Number of 0.82 and A L/D Ratio of 4	32
Figure 21	One-Third Octave Band Sound Pressure Level Spectra from the Front of the Cavity for a Mach Number of 0.82 and A L/D Ratio of 5	33
Figure 22	One-Third Octave Band Sound Pressure Level Spectra from the Front of the Cavity for a Mach Number of 0.82 and A L/D Ratio of 7	34
Figure 23	Suggested Shape for First, Second and Third Order Modes from Reference 2	35
Figure 24	Longitudinal Variation of Peak One-Third Octave Band Referenced to Free-Stream Dynamic Pressure Depicting Mode Shapes for L/D = 4	36
Figure 25	One-Third Octave Mode 2 Levels from the Front and Rear of the Cavities for 3,000 Feet Altitude and Mach Number 0.82	38
Figure 26	Comparison of Predicted Mode Shapes to Data for L/D = 4 from 3,000 Foot Altitude and Mach 0.82	40
Figure 27	Comparison of the Predicted Mode Shape to Data for L/D = 5 from 3,000 Foot Altitude and Mach 0.82	41
Figure 28	Comparison of the Predicted Mode Shape to Data for L/D = 7 from 3,000 Foot Altitude and Mach 0.82	42
Figure 29	Mode 2 Fluctuating Pressure Level Data with Prediction Curve	44
Figure 30	Maximum One-Third Octave Band Sound Pressure Level from the Rear of the Cavity as a Function of L/D for 3,000 Foot Altitude and Mach 0.82	45
Figure 31	One-Third Octave Band Peaks Depicting Mach Number Effect from the Front of the Cavity for L/D = 4 and 20,000 Foot Altitude	47
Figure 32	One-Third Octave Band Sound Pressure Level Peaks from the Front of the Cavity Depicting Mach Number Effect for L/D = 5 and 20,000 Foot Altitude	48

PAGE NR

Figure 33	One-Third Octave Band Sound Pressure Level Peaks from the Front of the Cavity Depicting Mach Number Effect for L/D = 7 and 20,000 Foot Altitude	49
Figure 34	Average Variation of Amplitude between Modes 1 and 2 as a Function of L/D	50
Figure 35	Average Variation of Amplitude between Modes 2 and 3 as a Function of Mach Number	52
Figure 36	One-Third Octave Band Spectra from the L/D = 5 Configuration Depicting Longitudinal Variation	53
Figure 37	One-Third Octave Band Sound Pressure Level Spectra from the Front of the L/D = 4 Cavity at 30,000 Foot Altitude	55
Figure 38	One-Third Octave Band Sound Pressure Level Spectra from the Rear of the Cavity for Mach Number 0.82 for all L/D Ratios	56
Figure 39	Mach Number Effect on the Average Variation between the Maximum One-Third Octave Broadband and Mode 2 Amplitudes	58
Figure 40	One-Third Octave Broadband Level Versus Strouhal Number	59
Figure 41	Comparison of One-Third Octave Band Sound Pressure Level Spectra from the L/D = 7 Empty and Store Configuration for an Altitude of 30,000 Feet	60
Figure 42	Comparison of One-Third Octave Band Sound Pressure Level Spectra from the L/D = 7 Empty and Store Configuration for an Altitude of 30,000 Feet	61
Figure 43	Chart for Determining Reference "q" Decibel Level	67
Figure 44	Comparison of Predicted Spectrum with Measured Spectra	68
Figure 45	Comparision of Predicted Spectrum with Measured Spectra	69
Figure 46	Comparison of Predicted Spectrum with Measured Spectra	70
Figure 47	Comparison of Predicted Levels with Measured Levels	71
Figure 48	Block Diagram of Data Acquisition Instrumentation	75
Figure 49	Data Reduction System	78

LIST OF TABLES

		PAGE NR
TABLE I	Pressure Reference Data	29
TABLE II	Values of the Sech Function	65

LIST OF SYMBOLS

P_{rms}, P	Root mean square fluctuating pressure
q	Free-stream dynamic pressure
M	Free-stream Mach number
P_c	Cavity static pressure
P_∞	Free-stream static pressure
L	Cavity length
X/L	Nondimensional cavity location
SPL	Sound pressure level
α	Constant
S	Strouhal number (fL/V)
f	Frequency
V	Free-stream velocity
D	Cavity depth
K	Ratio of the specific heats (C_p/C_v)
T	Temperature
L/D	Length to depth ratio
u	Local velocity
dB	Decibel - $10 \log (P^2/P^2_{ref})$
P_{ref}	Twenty Micronewtons per square meter - $20\mu N/m^2$
μ	Prefix 10^{-6}
N	Unit of Force-Newton
m	Unit of length-meter
g	Acceleration

h	Altitude
Z	Distance normal to surface
δ	Boundary Layer Thickness

SUBSCRIPTS

m	Integer that defines mode number
max	Maximum value
X/L	Nondimensional cavity location
b	Broadband
∞	Free-stream value

SECTION I

INTRODUCTION AND BACKGROUND

Cavities, or rectangular cutouts, exposed to fluid flow can produce an intense aero-acoustic environment. Past experience has shown that severe fluctuating pressures exist in aircraft weapons bays under certain flight conditions. The amplitude of the fluctuating pressures can be sufficiently high to cause structural damage, malfunction of equipment, and problems with store separation and trajectories.

The aero-acoustic phenomena associated with pressure oscillations excited by flow over open cavities have been studied during the past twenty years by several investigators (See list of Ref). Considerable knowledge has been gained about the phenomena but due to the complex nature of the problem, they are not completely understood. Most of the past investigations have been concerned with understanding the phenomena and the underlying mechanisms which control them. Several theoretical models describing flow induced cavity oscillations have been proposed but generally they did not agree with all aspects of the measured data. However, the Rossiter (Ref 11) frequency prediction model has been shown (Ref 3, 4, 12, 13, 14) to predict the modal frequencies with acceptable accuracy. The models proposed to predict the amplitudes have not been so successful. For example, the model developed in Ref 9 resulted in a prediction scheme for both the amplitudes and the modal frequencies. The predictions for deep cavities ($L/D<1$) are straight forward and easy to use and the results agree very well with the measured data. However, the associated response calculations for shallow cavities ($L/D>1$ which are most typical of weapons bays) require a substantial analytical effort and the results differ significantly from the measured data for various frequencies.

The models presented to date provide insight into the physical mechanisms but do not allow for reliable quantitative predictions.

An ideal prediction method, be it empirical or theoretical, should permit the estimation of both the modal frequencies and amplitudes for cavities with various length-to-depth (L/D) ratios and for Mach number and altitude variations. Also, it should account for variations in the amplitude within the cavity. An empirical prediction scheme was offered in Ref 4 which was derived from wind tunnel data. This scheme fell far short of an ideal method because it was a worst case prediction, i.e., the user could only predict the worst case expected for a given Mach number and altitude. No variation with L/D ratio or longitudinal position in the cavity was accounted for. In addition the scheme predicts the same level for each of the modal frequencies. Two noteworthy contributions resulted from the investigation. It was shown that the temperature in a cavity exposed to free-stream flow approaches the free-stream stagnation temperature instead of the free-stream static temperatures. The significance of this result is in the estimation of the modal frequencies. Rossiter (Ref 11) assumed the temperature in the cavity to approach the free-stream static temperature in the derivation of his frequency prediction equation. The error involved in assuming this becomes significant at high Mach numbers. The flight data verify that the temperature in the cavity approaches the stagnation temperature and the Rossiter equation modified to account for this change predicts the measured modal frequencies very well. The second contribution in Ref 4 was the determination of longitudinal mode shapes for the first three modal frequencies. These mode shapes were assumed to be valid for the flight test results and formed the bases for the longitudinal mode shape equations.

A flight test program was established in the Air Force Flight Dynamics Laboratory to verify and/or refine the worst case predictions offered in Ref 4. Four cavity and one flat plate configurations were flight tested. Figure 1 illustrates each of these configurations. The cavities were mounted in a modified SUU-41 munition dispenser

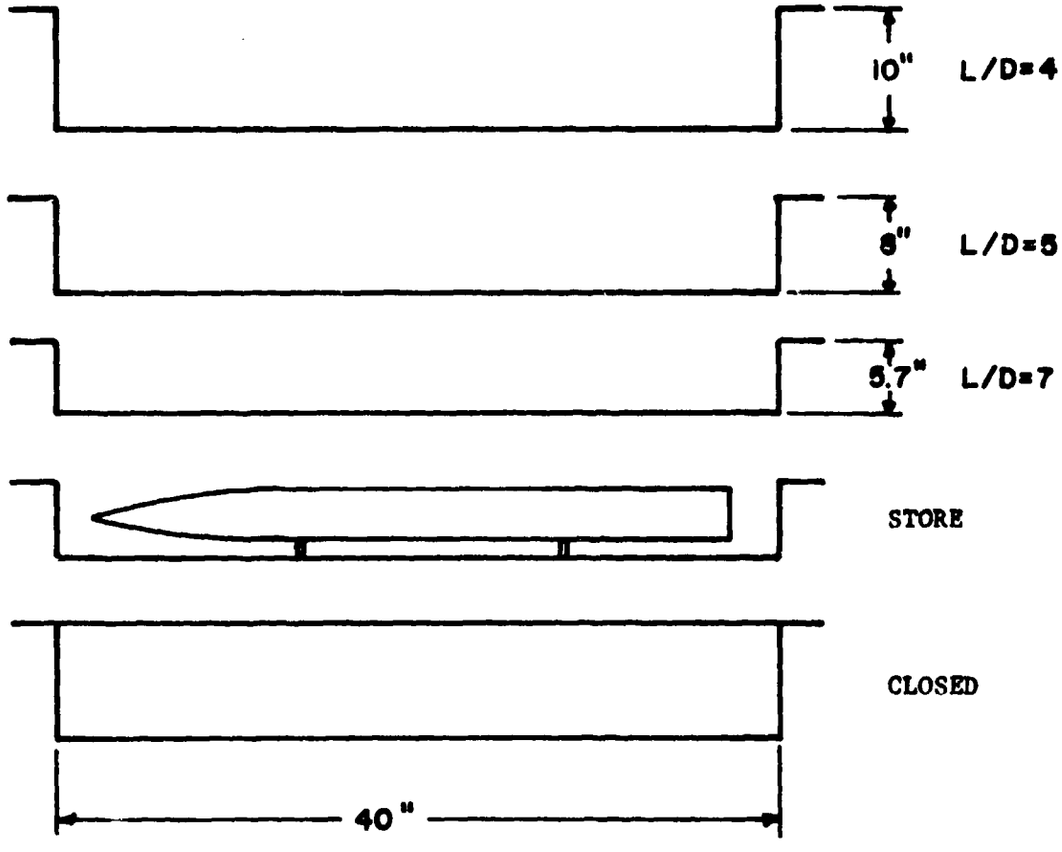

FIGURE 1 CAVITY CONFIGURATIONS TESTED

pod which is shown in Figure 2 along with a sketch of the standard pod. Figure 3 is a picture of the modified pod with the L/D = 4 cavity mounted in it. The pod was mounted on the triple ejection rack (TER) of the left inboard pylon on a RF-4C aircraft. A schematic of the aircraft with the pod mounted on it is shown in Figure 4. The cavities were instrumented with nine microphones, one accelerometer, one thermocouple, and three static pressure ports and the flat plate was instrumented with one microphone, one thermocouple, one static pressure port and a pressure rake. The location of the instrumentation is shown in Figures 5 and 6 with a typical microphone mounting also shown in Figure 5. Data were obtained for constant pressure altitudes of 3,000 ft, 20,000 ft, and 30,000 ft for Mach number ranges of 0.61 to 0.93, 0.61 to 1.30 and 0.61 to 1.30 respectively. More detailed information about the cavities, instrumentation, test procedures and data reduction are included in the Appendix.

The measured data were correlated with the empirical wind tunnel aero-acoustic predictions. An improved prediction method resulted which accounted for Mach number and altitude effects and longitudinal variation of amplitude for an L/D = 4 cavity. These results were reported in Ref 12. Similar expressions were developed for the L/D = 5 and L/D = 7 cavities and these results are offered in Ref 14. Expressions were then derived which accounted for the L/D effect and were valid for any L/D ratio in the range of 4 to 7 and Mach number in the range 0.6 to 1.3. These expressions were documented in Ref 13. Typical results from these references are included in Section II of this report. Data from the literature were used to extend the range of applications of the prediction equations to cavities with L/D ratios from 2 to 7 and for Mach numbers from 0.5 to 3.0. These results are also included in Section II.

The final prediction expressions summarized in Section III, are a function of four variables; cavity L/D ratio, normalized cavity longitudinal position (X/L), free-stream dynamic pressure (q), and

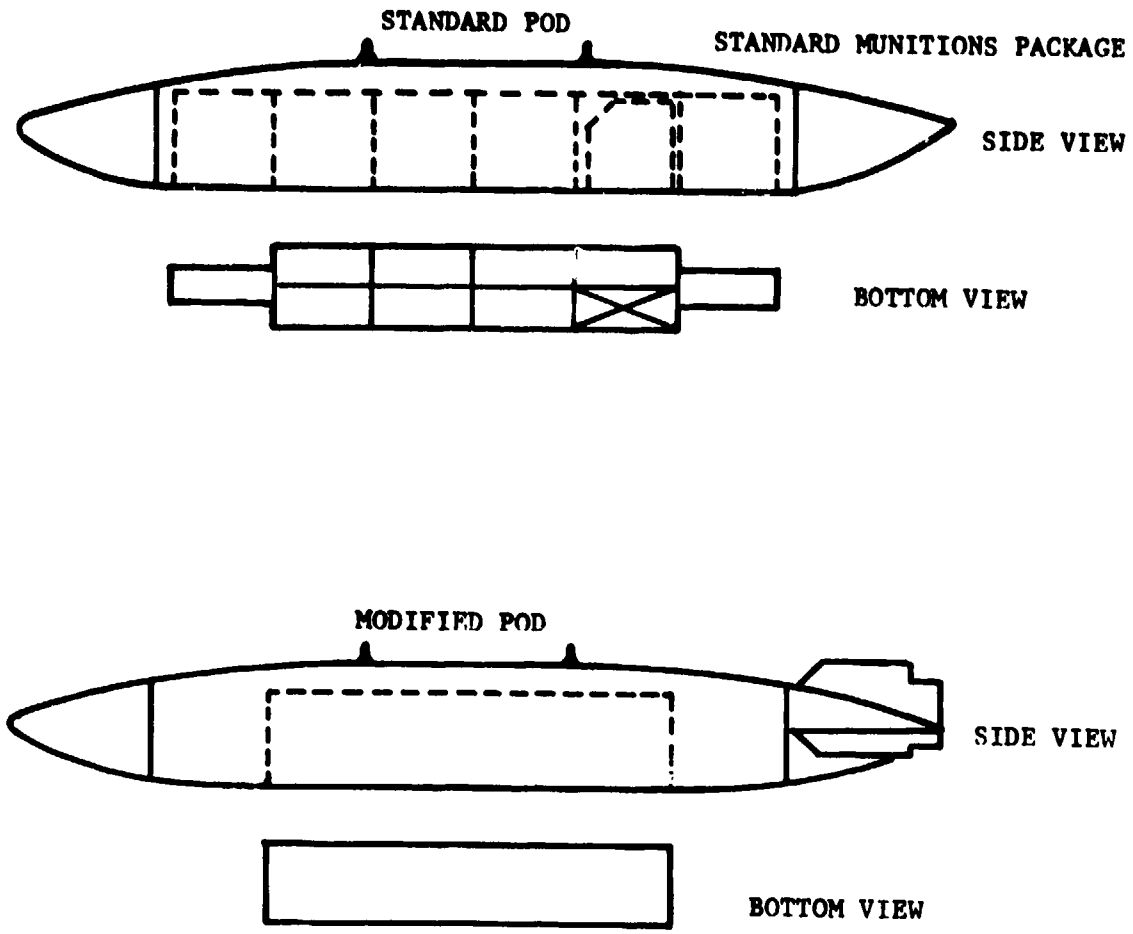

FIGURE 2 MODIFICATIONS TO THE STANDARD SUU-41 DISPENSER POD

FIGURE 3 TEN INCH DEEP CAVITY (L/D = 4) MOUNTED IN MODIFIED SUU-41 POD

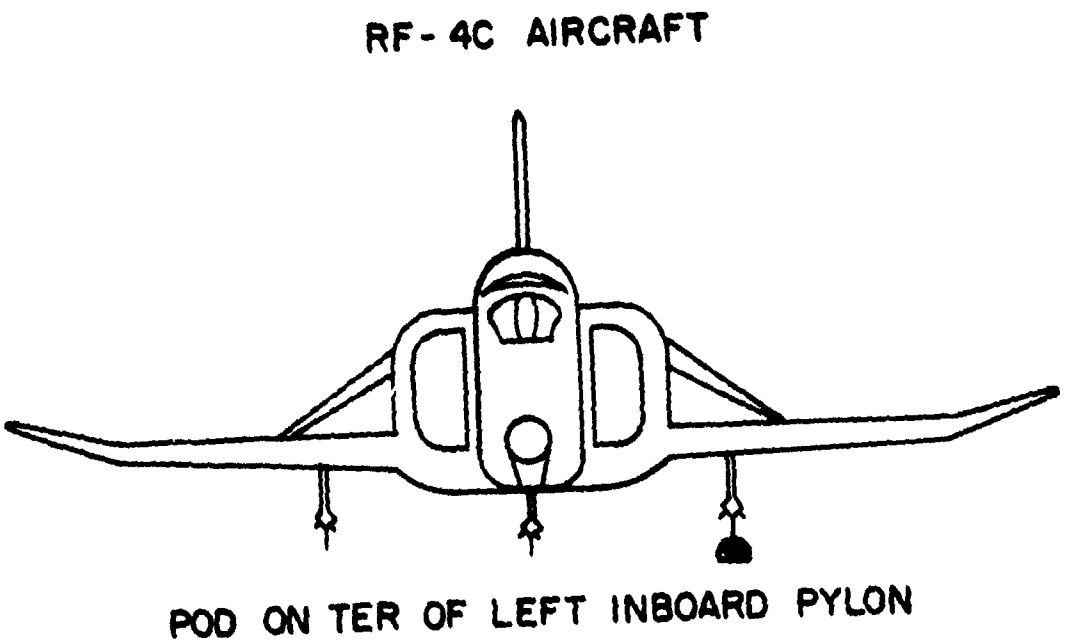

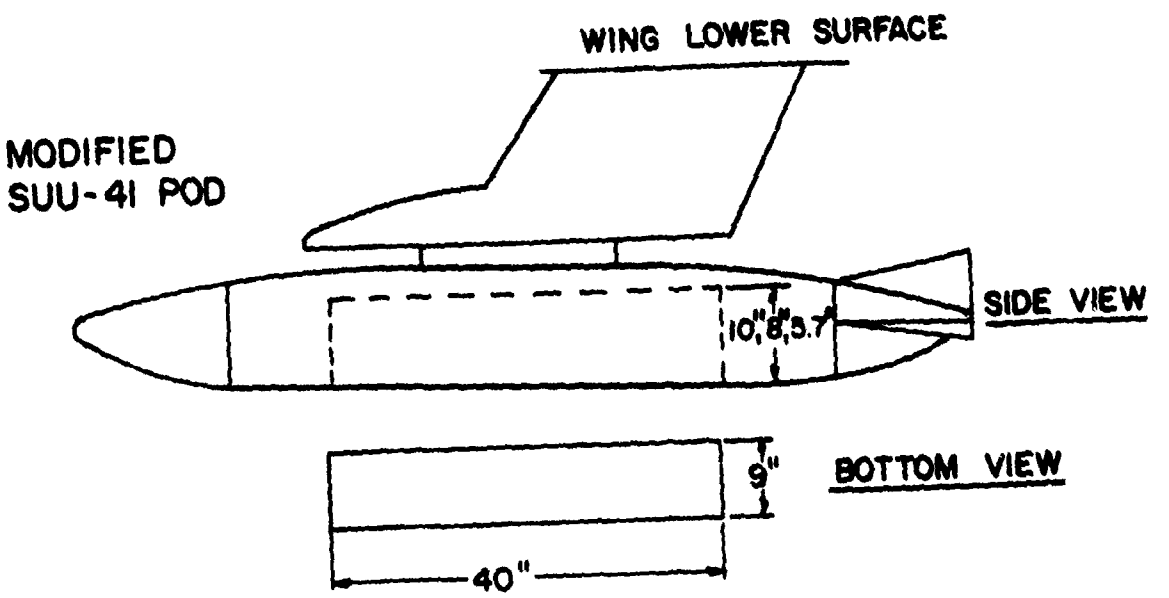

FIGURE 4 MODIFIED SUU-41 POD MOUNTED ON RF-4C TEST AIRCRAFT

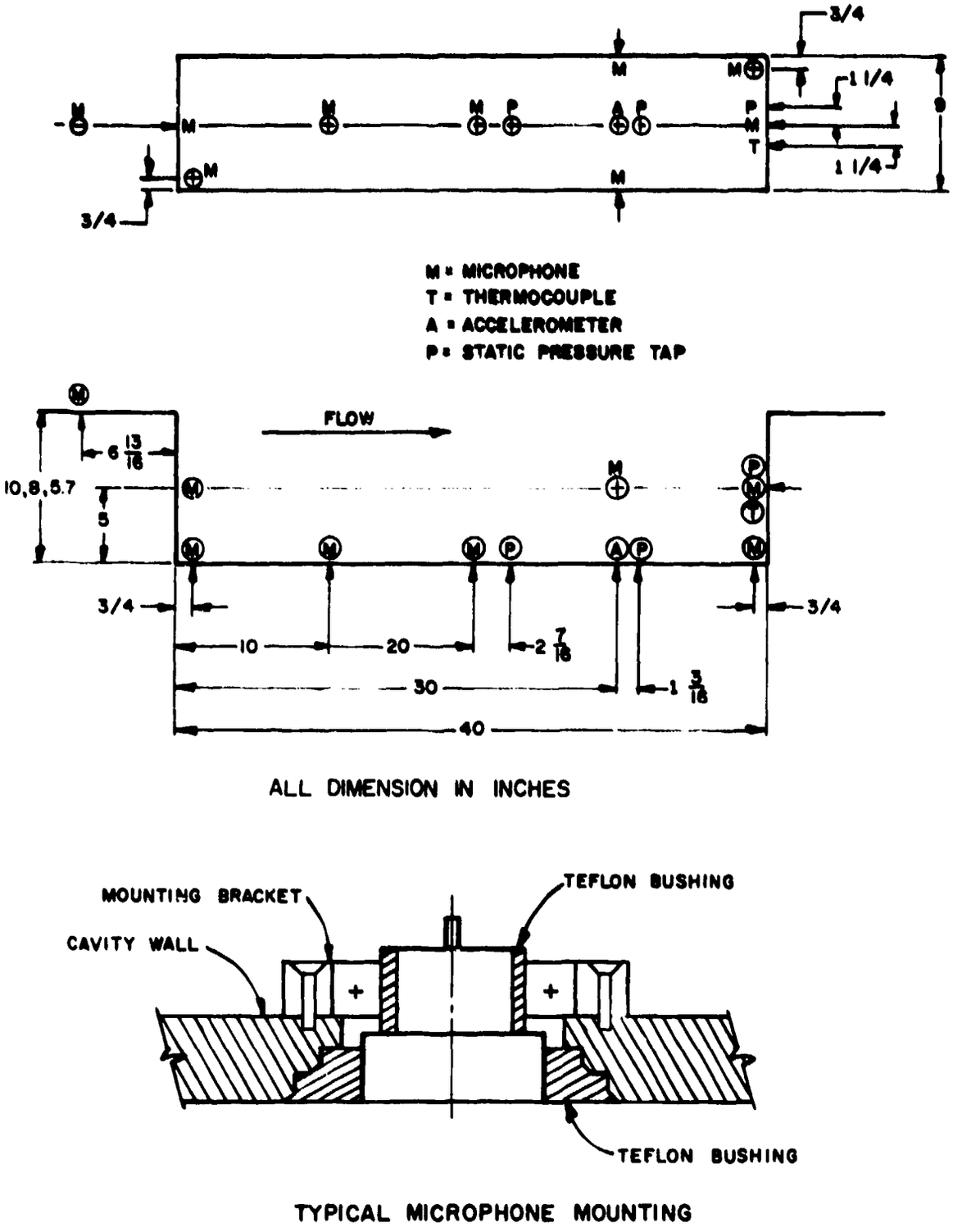

FIGURE 5 CAVITY INSTRUMENTATION LOCATION

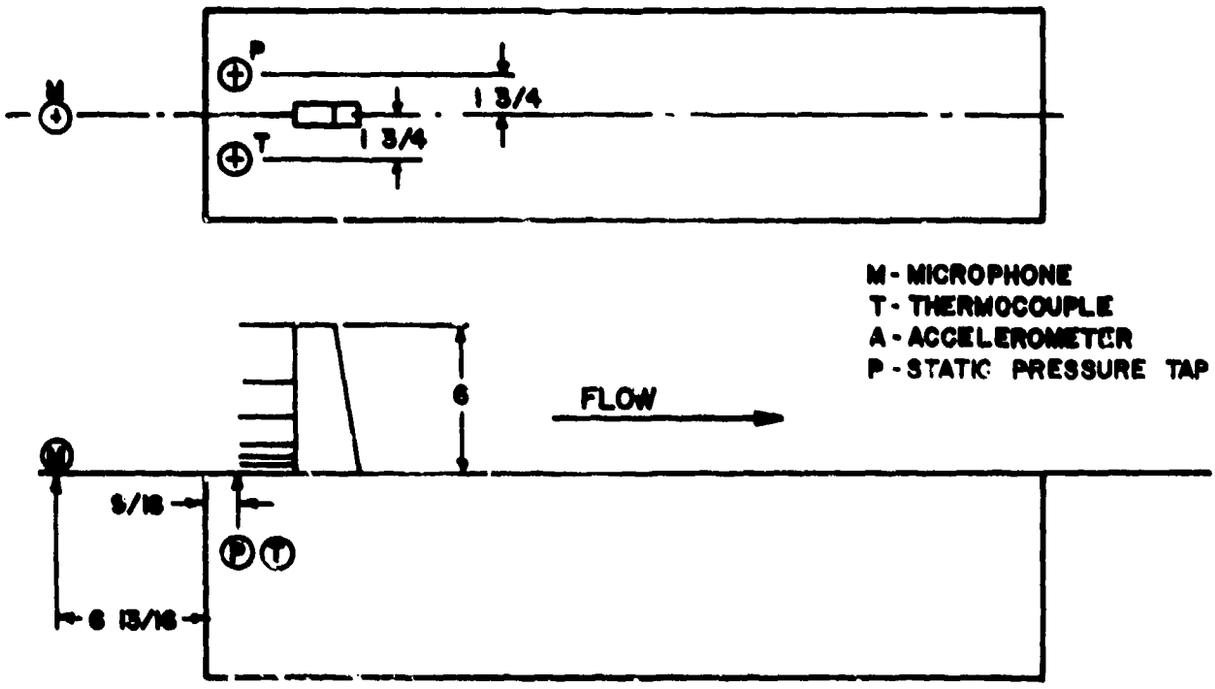

ALL DIMENSIONS IN INCHES

FIGURE 6 CLOSED CAVITY INSTRUMENTATION LOCATION

free-stream Mach number M. With these four variables the equations can account for all of the significant trends that were observed in the flow induced cavity pressure oscillation phenomena.

Section IV summarizes the significant results of the entire effort.

SECTION II

TEST RESULTS

1. Boundary Layer Characteristics

In order to define the flow conditions for which subsequent data were taken, boundary layer profiles were obtained for each altitude and representative Mach numbers. A boundary layer profile rake, thermocouple, and a static pressure transducer were mounted on the flat plate covering the cavity as shown in Figure 6. The resulting normalized velocity profiles are presented in Figure 7 along with the conventional 1/7th power law for fully developed turbulent boundary layers. The data indicate that the profiles existing at the leading edge of the cavity agree reasonably well with those for fully developed turbulent flow. It should be mentioned that the boundary layer that exists at the leading edge of the cavities was not expected to be the same as that for the flat plate because of upstream propagation of the fluctuating pressures generated in the cavity. A microphone located upstream of the cavity (Figure 6) enabled the fluctuating pressures in the boundary layer to be measured which revealed upstream propagation of the pressures generated in the cavity. Figure 8 presents boundary layer spectra from the microphone located upstream of the cavity for the flat plate configuration for various Mach numbers.

The data are presented normalized, i.e., referenced to the free-stream dynamic pressure (q) instead of the standard $20\mu N/m^2$ reference. Results for only the 20,000 ft altitude are shown in the figure. The peak that occurs at 400 Hz in the boundary layer spectra is due to the aircraft power supply.

The normalized boundary layer noise is seen to decrease with increasing Mach number as was expected since it has been shown (Ref 6) that the normalized boundary layer noise follows the expression:

$$\frac{P_{rms}}{q} = \frac{C_1}{1 + C_2 M^2} \qquad (1)$$

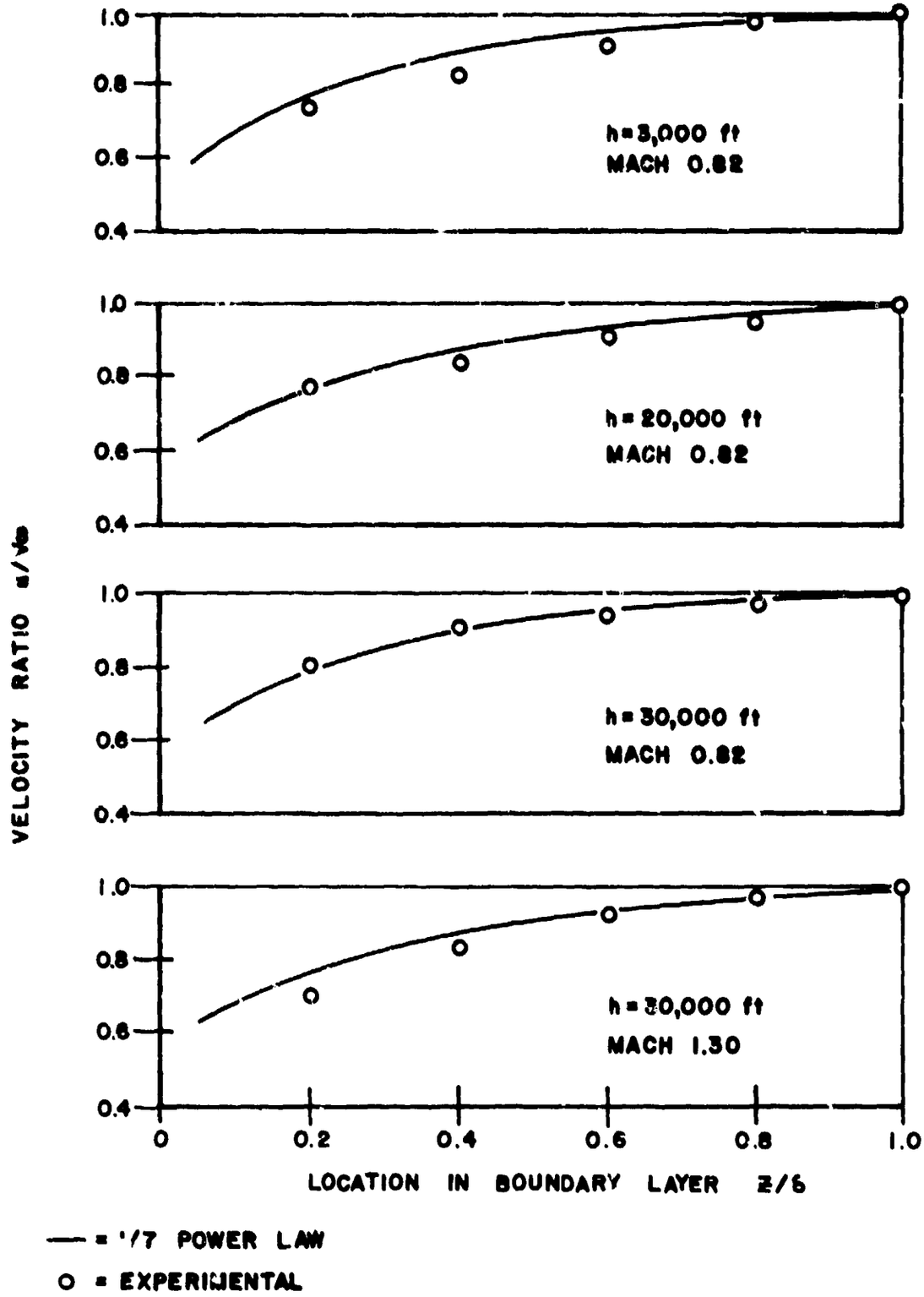

FIGURE 7 BOUNDARY LAYER PROFILES FROM THE MODIFIED SUU-41 POD

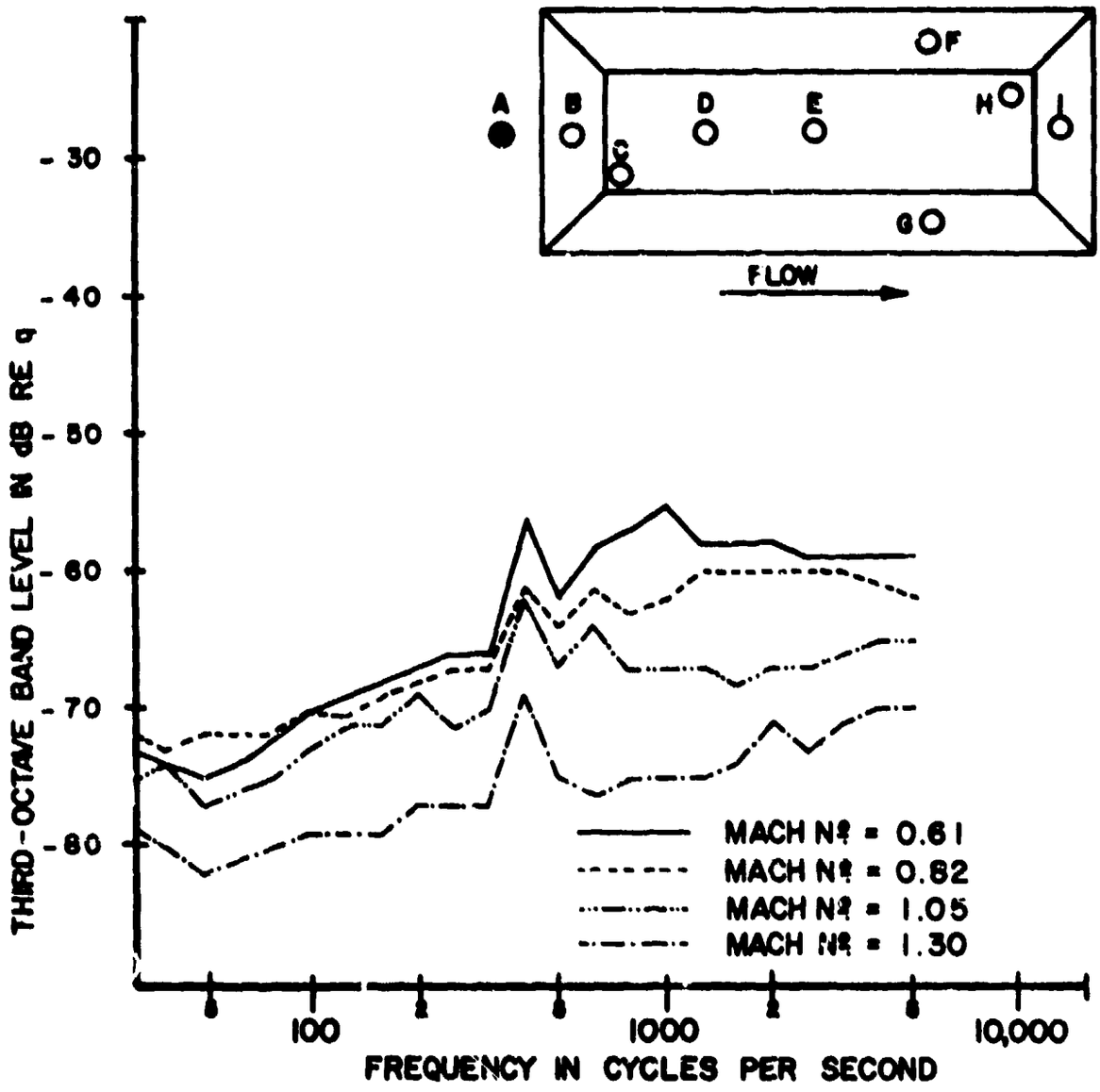

FIGURE 8 ONE-THIRD OCTAVE BAND NORMALIZED PRESSURE LEVEL SPECTRA FROM MICROPHONE A OF THE FLAT PLATE CONFIGURATION FOR 20,000 FOOT ALTITUDE

with constants C_1 and C_2 depending upon the type of boundary layer. The dynamic pressure (q) may be defined for air as 0.7 $P_o M^2$ where P_o is the local static pressure and Equation 1 may then be written as:

$$P_{rms} = \frac{C_3 P_o}{\frac{1}{M^2} + C_2} \qquad (1.a)$$

It is noted from Equation 1.a that for a constant pressure altitude the rms pressure will increase with an increase in Mach number.

The data shown in Figure 8 follow the trend given by equation (1). However, this relation is for the overall rms pressure and due to the instrumentation limitations the true overall level was not obtained for all conditions. For the higher Mach numbers there is significant energy at frequencies above 10 KHz which was beyond the frequency limits of the instrumentation. The shape of the one-third octave spectra in Figure 8 agree with the shape expected for the turbulent boundary layer and do indicate that the peak in the spectra increases with increasing Mach numbers.

One-third octave band spectra from the microphone located ahead of the cavity for the flat plate and for the L/D = 5 cavity configuration are presented in Figure 9 along with the data from a microphone located in the front of the L/D = 5 cavity. The spectra obtained from the microphone located at the front of the cavity are seen to be very similar to that measured in the cavity indicating that the cavity induced pressure oscillations are propagated upstream with little or no attenuation. This upstream propagation was also noted for supersonic flight speeds indicating that the propagation is occurring in the subsonic portion of the boundary layer. Additional boundary layer data may be found in Ref 12 and 14.

2. Static Pressures

Static pressures were measured at three locations in the cavity. Two pressure transducers were located in the rear half of the floor and one in the aft wall (see Figure 5). The data are presented as the difference between the cavity static pressure P_c

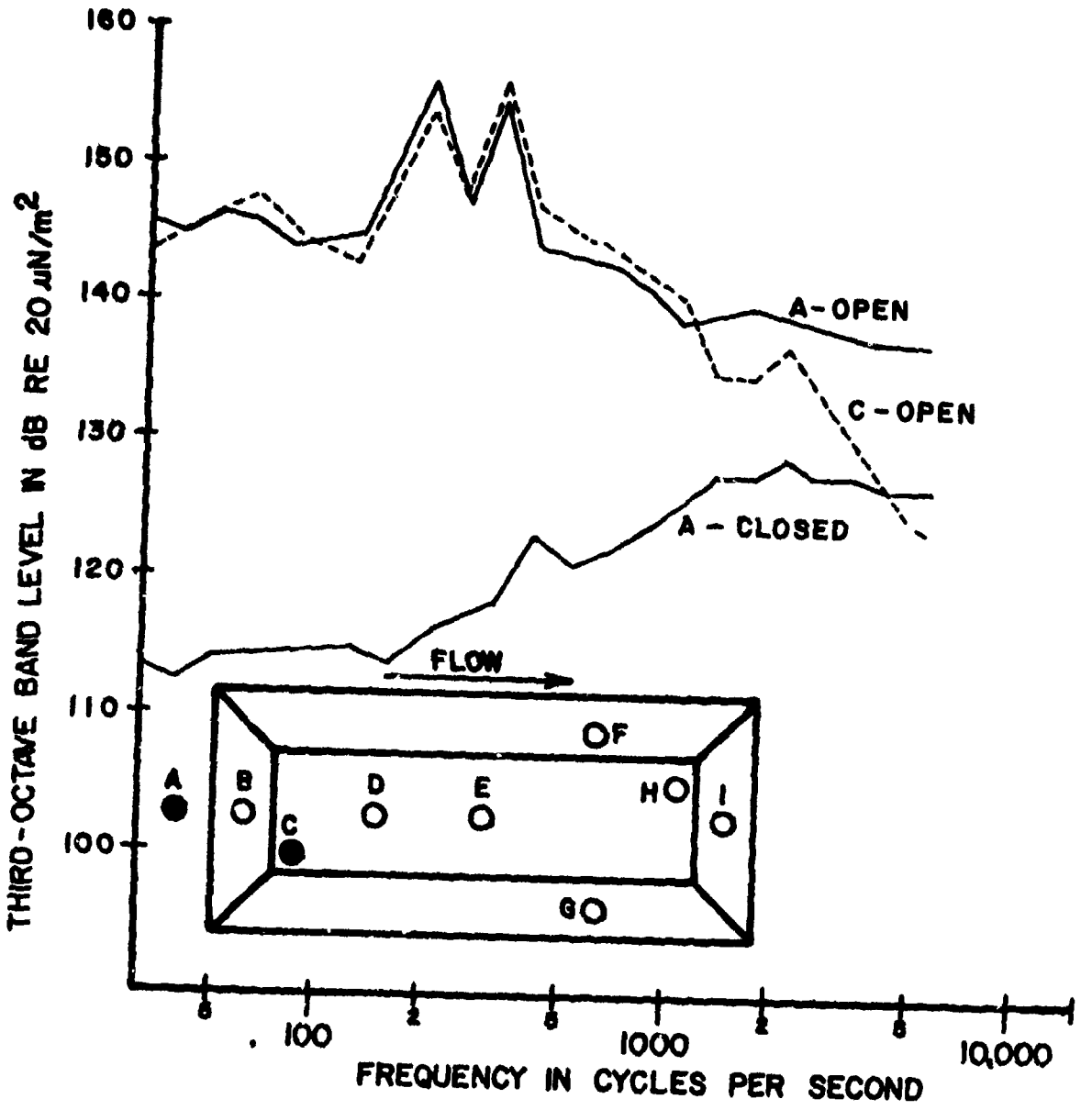

FIGURE 9 ONE-THIRD OCTAVE BAND SOUND PRESSURE LEVEL SPECTRA FROM THE FLAT PLATE AND L/D = 5 CAVITY AT 3,000 FOOT ALTITUDE AND MACH 0.82

and the free-stream static pressure P_∞ normalized with the free-stream static pressure. The data shown in Figure 10 are typical of that for the entire test. It is seen that the cavity static pressure increases toward the rear of the cavity as earlier investigators (Ref 4, 9, and 11) observed. As the Mach number is increased the static pressure increases reaching its maximum at the maximum speed. It must be pointed out that one cannot extrapolate this observation very far beyond the range of the test because it was found in Ref 4 (for wind tunnel tests) that the static pressure at the rear of the cavity starts to decrease around M = 2. This trend was also noted in Ref 9. The static pressure results for the L/D = 7 with the ogive store mounted in it were compared to the other results with no significant variations being observed.

3. Cavity Temperatures

In the past, investigators have assumed the temperature in the cavity to be nearly equal to the free-stream static temperature as opposed to the free-stream stagnation temperature. Cavity temperatures for wind tunnel tests were presented for the first time in Ref 4 and it was shown that the temperatures inside the cavity approach the free-stream stagnation temperature.

Cavity temperatures were measured in the flight test with a thermocouple mounted near the center of the aft wall (see Figure 5). The results for the L/D = 7 with store configuration are shown in Figure 11, along with wind tunnel results from Ref 4. It can be seen that the wind tunnel data show a trend for the cavity temperature to approach the stagnation temperature with increasing Mach number. At the lower Mach numbers the flight data fall well above the wind tunnel results but at supersonic speeds the data agree quite well. The reason for high recovery factors at the lower speeds is believed to be due to the flight profiles. The sequency of recording data was generally from the lowest altitude to the highest, thus the cavity walls would be at a temperature above the stagnation temperature each time the aircraft

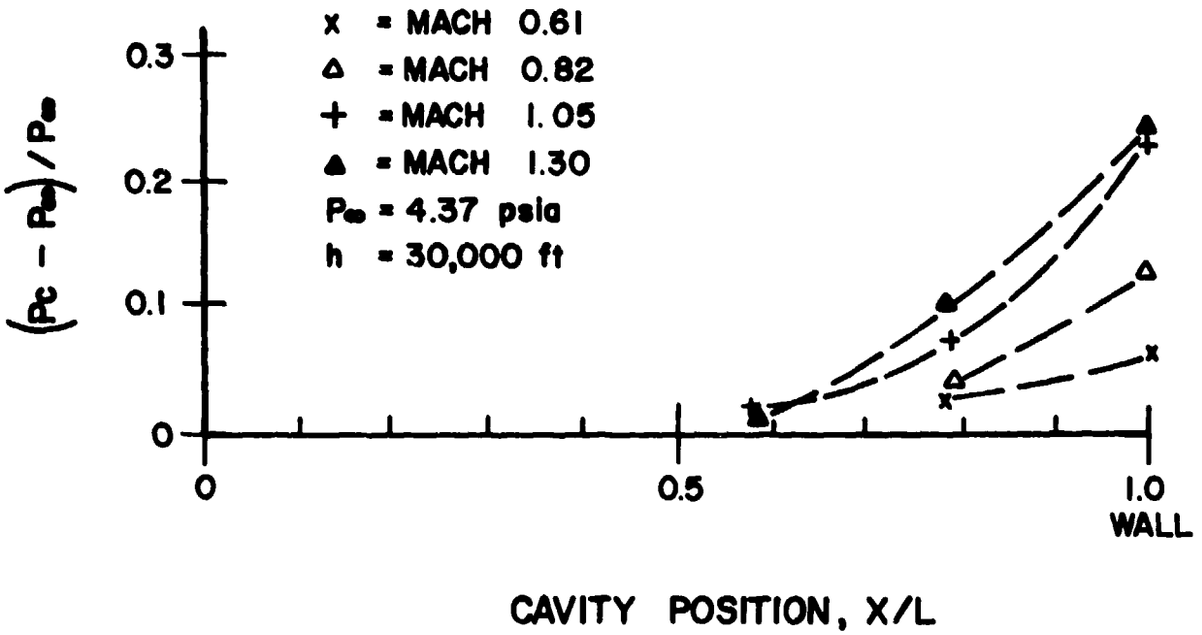

FIGURE 10 LONGITUDINAL VARIATION OF STATIC PRESSURE ALONG THE L/D = 4 CAVITY FLOOR

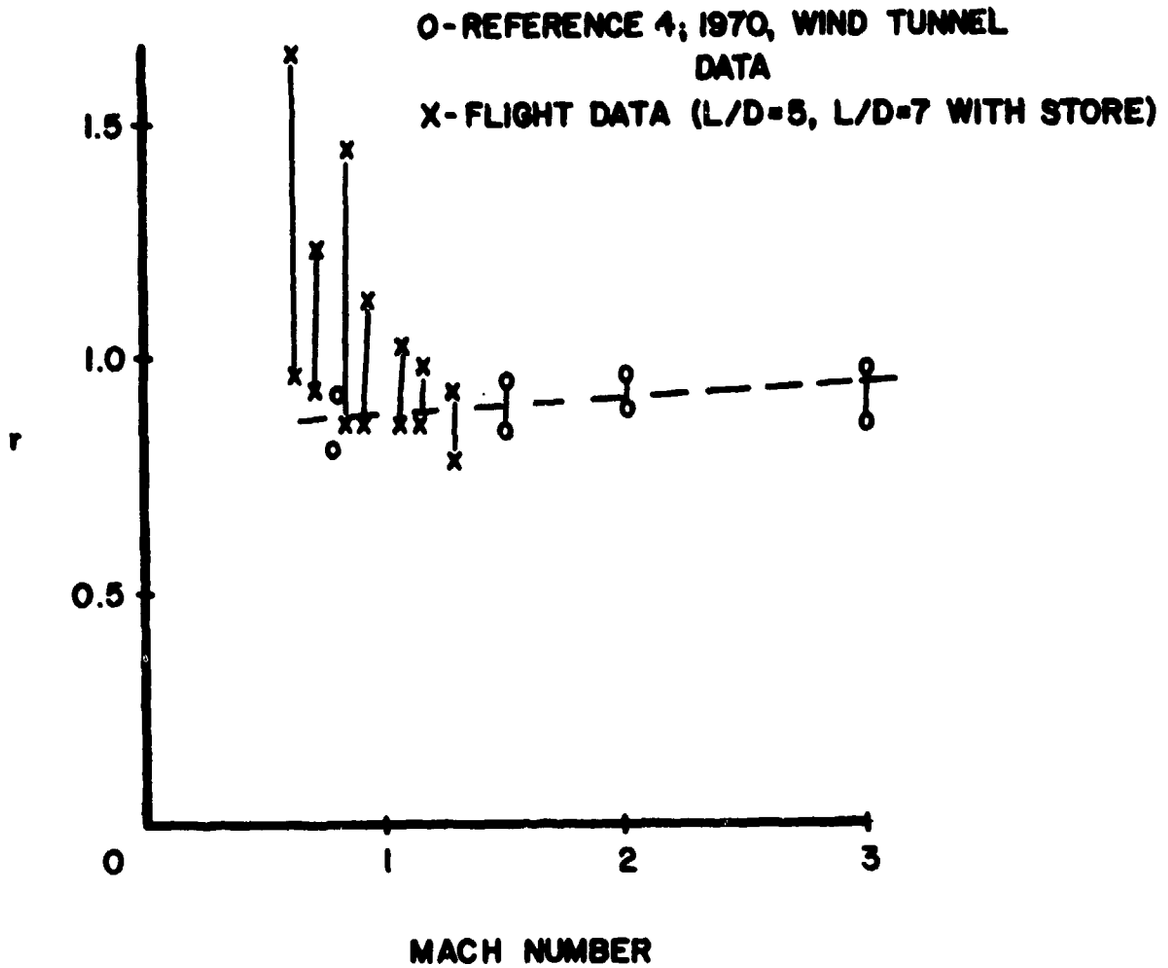

$$r = \frac{T_C - T_\infty}{T_0 - T_\infty}$$

T_C - CAVITY TEMPERATURE

T_0 - FREE STREAM STAGNATION TEMPERATURE

T_∞ - FREE STREAM STATIC TEMPERATURE

FIGURE 11 COMPARISON OF THE RECOVERY FACTORS FOR THE FLIGHT DATA TO WIND TUNNEL RESULTS FROM REFERENCE 4

changed altitude. It is believed that this temperature excess is the cause of the higher recovery factors at the lower Mach numbers. Figure 12 shows two consecutive runs at an altitude of 20,000 ft displaying a reduction in recovery factors for the second set of temperature measurements. This tends to substantiate the above explanation since the second temperature measurements are for the same flight conditions at a later time and the cavity wall temperature was lower due to the increased soak time. The reduction in recovery factors for the second set indicates that the measured temperature is affected by the duration of time the aircraft is at the same altitude.

Due to anomalies in the temperature measurements, acceptable data were obtained for only two test configurations, L/D = 7 with store and L/D = 5. Since data for only these two configurations were obtained it was not possible to determine the effect that the L/D ratio or store had on the cavity temperatures. However, it can be concluded that the temperature in a cavity exposed to free-stream flow approaches the free-stream stagnation temperature as was found in the wind tunnel tests of Ref 4.

4. Vibration Levels

The vibration levels were measured by an accelerometer mounted on the floor of the cavity at 3/4 of the cavity length from the leading edge (see Figure 5). Data were recorded continuously by the same instrumentation as that used with the microphones and one-third octave band analyses were performed for various test conditions. A typical spectrum for each test configuration is shown in Figure 13. A significant reduction in the low frequencies is seen in the spectrum for the store configuration.

The vibration sensitivity of the microphones used was low enough that 1g of acceleration of the microphone would produce not more than a 90 dB reading. Figure 14 shows the measured spectrum for Microphone E (the nearest one to the accelerometer, see Figure 5) along with the corresponding spectrum induced in a microphone due to

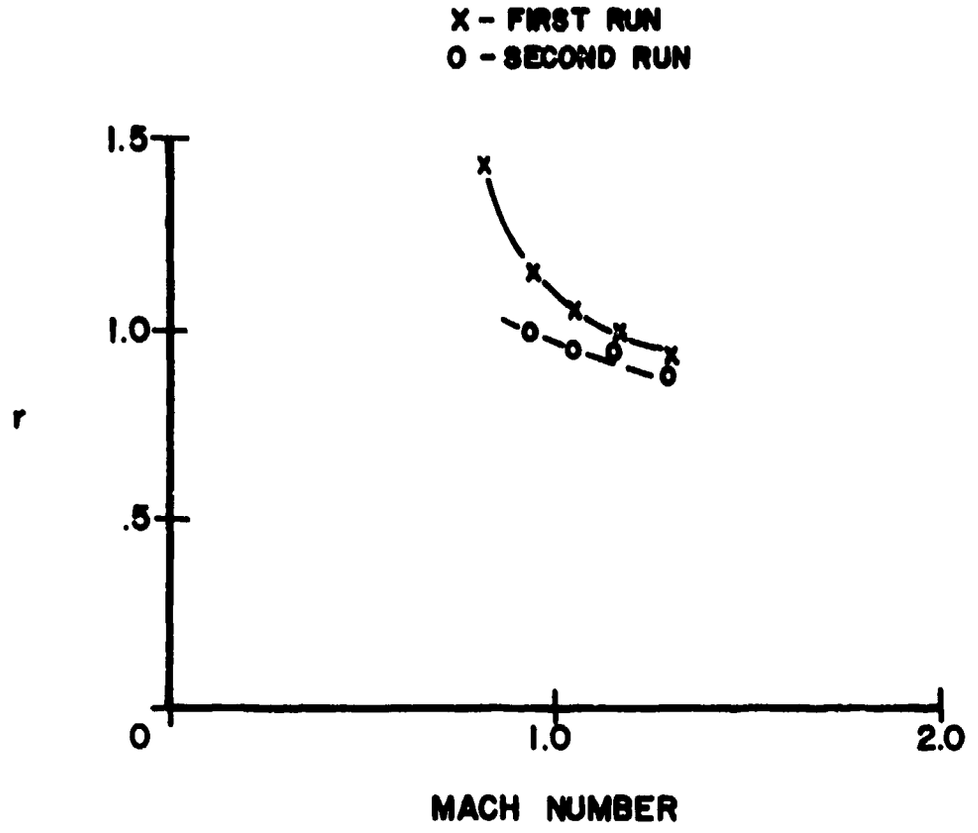

$$r = \frac{T_c - T_\infty}{T_o - T_\infty}$$

T_c - CAVITY TEMPERATURE

T_o - FREE STREAM STAGNATION TEMPERATURE

T_∞ - FREE STREAM STATIC TEMPERATURE

FIGURE 12 THERMAL RECOVERY FACTORS AS A FUNCTION OF MACH NUMBER FOR L/D = 7 WITH OGIVE STORE AT AN ALTITUDE OF 20,000 FEET

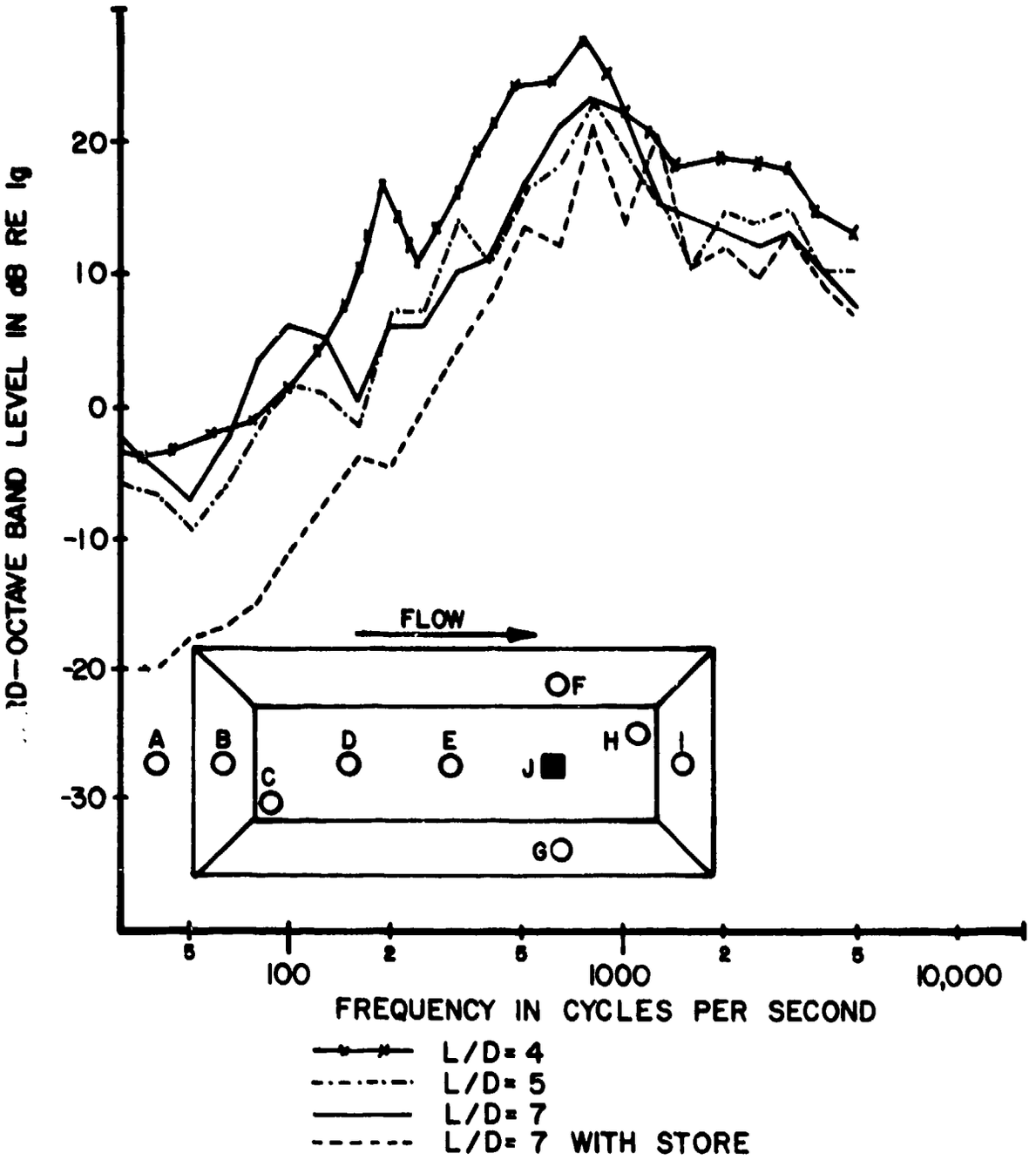

FIGURE 13 ACCELERATION SPECTRA FROM ACCELEROMETER J AT AN ALTITUDE OF 3000 FEET AND MACH NUMBER OF 0.82

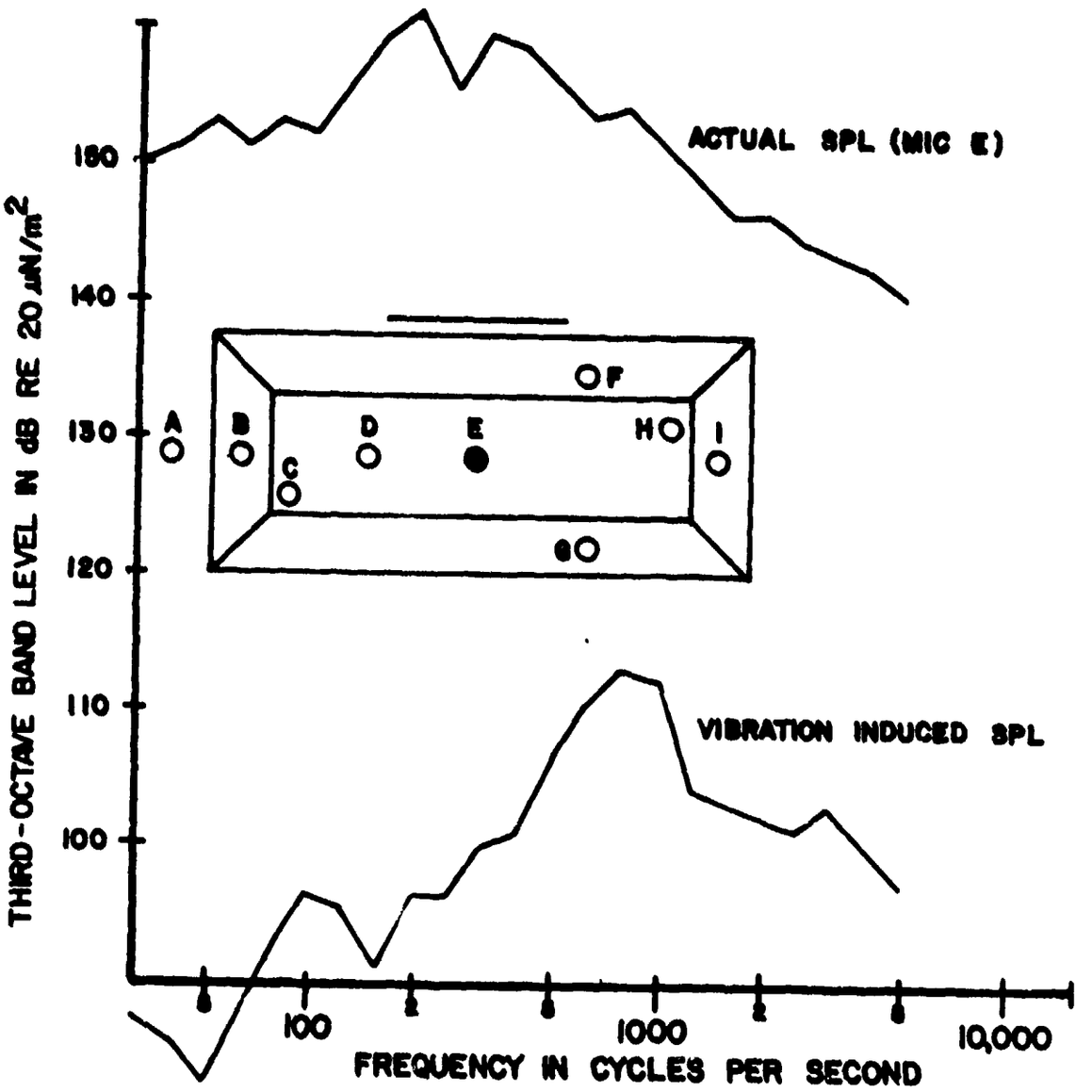

FIGURE 14 COMPARISON OF ACTUAL AND VIBRATION INDUCED SPL FOR THE L/D = 7 CONFIGURATION AT A MACH NUMBER OF 0.82 AND ALTITUDE OF 3,000 FEET

the measured acceleration for an altitude of 3,000 ft and a Mach number of 0.82. There is a 30 dB or more difference between the two curves at all frequencies; therefore, it can be assumed that the vibration effect on the microphones was insignificant. It was also assumed throughout the report that the acoustic energy input to the system from the vibration of the walls was negligible.

5. Resonant Frequencies

Narrowband (2 Hz) frequency spectra were obtained from various microphone locations to identify the discrete resonant frequencies in the recorded data. Typical narrowband spectra are shown in Figures 15-17 for Microphone C at an altitude of 20,000 ft and Mach number of 1.30 for the three test configurations. The predicted resonant frequencies are depicted in the figures by dashed lines for the first three modes. Note that the same frequencies were measured and predicted for the three L/D configurations as they were all the same length. The nondimensional resonant frequencies or Strouhal numbers ($S = fL/V$) were calculated for each observed resonant frequency f. The free-stream velocity was calculated from the free-stream static temperature and measured Mach number. Only those resonant frequency amplitudes that were about 5 dB or more above the broadband level were used to calculate the nondimensional frequencies. The calculated Strouhal numbers for all three L/D ratios are presented in Figure 18 along with the data from Ref 4 for L/D ratios of 4, 5.7, and 7. The solid curves represent the modified Rossiter equation for the Strouhal relation given by:

$$S = \frac{m - 0.25}{\dfrac{M}{\left(1 + \frac{K-1}{2} M^2\right)^{1/2}} + 1.75} \qquad m = 1,2,3 \qquad (2)$$

where K is the ratio of specific heats and M is the free-stream Mach number. It is seen that the nondimensional resonant frequencies vary only a small amount with the L/D ratio with the largest variation occurring for the lowest modal frequency. Variations in the ambient

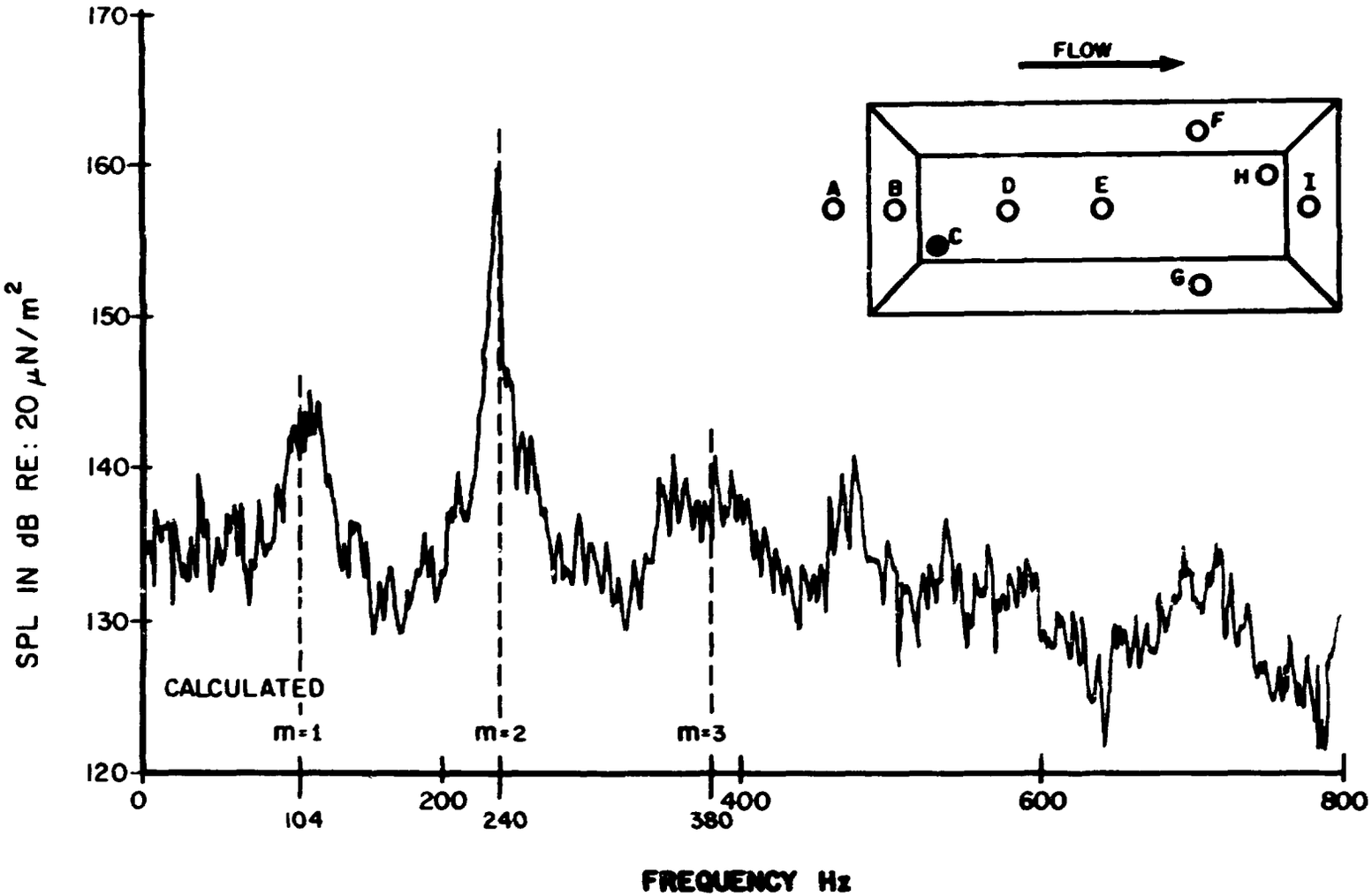

FIGURE 15 NARROWBAND (2 Hz) SPECTRUM FROM THE FRONT OF THE L/D = 4 CAVITY FOR AN ALTITUDE OF 20,000 FEET AT MACH NUMBER 1.30

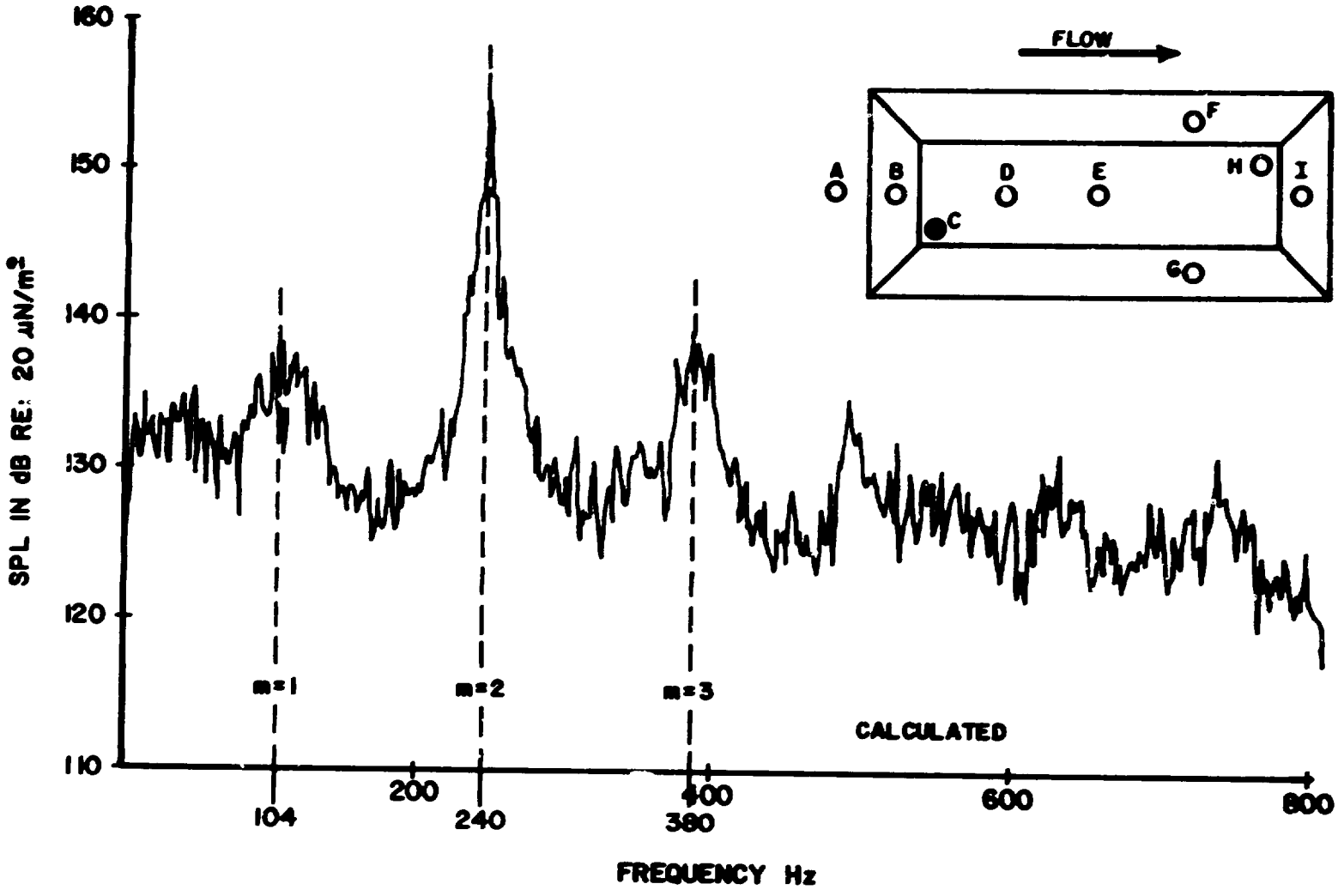

FIGURE 16 NARROWBAND (2 Hz) SPECTRUM FROM THE FRONT OF THE L/D = 5 CAVITY FOR AN ALTITUDE OF 20,000 FEET AT MACH NUMBER 1.30.

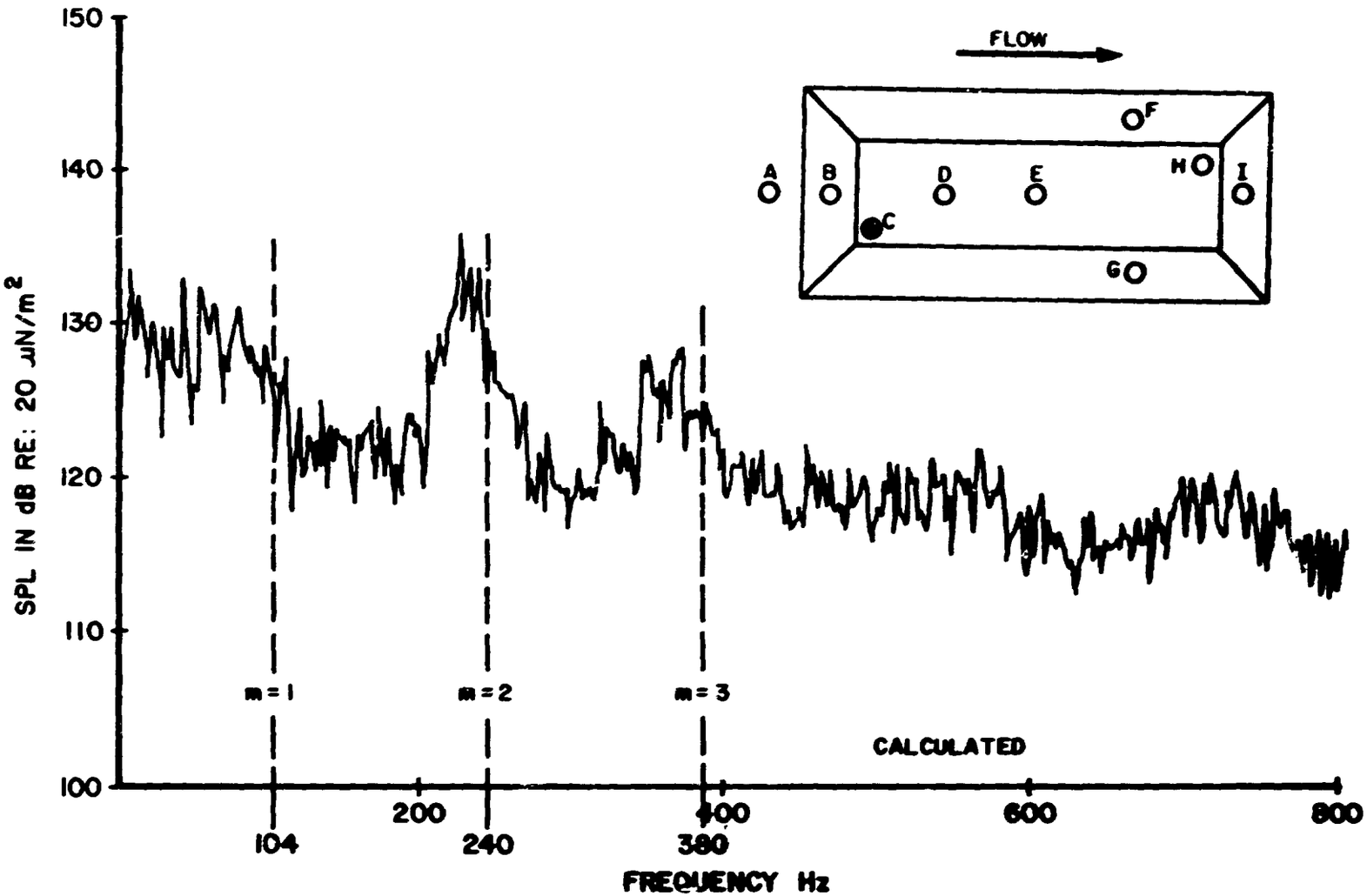

FIGURE 17 NARROWBAND (2 Hz) SPECTRUM FROM THE FRONT OF THE L/D = 7 CAVITY FOR AN ALTITUDE OF 20,000 FEET AT MACH NUMBER 1.30

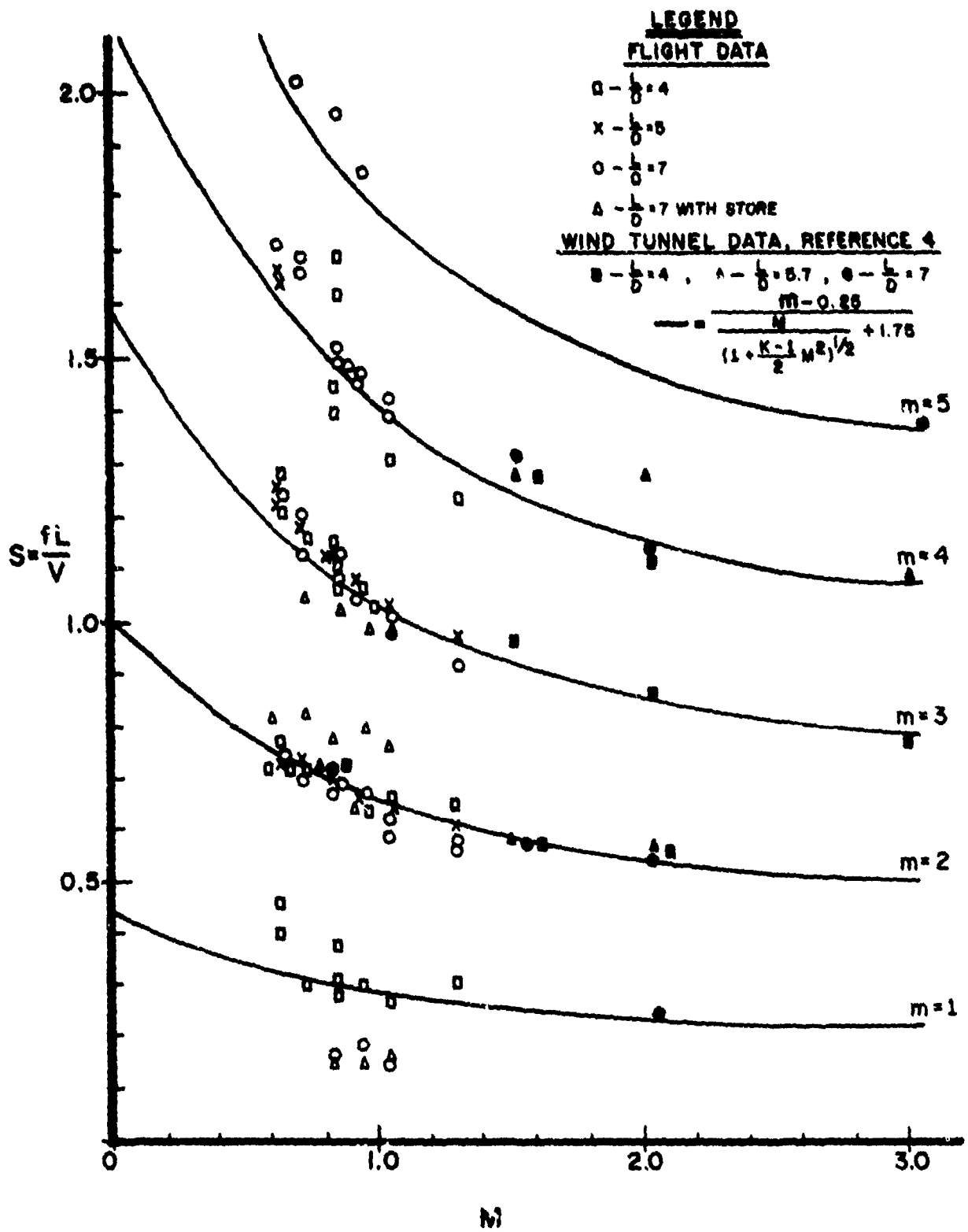

FIGURE 16 NONDIMENSIONAL RESONANT FREQUENCIES AS A FUNCTION OF MACH NUMBER

pressure (altitude) also had little effect as seen in the data in Figure 18 which include all test altitudes. The addition of a store did not affect the frequency as can also be seen in this figure. It was observed in Ref 4 that the resonant frequencies were relatively insensitive to variations in these variables but they determine in an unknown way the "occurrence" of the discrete frequencies.

The modified Rossiter formula, Equation (2), is seen in Figure 18 to be a good fit to the flight data and is thus recommended for predicting the resonant frequencies for rectangular cavities.

6. Fluctuating Pressures

Fluctuating pressures were measured at the nine locations shown in Figure 5 for all three test altitudes. The data were obtained from microphones at these locations and were recorded continuously as the aircraft slowly accelerated from the lowest to the highest Mach number. The recorded data were analyzed at approximately every 0.1 Mach number using a two second sample time. For the frequencies of interest this insures a good statistical representation of the data. Throughout the report the fluctuating pressures are either presented as sound pressure levels referenced to 20 $\mu N/m^2$ or are normalized to the free-stream dynamic pressure (q) and presented logarithmically. The dynamic pressures were computed from the free-stream Mach number and free-stream static pressures. These are presented in Table 1 for each pressure altitude and Mach number. In addition Table 1 includes the quantity required to convert the logarithmic normalized fluctuating pressures to sound pressure levels, i.e., add the last column of Table 1 to 20 log p/q to obtain the sound pressure level referenced to 20 $\mu N/m^2$.

Figure 19 presents overall fluctuating pressure levels as a function of Mach number for each of the cavity configurations tested. Data are presented from the front of the cavities for altitudes of 3000 and 20,000 feet. From these data it is seen that the overall fluctuating pressure levels in the cavities, for constant altitude, increase with increasing Mach number throughout the subsonic flight

TABLE I PRESSURE REFERENCE DATA

ALTITUDE Kft	MACH NR	STATIC PRESSURE P_∞ (psia)	DYNAMIC PRESSURE q_∞ (psia)	$-20 \text{ LOG } \left(\frac{P_{ref}}{q_\infty}\right)$ (dB)
30	0.61	4.37	1.12	172
20		6.76	1.73	175
3		13.17	3.37	181
30	0.71	4.37	1.56	174
20		6.76	2.41	178
3		13.17	4.69	184
30	0.82	4.37	2.06	177
20		6.76	3.19	181
3		13.17	6.21	186
30	0.93	4.37	2.66	179
20		6.76	4.11	183
3		13.17	8.01	189
30	1.05	4.37	3.35	181
20		6.76	5.19	185
3		13.17	10.11	191
30	1.17	4.37	4.18	183
20		6.76	6.47	187
3		13.17	12.60	193
30	1.30	4.37	5.17	185
20		6.76	8.00	189
3		13.17	15.58	194

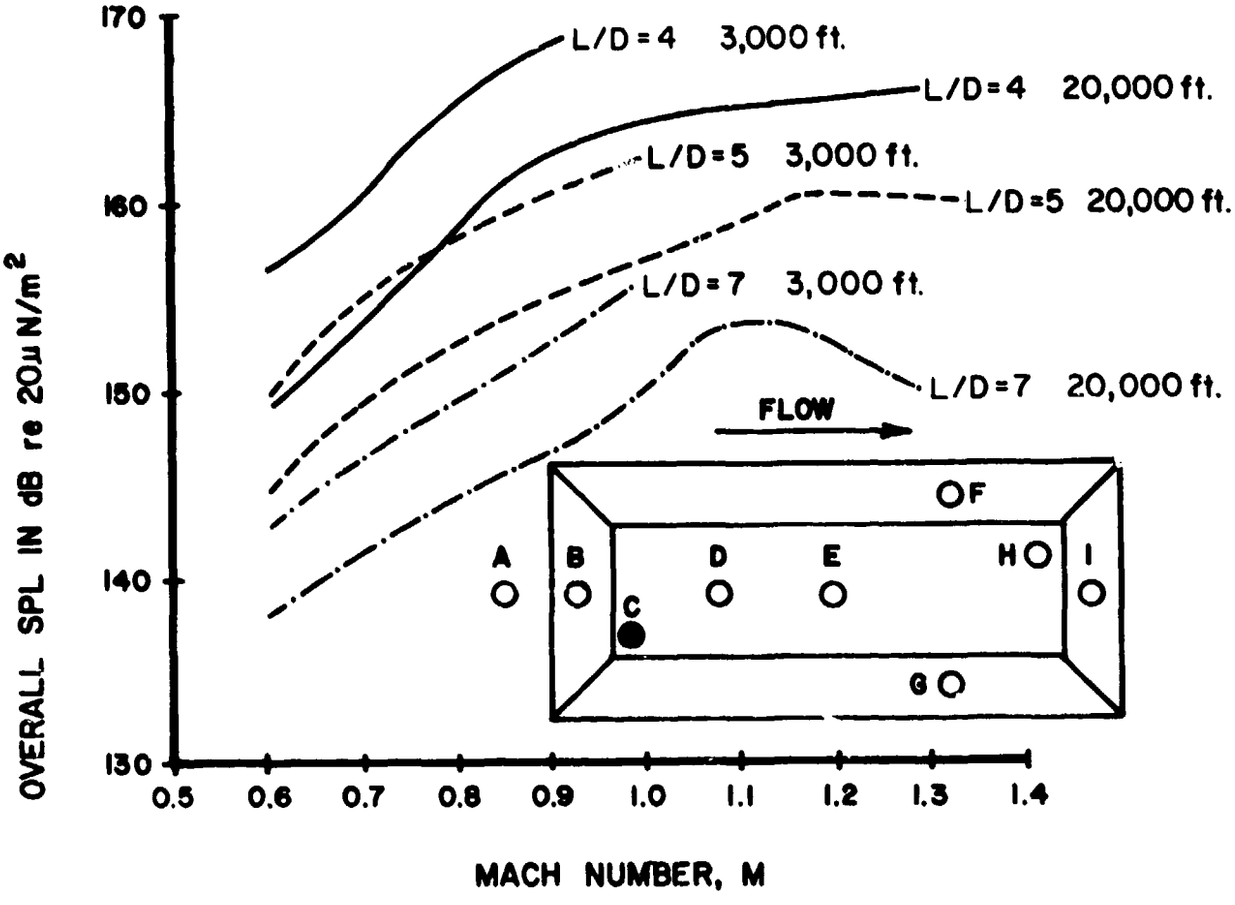

FIGURE 19 OVERALL FLUCTUATING PRESSURE LEVELS FROM THE FRONT OF THE CAVITIES

regime. However, the data from the shallow cavities (L/D = 5-7) show that at a somewhat higher Mach number a maximum pressure level is reached beyond which there is a decrease in level. The Mach numbers that correspond to the maximum overall level appear to be a function of the L/D ratio of the cavity. The Mach number that results in a maximum overall level for the L/D = 7 cavity is near 1.1 and near 1.2 for the L/D = 5 cavity. No maximum level was observed up to Mach 1.3 for the L/D = 4 cavity. However, it is expected that if the F-4 aircraft could have achieved a higher Mach number a maximum level would have been measured for the L/D = 4 cavity. The overall levels presented in Figure 19 are representative of all the data observed except that the spread between the data at each altitude differs for the different positions along the cavity. This results in a lack of free-stream dynamic pressure scaling at certain longitudinal cavity locations. This lack of scaling will be discussed in greater detail below when the mode shapes are presented.

One-third octave band spectra from the front of each of the three cavities are presented in Figures 20-22 for the three pressure altitudes. The resonant peaks are very evident for the deepest cavity, L/D = 4, and are much less pronounced for the shallowest cavity, L/D = 7. These data are typical of the results from the other locations in the cavity except, as was also noted in the overall levels, the spread between the curves varies with cavity longitudinal position. One-third octave band spectra from all microphone locations are presented in Ref 12 and 14.

It was shown in Ref 4 that the longitudinal variation of the resonant pressure amplitudes could be described as ordered modes. Suggested shapes for the first three modes, as determined from the wind tunnel data, are presented in Figure 23. In order to determine if the flight data followed the same mode shapes the amplitudes for the first three resonant frequencies are summarized in Figure 24 for the L/D =4 cavity. The levels are referenced to q and include results from all three altitudes (for a Mach number of 0.8). The data from the 20,000 ft altitude for a Mach number of 1.3 are presented to show that

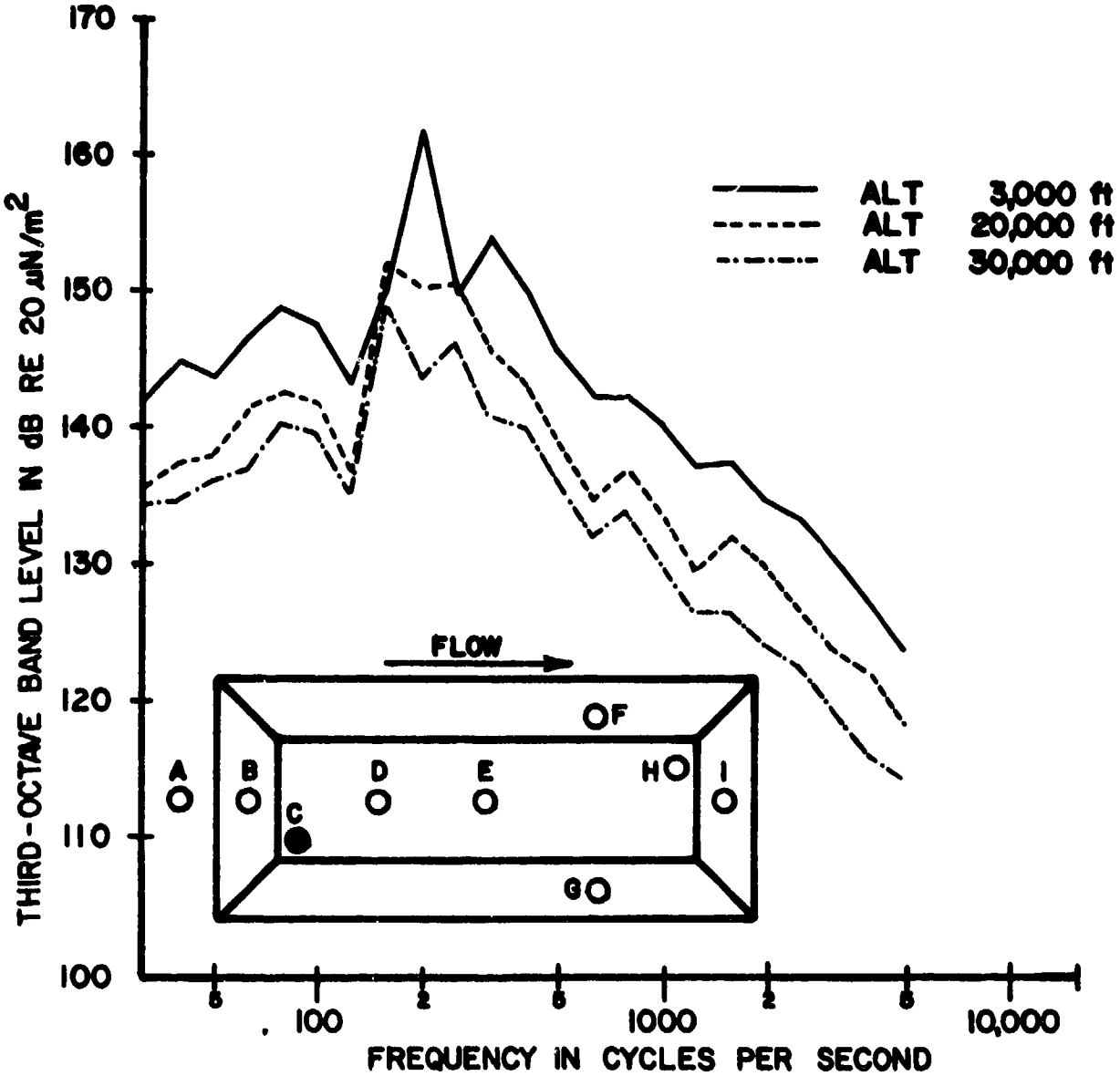

FIGURE 20 ONE-THIRD OCTAVE BAND SOUND PRESSURE LEVEL SPECTRA FROM THE FRONT OF THE CAVITY FOR A MACH NUMBER OF 0.82 AND A L/D RATIO OF 4

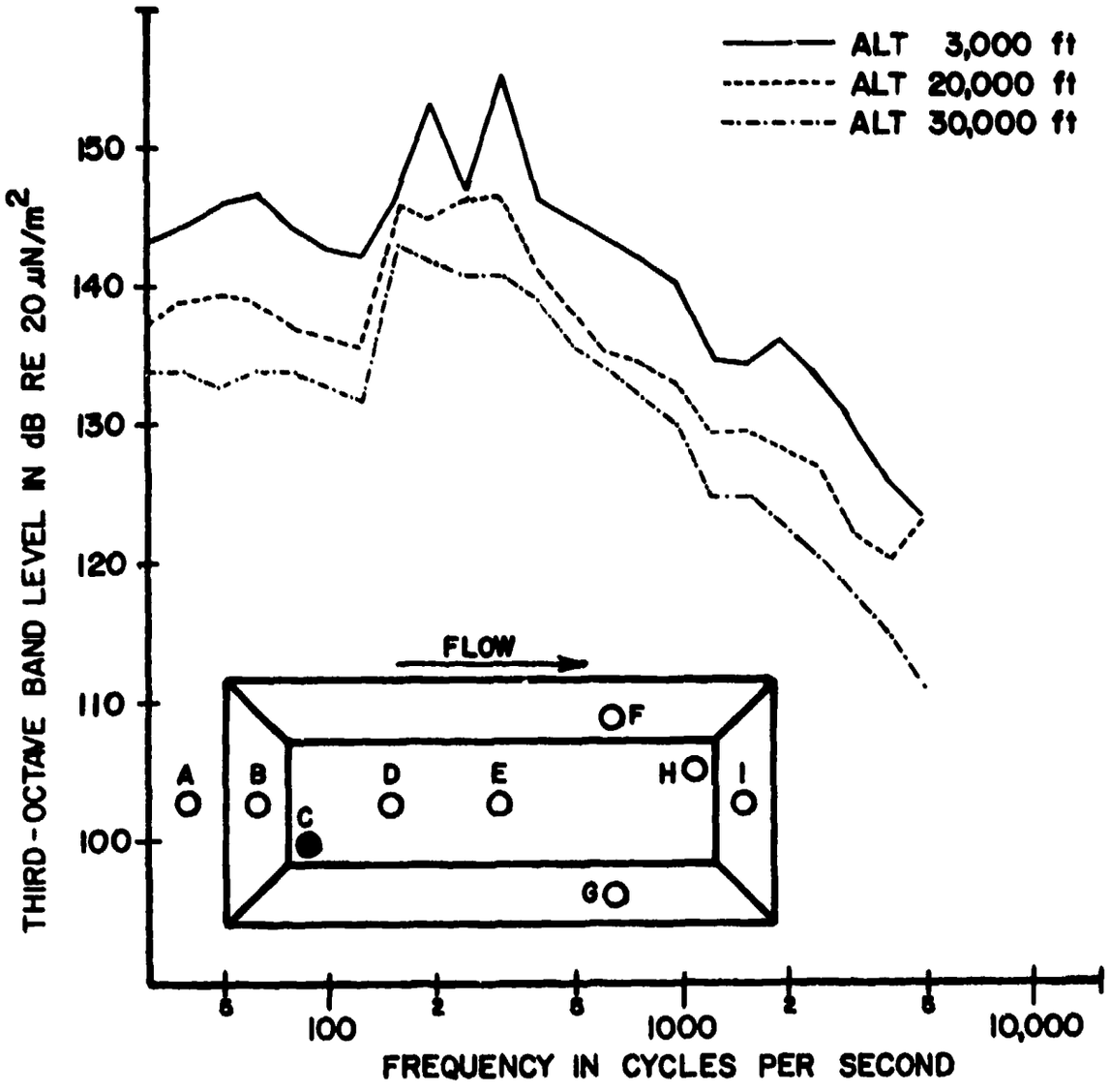

FIGURE 21 ONE-THIRD OCTAVE BAND SOUND PRESSURE LEVEL SPECTRA FROM THE FRONT OF THE CAVITY FOR A MACH NUMBER OF 0.82 AND A L/D RATIO OF 5

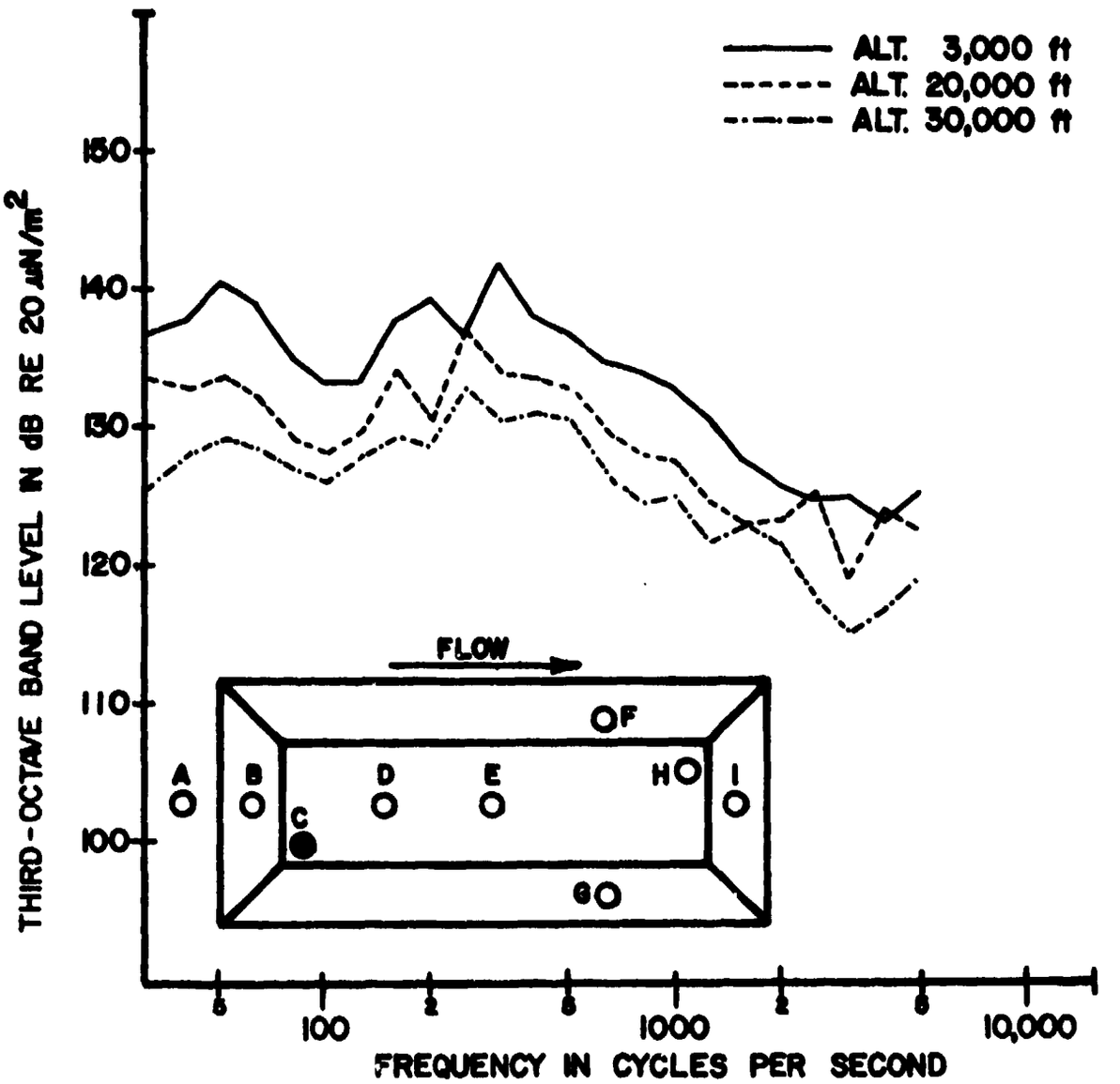

FIGURE 22 ONE-THIRD OCTAVE BAND SOUND PRESSURE LEVEL SPECTRA FROM THE FRONT OF THE CAVITY FOR A MACH NUMBER OF 0.82 AND A L/D RATIO OF 7

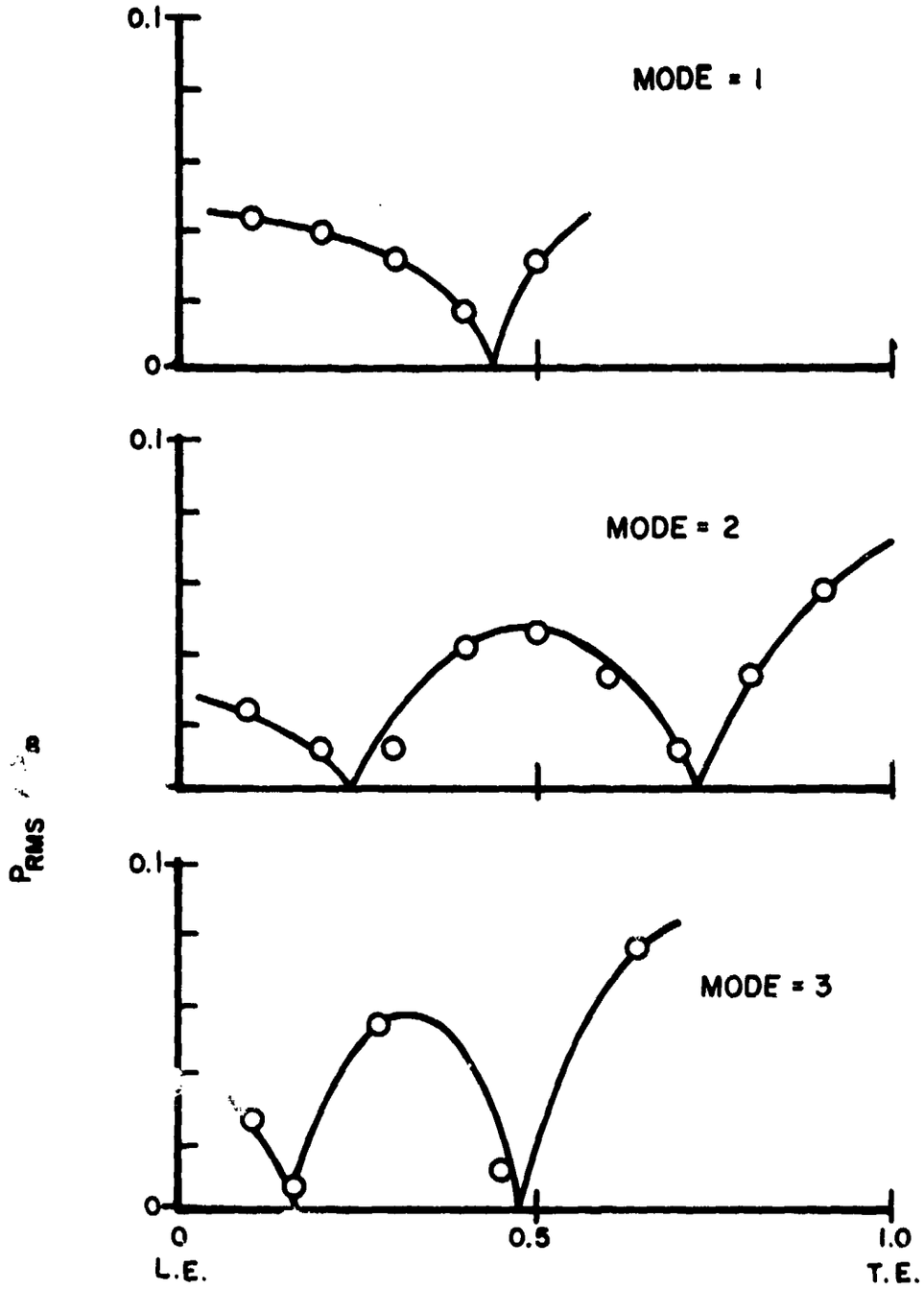

FIGURE 23 SUGGESTED SHAPE FOR FIRST, SECOND AND THIRD ORDER MODES FROM REFERENCE 2.

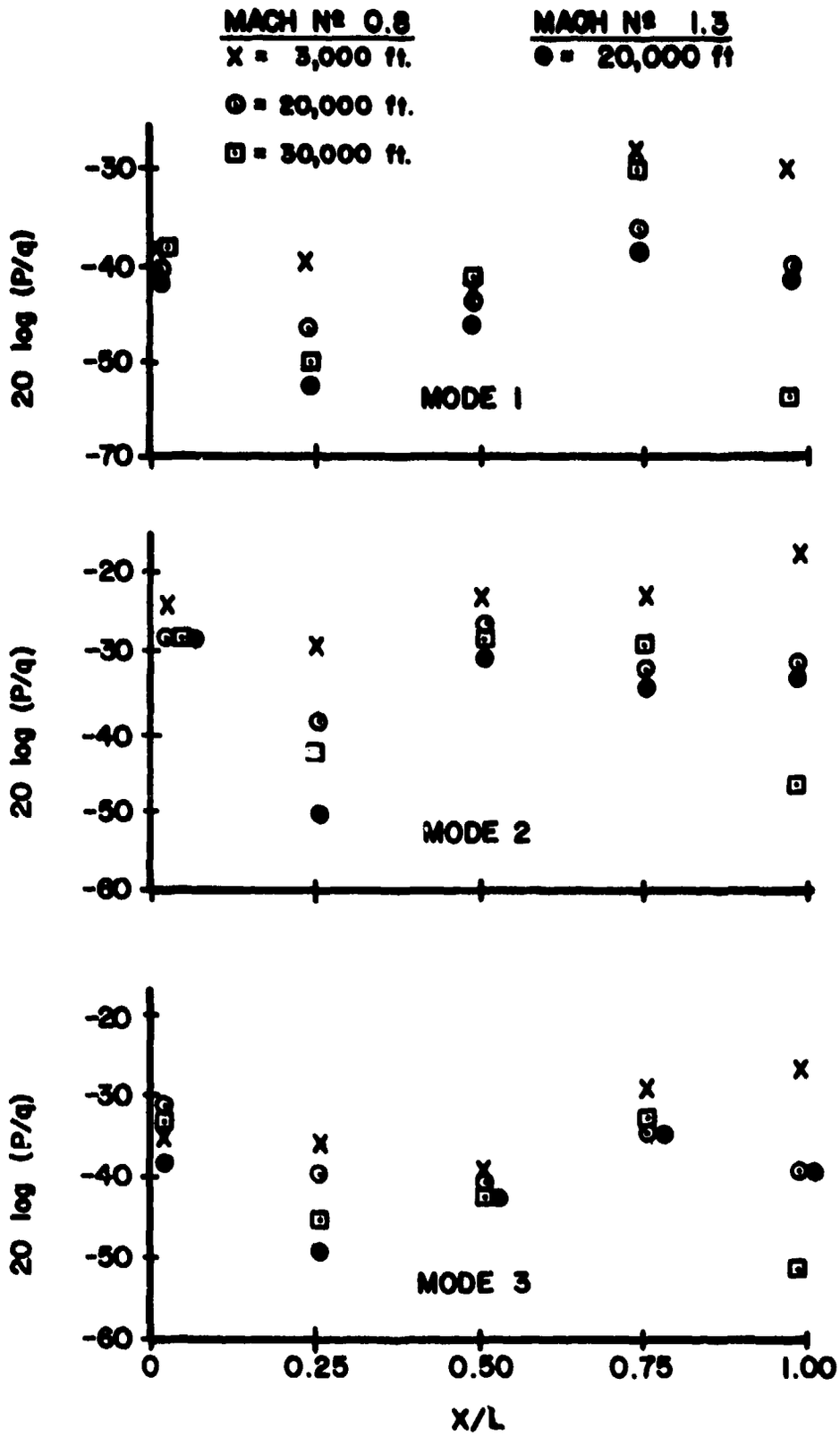

FIGURE 24 LONGITUDINAL VARIATION OF PEAK ONE-THIRD OCTAVE BAND REFERENCED TO FREE-STREAM DYNAMIC PRESSURE DEPICTING MODE SHAPES FOR L/D = 4

essentially the same mode shape exists at the higher airspeeds. Failure of the data to scale with q is quite evident at the rear of the cavity (X/L = 1). The only longitudinal cavity locations that scale well with q are X/L = 0.0 and X/L = 0.5. An adequate explanation as to why the other locations do not scale is not readily apparent. Thus the conclusion in Ref 4 that the fluctuating pressures scale with free-stream dynamic pressure, as determined from wind tunnel data, does not appear to be valid for all positions in the cavity.

In Ref 12 longitudinal mode shape equations were developed in the form of ramped sinusoidal functions for the L/D = 4 cavity from data obtained at an altitude of 3,000 ft. In Ref 14 the same approach was used to develop mode shape equations for the L/D = 5 and 7 cavity data. The form of the equation used for each L/D ratio was

$$20 \log (P_m/q)_{X/L} = 20 \log (P_m/q)_{X/L = 1} - (A_1 + A_2\, X/L + A_3 \left|\cos \alpha_m X/L\right|) \qquad (3)$$

$$m = 1, 2, 3$$

where: $20 \log (P_m/q)_{X/L}$ are the one-third octave band level of the rms sound pressures normalized with q for the modal frequencies at non-dimensional locations in the cavity, $20 \log (P_m/q)_{X/L = 1}$ are the one-third octave band level of the rms sound pressures normalized with q for the mode frequencies at the rear of the cavity, A_1, A_2, A_3 and α are empirical constants determined with the measured data from each cavity. It was found for these L/D ratios that the only variations were in the empirical constants A_1 and A_2 which define the increase in level from the front to the rear of the cavity. The increase in level from the front to the rear of the cavity was different for each cavity L/D ratio. Figure 15 shows this increase for the mode 2 frequency as

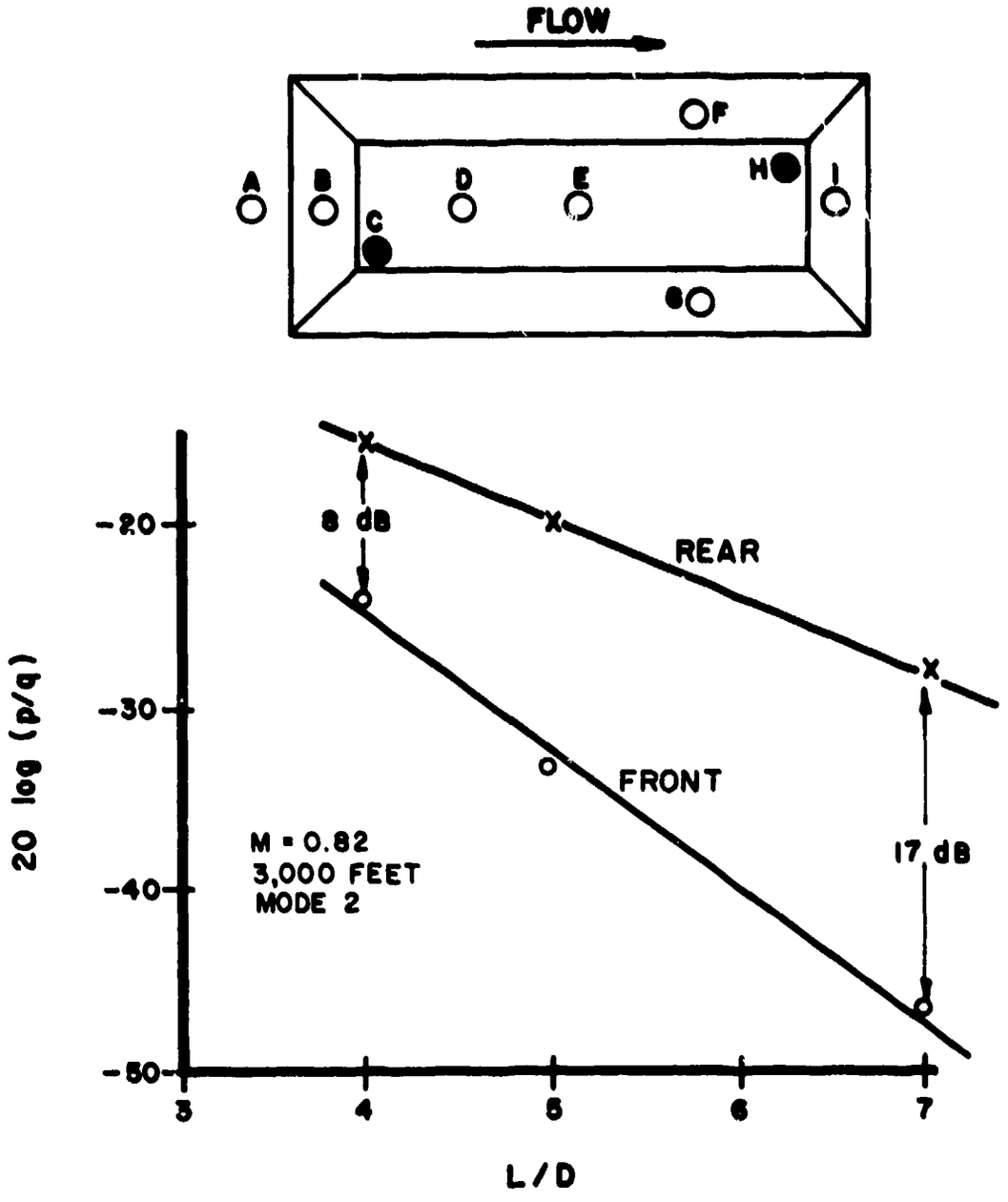

FIGURE 25, ONE-THIRD OCTAVE MODE 2 LEVELS FROM THE FRONT AND REAR OF THE CAVITIES FOR 3,000 FEET ALTITUDE AND MACH NUMBER 0.82.

a function of the L/D ratio. The increase was nearly 8 dB for the L/D = 4 cavity and 17 dB for the L/D = 7. Modes 1 and 3 displayed similar increases in level from the front to the rear of the cavities. A final mode shape equation accounting for the increase in level from the front to the rear of the cavity was determined to be:

$$20 \log (P_m/q)_{X/L} = 20 \log (P_m \max/q) - 10 \left[1 - \left|\cos \alpha_m X/L\right| + (0.33\ L/D - 0.6)(1 - X/L)\right] \qquad (4)$$

$$m = 1, 2, 3$$

where:

$20 \log (P_m/q)_{X/L}$ = one-third octave band level of the rms sound pressures normalized with q

$20 \log (P_m \max/q)$ = one-third octave band level of the rms sound pressures from the rear of the cavity normalized with q

X/L = normalized longitudinal cavity locations

$\alpha_1 = 3.5$

$\alpha_2 = 6.3$

$\alpha_3 = 10.0$

Figures 26-28 compare calculated mode shapes from equation (4) to the measured data at Mach 0.82 from all these cavities for modes 1, 2, and 3. The agreement is seen to be very good.

In order to use Equation 4 for predicting the absolute sound pressure levels in the cavity the maximum level for each mode frequency must be known. Mode 2 was observed, in most cases, to have the highest amplitude of the first three modes. In Ref 12 and 14 a second order least squares curve fit was used to define the normalized mode 2 amplitude as a function of Mach number and then sound pressure levels of modes 1 and 3 were related to mode 2. This proved to be very acceptable over the limited flight test Mach number range of 0.6 to 1.3; however,

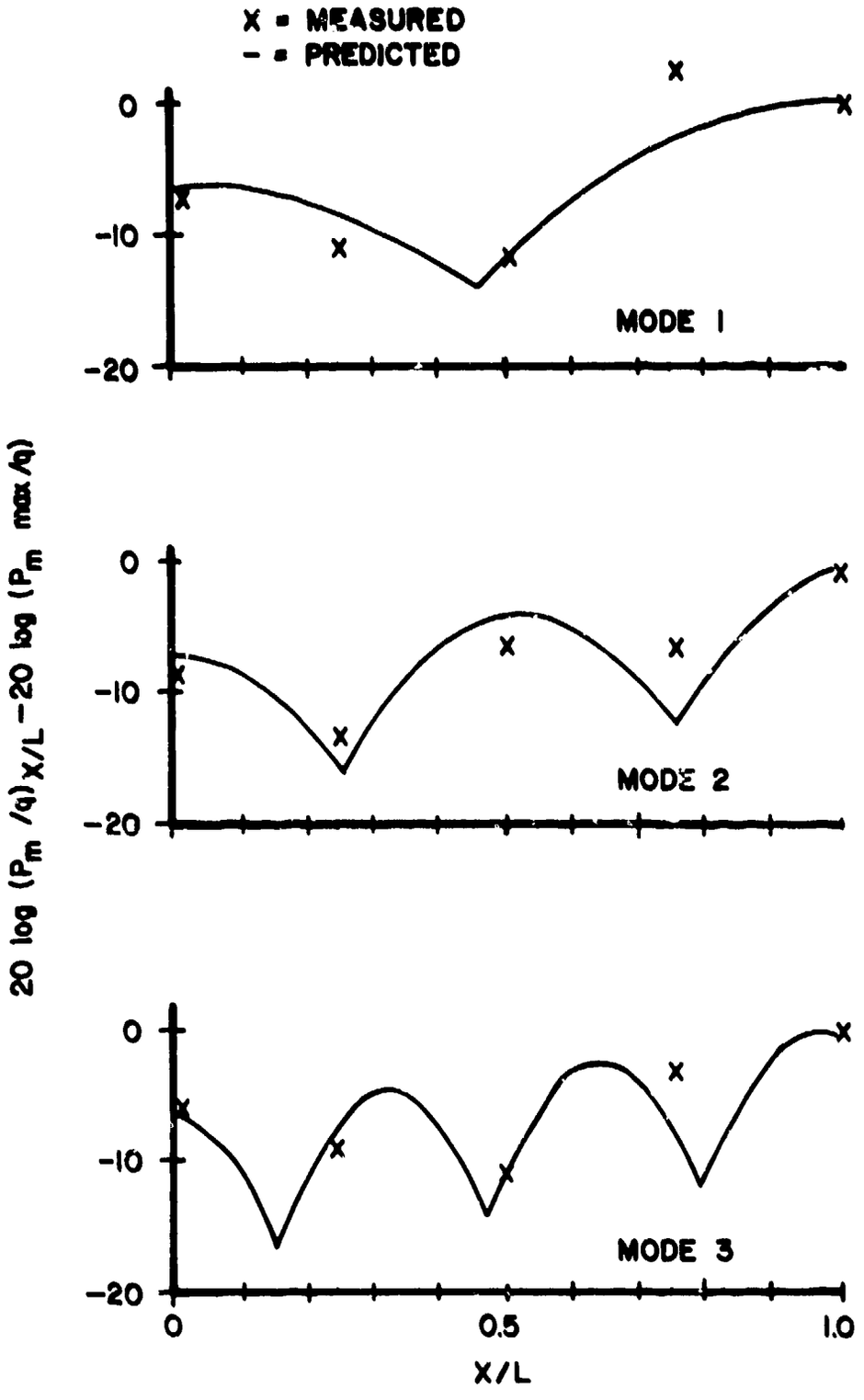

FIGURE 26 COMPARISON OF PREDICTED MODE SHAPES TO DATA FOR L/D = 4 FROM 3,000 FOOT ALTITUDE AND MACH 0.82

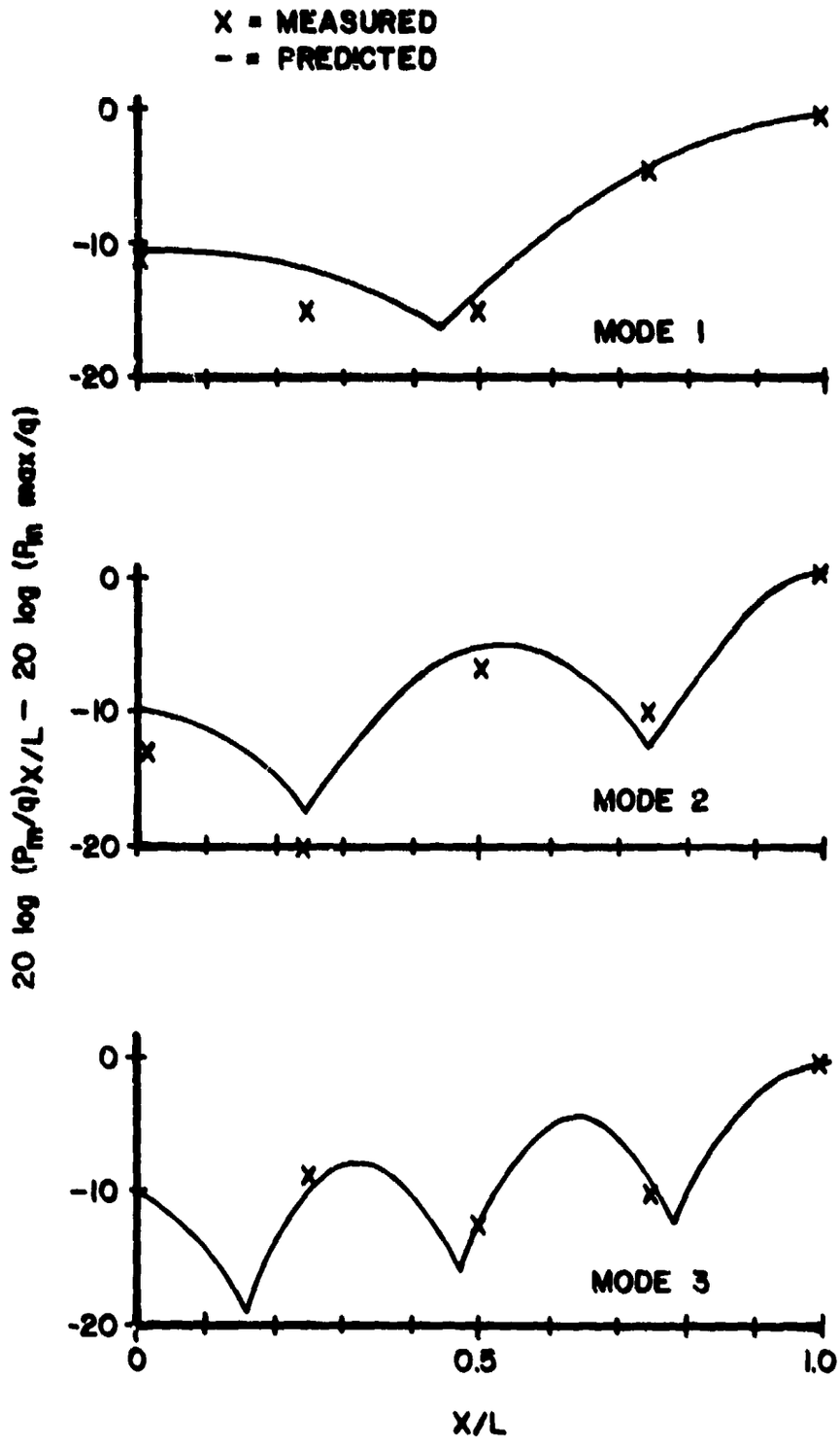

FIGURE 27 COMPARISON OF THE PREDICTED MODE SHAPE TO DATA FOR L/D = 5 FROM 3,000 FOOT ALTITUDE AND MACH 0.82

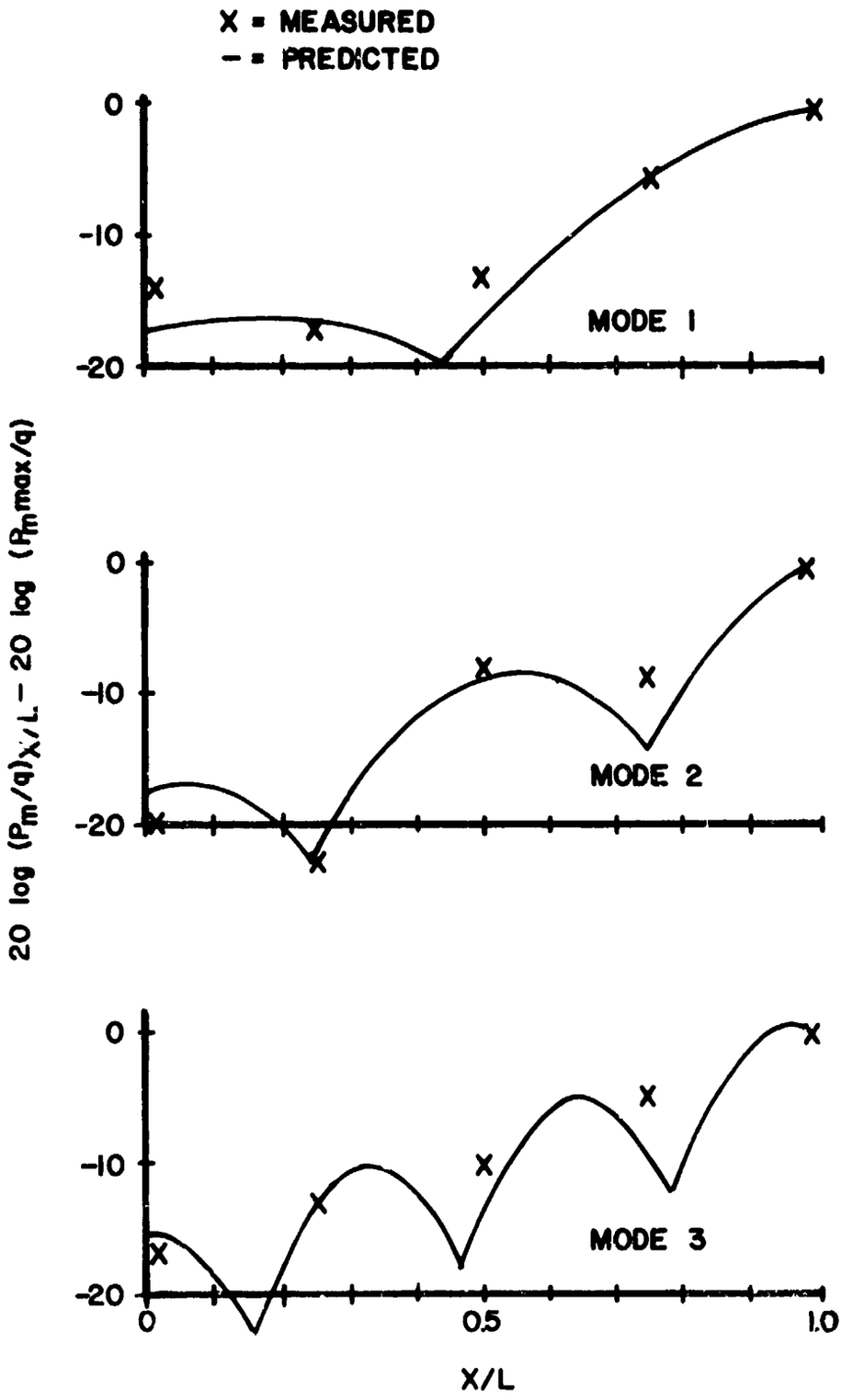

FIGURE 28 COMPARISON OF THE PREDICTED MODE SHAPE TO DATA FOR L/D = 7 FROM 3,000 FOOT ALTITUDE AND MACH 0.82

it could not be relied on to give valid results at Mach numbers above or below that range. It was desired to obtain a prediction scheme valid over a much larger speed range incorporating L/D effects.

It can be seen in the upper curve of Figure 25 that the mode 2 level was a function of L/D ratio and the prediction equation should reflect this variation in the maximum mode 2 level. The slope of the upper curve in Figure 25 was used to define the variation in the maximum mode 2 level with L/D ratio. This slope is 3.3. Since the normalized levels tended to increase with subsonic Mach number and decrease with supersonic Mach number, a function with these characteristics is required. Flight data were not available for the low subsonic and high supersonic speeds so wind tunnel data were used in conjunction with the flight data to develop an expression for the normalized maximum mode 2 sound pressure level as a function of Mach number. This expression is given by:

$$20 \log (P_2 \max/q) = 25 \operatorname{sech} \left[2 (M-1)\right] - 3.3 \, L/D - 27 \qquad (5)$$

where $\operatorname{sech} X = 2/ (e^{X} + e^{-X})$

Figure 29 presents the flight data and wind tunnel data from Ref 4 and 11 along with the curve defining the normalized mode 2 level from equation (5). The curve fits the flight data well but tends to deviate from the wind tunnel results. It is desirable to verify the curve with more data, at both low and high Mach numbers.

Equation 4 allows determination of the normalized mode 2 amplitude as a function of Mach number and L/D ratio. Equations defining modes 1 and 3 amplitudes still remain to be identified. These two modes will be referenced to mode 2 and for simplicity only constant or linear variations of Mach number or L/D ratio were considered. Figure 30 presents the one-third octave band levels from the rear of the cavity for modes 1, 2, and 3 as a function of L/D ratio at a Mach number of 0.82. Mode 1 is seen to be the lowest level for all L/D ratios and mode 3 is

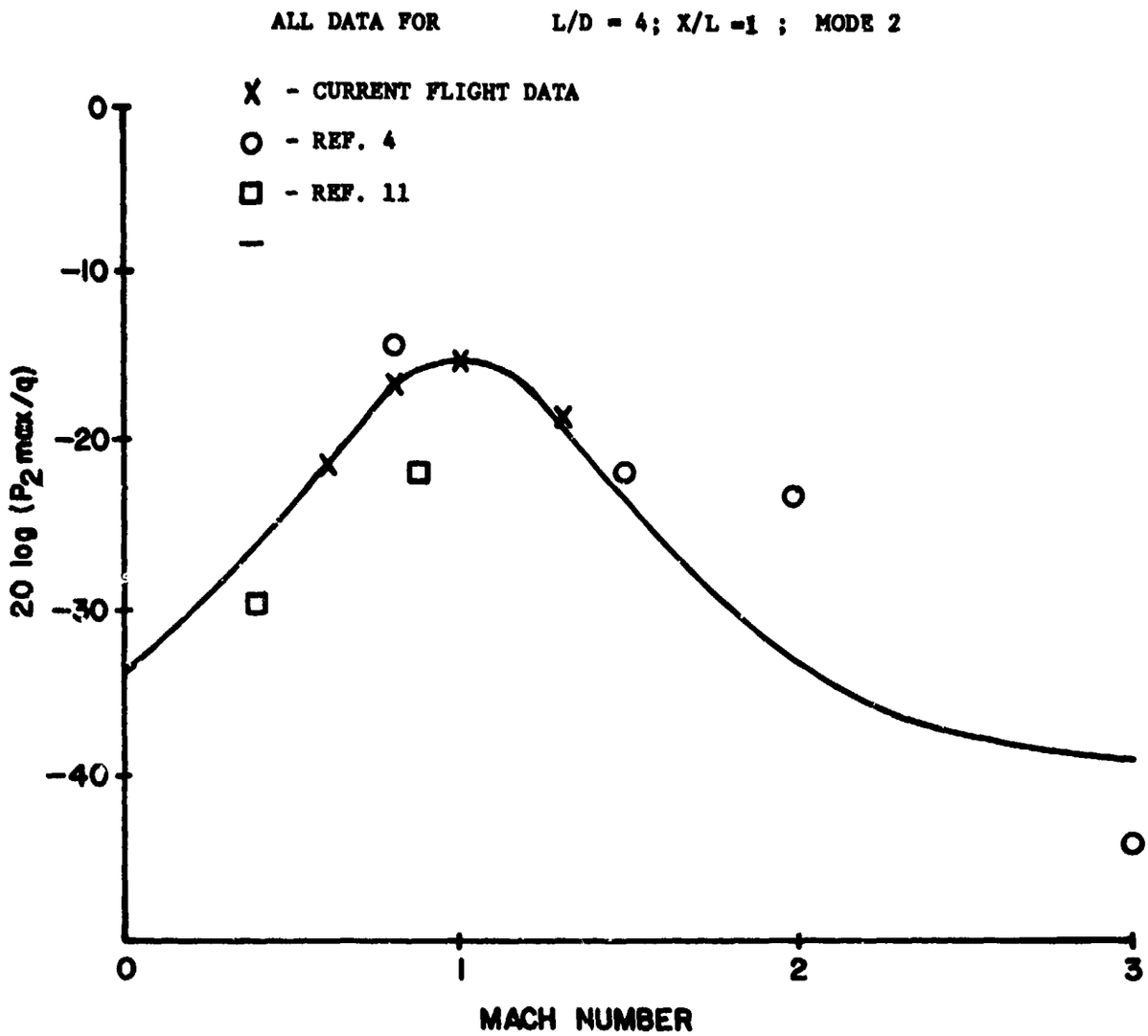

FIGURE 29 MODE 2 FLUCTUATING PRESSURE LEVEL DATA WITH PREDICTION CURVE

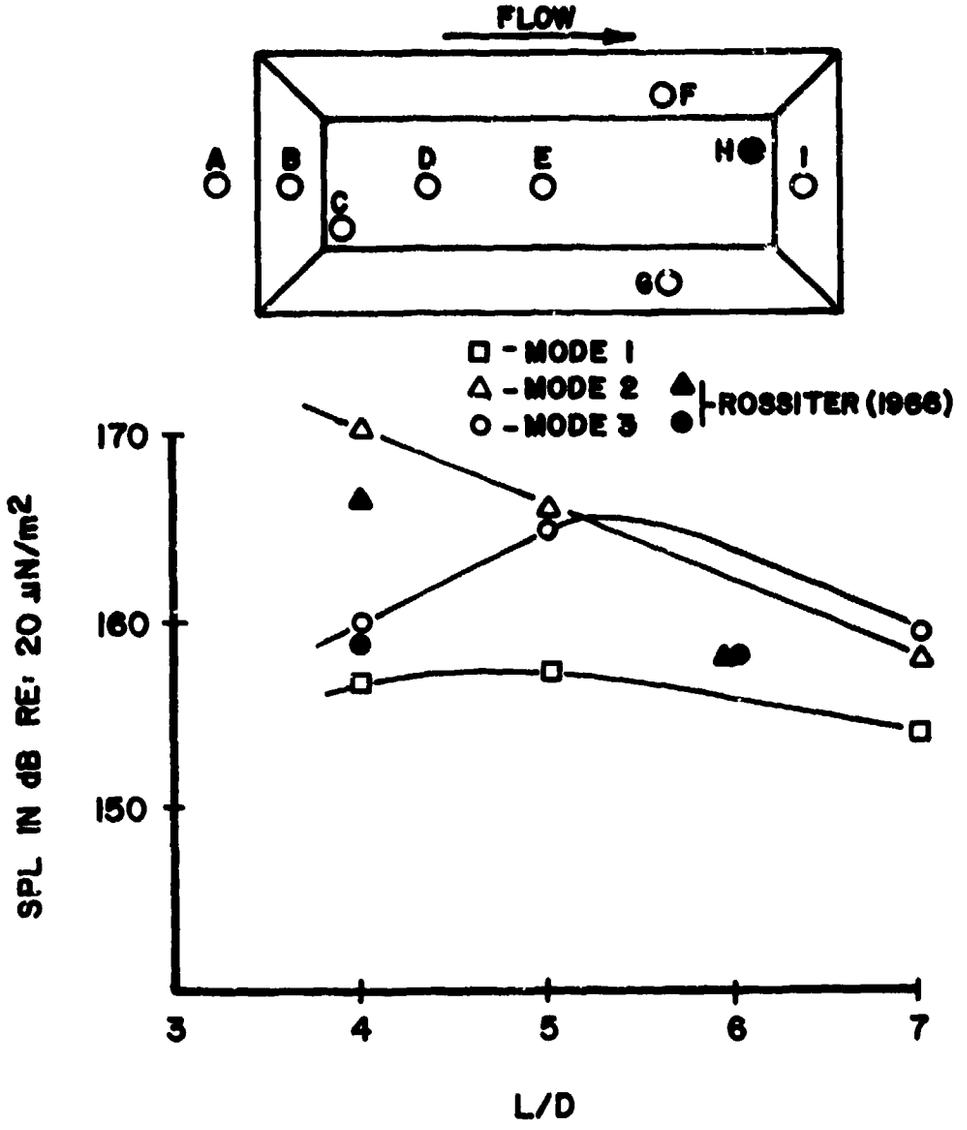

FIGURE 30 MAXIMUM ONE-THIRD OCTAVE BAND SOUND PRESSURE LEVEL FROM THE REAR OF THE CAVITY AS A FUNCTION OF L/D FOR 3,000 FOOT ALTITUDE AND MACH 0.82

very close to mode 2 except at the lower L/D ratios. Mode 1 relative to mode 2 has a nearly linear variation with L/D ratio for a Mach number of 0.82.

Figures 31 through 33 present the Mach number effects on the amplitudes of the three modal frequencies for each L/D ratio. As the L/D ratio increases from 4 to 7 the variation between mode levels decreases. This was anticipated because past data reveal that the mode amplitudes tend to decrease with increasing L/D ratio. As seen in Figure 33 for the L/D = 7 cavity, the amplitudes of the resonant peaks clearly display a maxima, whereas, this was not the case for the L/D = 4 and L/D = 5 cavities (Figures 31 and 32). It was concluded from these figures that the nearly linear variation (with L/D ratio) shown in Figure 34 between the amplitudes of modes 1 and 2 was a good approximation over the entire Mach number range of the flight test. It was also concluded that the Mach number effects on the variation between the mode 2 and 3 amplitudes were more significant than the L/D effects presented in Figure 30 and should be used in collapsing the data. It still remains to be determined if these two approximations are good for increased L/D ratios and Mach number ranges.

In Figure 34 the differences between amplitudes of modes 1 and 2 for L/D ratios from 2 to 7 are plotted. The difference between the amplitudes of modes 1 and 2 were obtained by averaging results over the respective Mach number ranges indicated in the figure. Data from several sources are included. The scatter appears fairly large at the lower L/D values; however, considering the data cover Mach numbers from 0.21 to 3.00, this data scatter is considered reasonable. The line shown in this figure was obtained by a least squares fit. It is the proposed prediction for the mode 1 amplitude and results in the following expression:

$$20 \log (P_1 \max/q) = 20 \log (P_2 \max/q) + 1.5 \text{ L/D} - 13 \qquad (6)$$

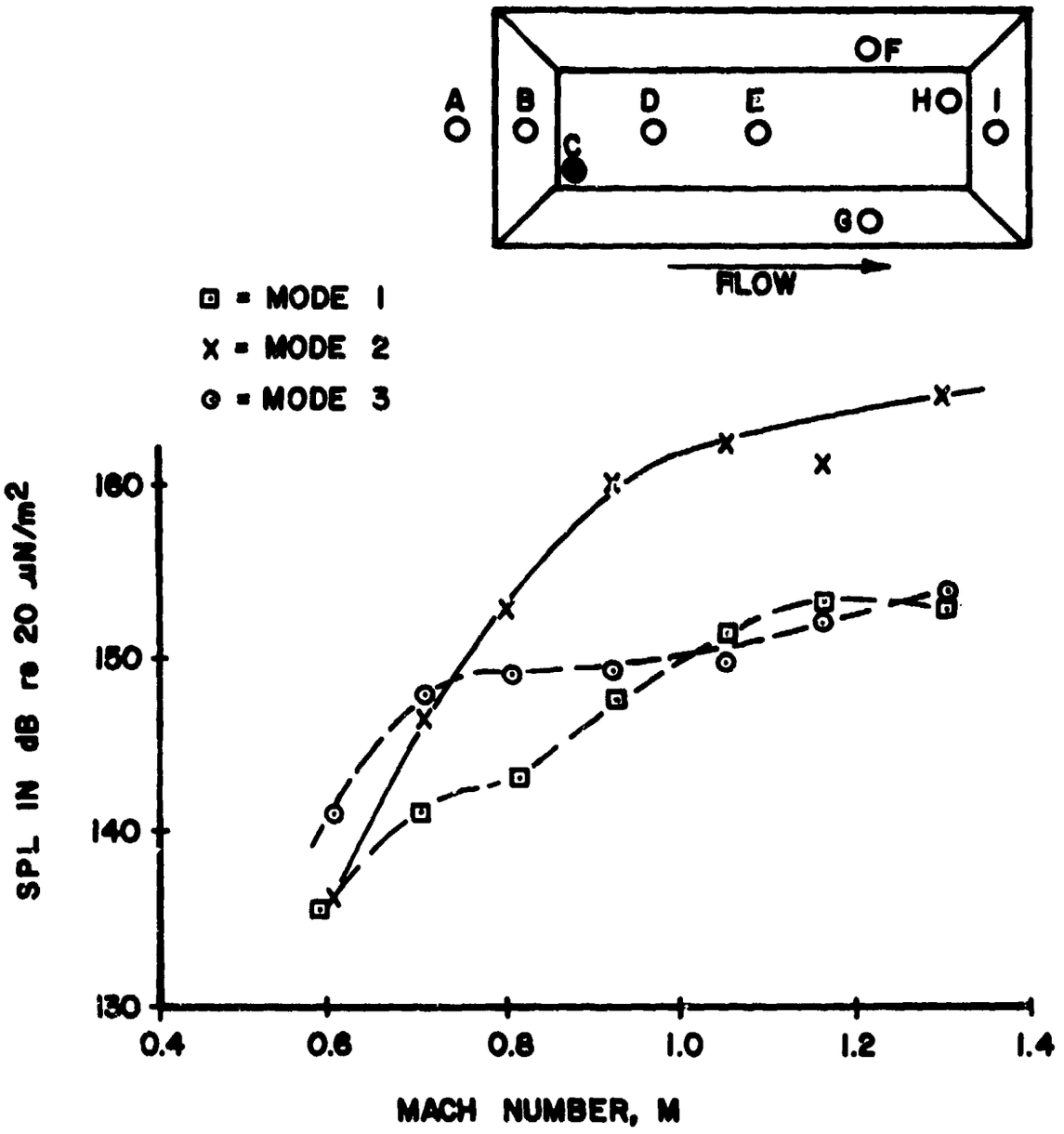

FIGURE 31 ONE-THIRD OCTAVE BAND PEAKS DEPICTING MACH NUMBER EFFECT FROM THE FRONT OF THE CAVITY FOR L/D = 4 AND 20,000 FOOT ALTITUDE

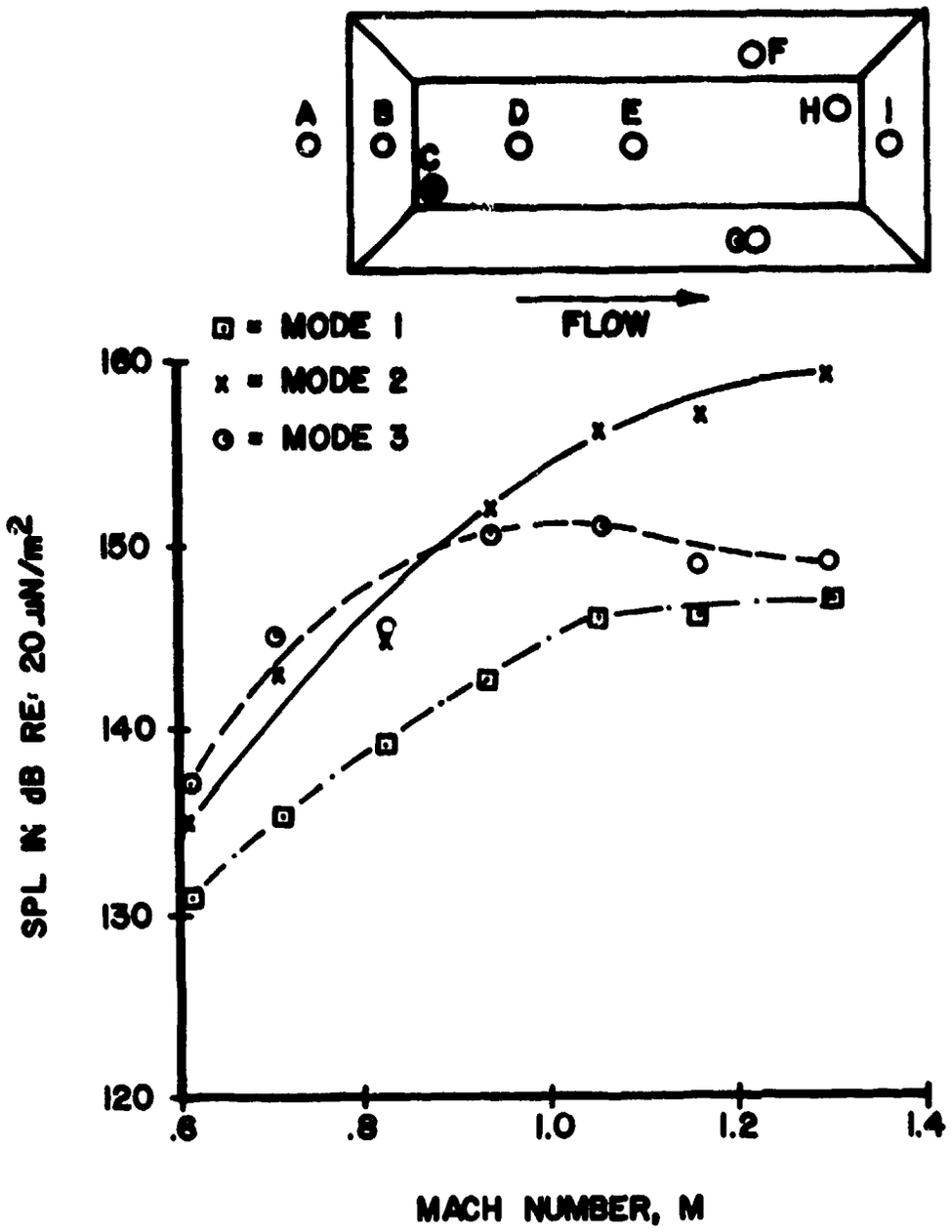

FIGURE 32 ONE-THIRD OCTAVE BAND SOUND PRESSURE LEVEL PEAKS FROM THE FRONT OF THE CAVITY DEPICTING MACH NUMBER EFFECT FOR L/D = 5 AND 20,000 FOOT ALTITUDE

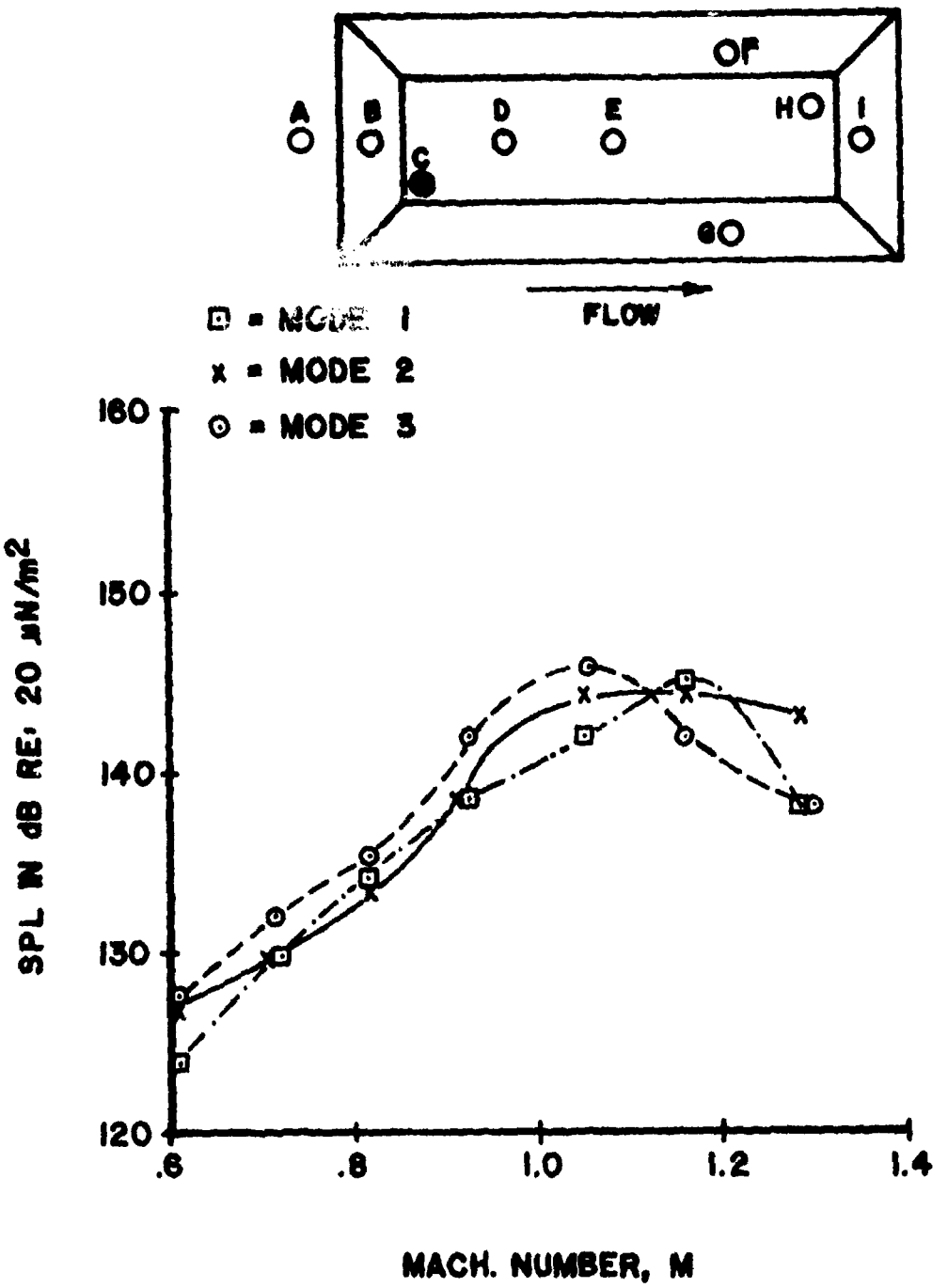

FIGURE 33 ONE-THIRD OCTAVE BAND SOUND PRESSURE LEVEL PEAKS FROM THE FRONT OF THE CAVITY DEPICTING MACH NUMBER EFFECT FOR L/D = 7 AND 20,000 FOOT ALTITUDE

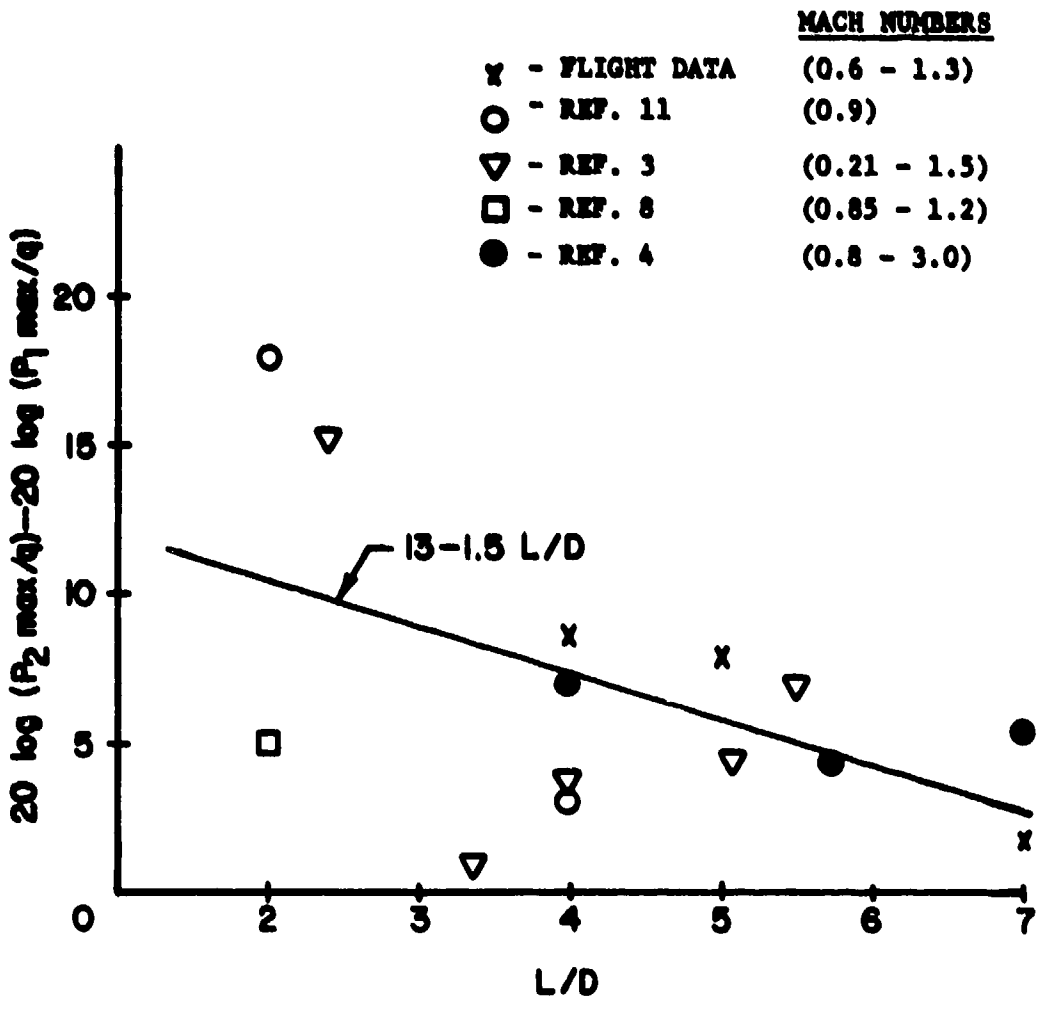

FIGURE 34 AVERAGE VARIATION OF AMPLITUDE BETWEEN MODES 1 AND 2 AS A FUNCTION OF L/D

The flight data were weighted twice as heavy as the wind tunnel data. Equation 6 allows an estimation of the maximum mode 1 one-third octave band amplitude. A similar expression is required for the mode 3 amplitude.

Basically the same approach was used to determine an expression for the mode 3 amplitude. The differences between mode 2 and mode 3 amplitudes were obtained as a function of Mach number assuming no L/D effect. It was previously noted from Figures 30-33 that the Mach number had a larger effect than the L/D ratio on the difference between the mode 2 and mode 3 amplitudes. The averages are shown in Figure 35 as a function of Mach numbers which include flight and wind tunnel data. The flight data follow a linear variation with Mach number and the wind tunnel data agree quite well. No data are shown above Mach 1.5 since the mode 3 amplitudes were not sufficiently above the broadband level to determine a difference. The recommended prediction curve for the mode 3 amplitude is shown in the figure and results in the following equation:

$$20 \log (P_3 \max/q) = 20 \log (P_2 \max/q) - 13 M + 9 \qquad (7)$$

The equations presented thus far enable the estimation of the resonant frequencies, one-third octave band sound pressure amplitude for these frequencies and the longitudinal distribution of the amplitudes. The determination of the complete aero-acoustic environment in a cavity requires the broadband levels, as well as the narrowband levels. It was observed in Ref 4, 9, and 11 that the broadband levels increase toward the rear of the cavity. The flight data essentially displayed the same result. In general, this increase was approximately 10 dB from the front to the rear of the cavity for a L/D = 4 cavity, 13 dB for a L/D = 5 cavity and 17 dB for the L/D = 7 cavity. For prediction purposes linear variations were assumed. Figure 36 shows the longitudinal broadband variation for the L/D = 5

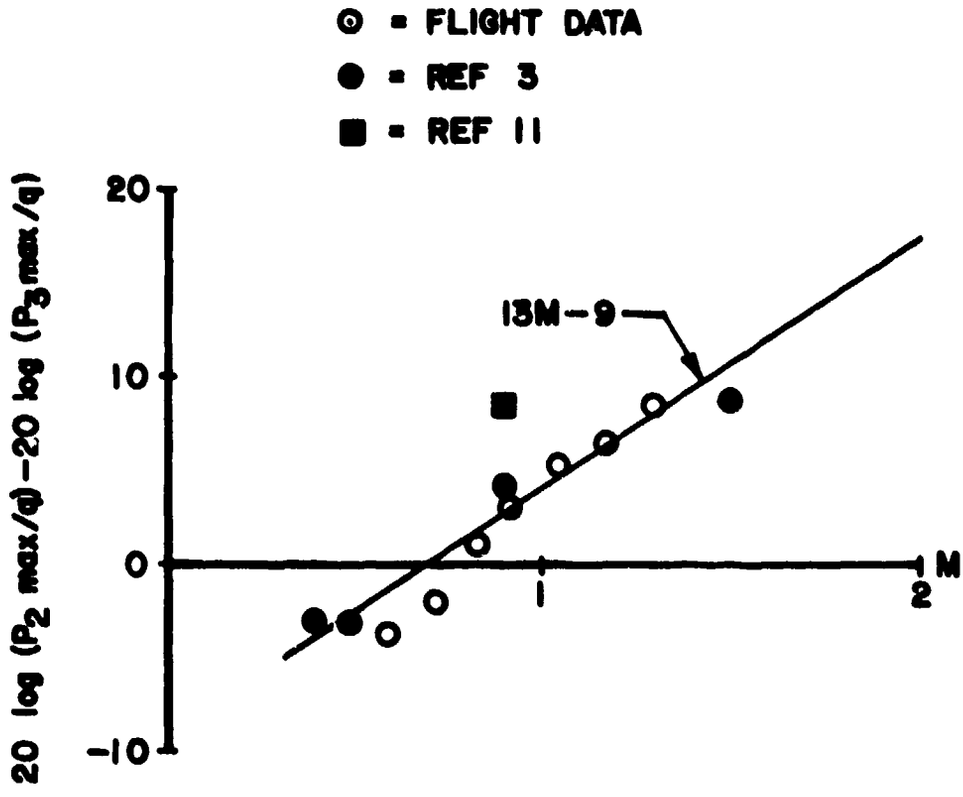

FIGURE 35 AVERAGE VARIATION OF AMPLITUDE BETWEEN MODES 2 AND 3 AS A FUNCTION OF MACH NUMBER

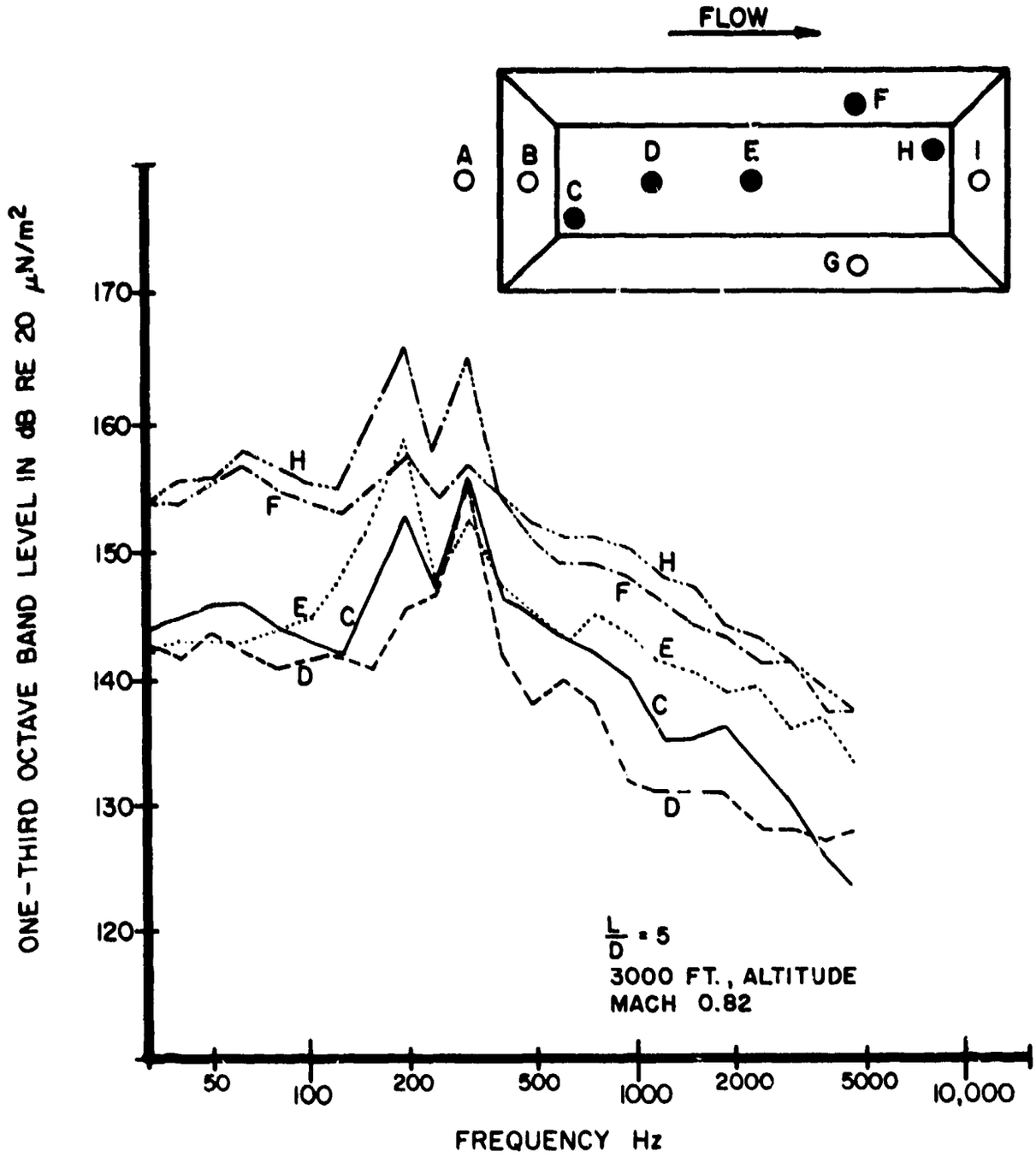

FIGURE 36 ONE-THIRD OCTAVE BAND SPECTRA FROM THE L/D = 5 CONFIGURATION DEPICTING LONGITUDINAL VARIATION

cavity at a Mach number of 0.82 and an altitude of 3000 feet. It is apparent that the shape of the broadband spectrum remains fairly constant over the entire cavity length. It also remains to be determined if the shape of the broadband spectrum varies with Mach number or L/D ratio.

Figure 37 presents the normalized spectra from the front of the L/D = 4 cavity for several Mach numbers. The shape of the spectra is seen to be essentially the same for the entire Mach number range of the test. It can also be noted in this figure that the normalized broadband levels increase with Mach number. Variation of the broadband spectra with L/D ratio is shown in Figure 38. It is evident that the shape is not a function of L/D ratio. Thus it was assumed that the shape of the broadband spectrum did not vary significantly with X/L, L/D or Mach number. However, the maximum broadband level was a function of these three variables. The maximum normalized broadband level was referenced to the maximum normalized mode 2 amplitude. The first variable accounted for was the difference between the maximum mode 2 amplitude and the maximum broadband level. Figure 38 indicates differences in the mode 2 amplitude and the broadband levels of about 15 dB for L/D = 4, 11 dB for L/D = 5 and 5 dB for L/D =7. This resulted in a linear relation between the mode 2 amplitude and the broadband level given by the following expression:

$$20 \log (P_b \max/q) = 20 \log (P_2 \max/q) + 3.3\ L/D - 28 \qquad (8.a)$$

where P_b max is the maximum one-third octave band rms broadband pressure which occurs at the rear of the cavity. This expression does not account for the longitudinal variation of the broadband level. The longitudinal variations presented earlier were 10 dB for the L/D = 4 cavity, 13 dB for the L/D = 5 cavity and 17 dB for the L/D = 7 cavity. With these longitudinal variations the prediction equation becomes:

$$20 \log (P_b \max/q) = 20 \log (P_2 \max/q) + 3.3\ L/D - 28 + 3(1-L/D)(1-X/L) \qquad (8.b)$$

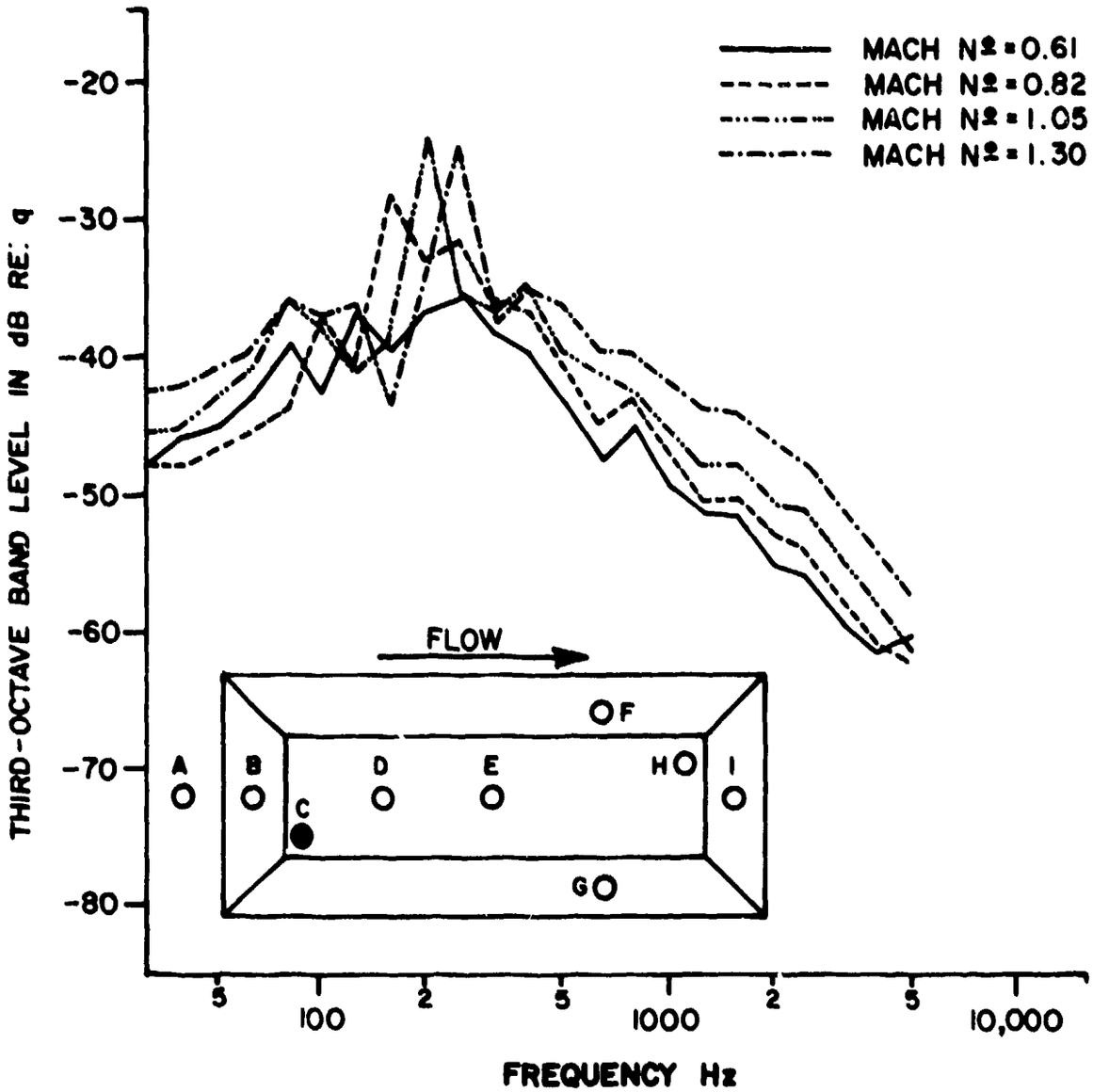

FIGURE 37 ONE-THIRD OCTAVE BAND SOUND PRESSURE LEVEL SPECTRA FROM THE FRONT OF THE L/D = 4 CAVITY AT 30,000 FOOT ALTITUDE

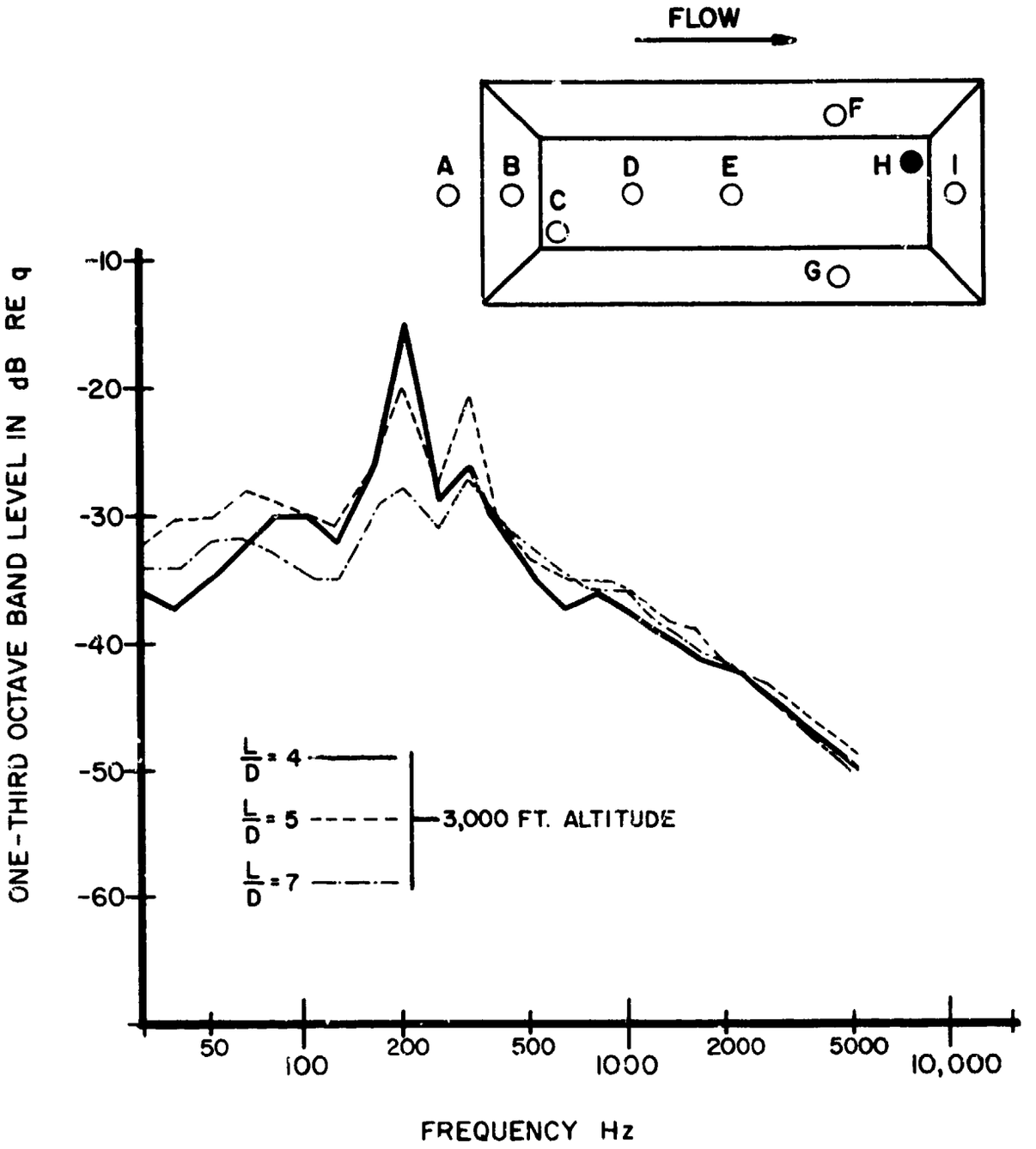

FIGURE 38 ONE-THIRD OCTAVE BAND SOUND PRESSURE LEVEL SPECTRA FROM THE REAR OF THE CAVITY FOR MACH NUMBER 0.82 FOR ALL L/D RATIOS

This expression still does not account for a Mach number effect. It was observed, from Ref 4 that as Mach number increases the difference between the maximum mode 2 amplitude and the maximum broadband level decreases. An average difference, for the different L/D ratios, was determined from the flight data and from the data in Ref 4. These results are shown in Figure 39. These data indicate that the difference between the maximum mode 2 peak and the maximum broadband level linearly decreases from low Mach numbers and reaches zero near Mach 3. With this effect considered the final form of the expression to predict the maximum broadband level becomes:

$$20 \log (P_b \max/q) = 20 \log (P_2 \max/q) + [3.3\ L/D - 28 + 3\ (1-L/D)(1-X/L)]\ [1.2 - 0.4M] \quad (8.c)$$

Since it has been shown that the general shape of the broadband spectrum is fairly constant, a single spectrum shape is recommended for prediction purposes. Figure 40 presents the recommended broadband spectrum shape determined from the flight data. The levels are presented normalized with q and as a function of Strouhal number based on free stream velocity and the length of the cavity. Equation 8.c is used to determine the maximum one-third octave broadband level and then Figure 40 is used to determine the one-third octave broadband levels for the frequency range of interest.

7. Effect of Store Insertion

In order to determine the effect a store has on the fluctuating pressure environment in the cavity an ogive store was mounted in the L/D = 7 configuration as shown in Figure 1. This configuration was tested for the same flight conditions as the empty cavities and the same data were obtained. Figures 41 and 42 illustrate the differences between the empty and store-containing configurations by comparing the spectra from the empty and the store containing cavities

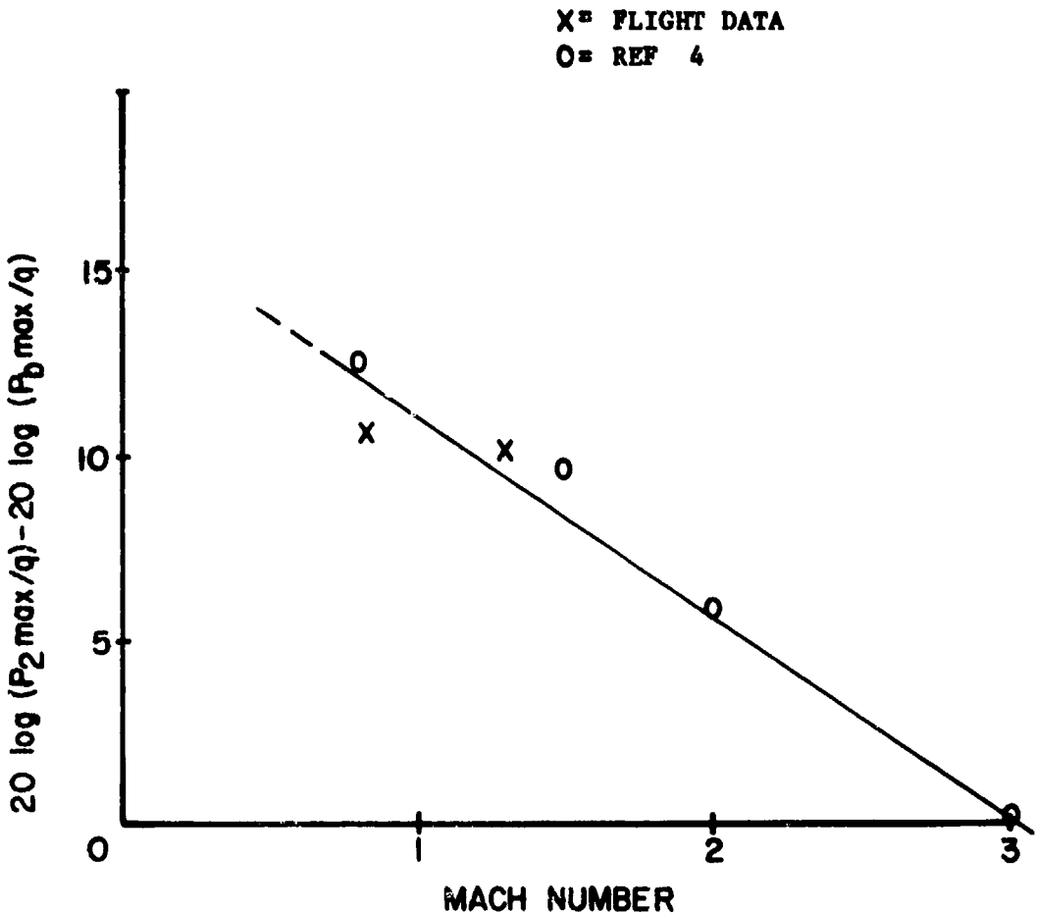

FIGURE 39 MACH NUMBER EFFECT ON THE AVERAGE VARIATION BETWEEN THE MAXIMUM ONE-THIRD OCTAVE BROADBAND AND MODE 2 AMPLITUDES

$$20 \log(P_b max./q) = 20 \log (P_2 max./q) + [3.3\ L/D - 28 + 3(1-L/D)(1-X/L)][1.2-0.4M]$$

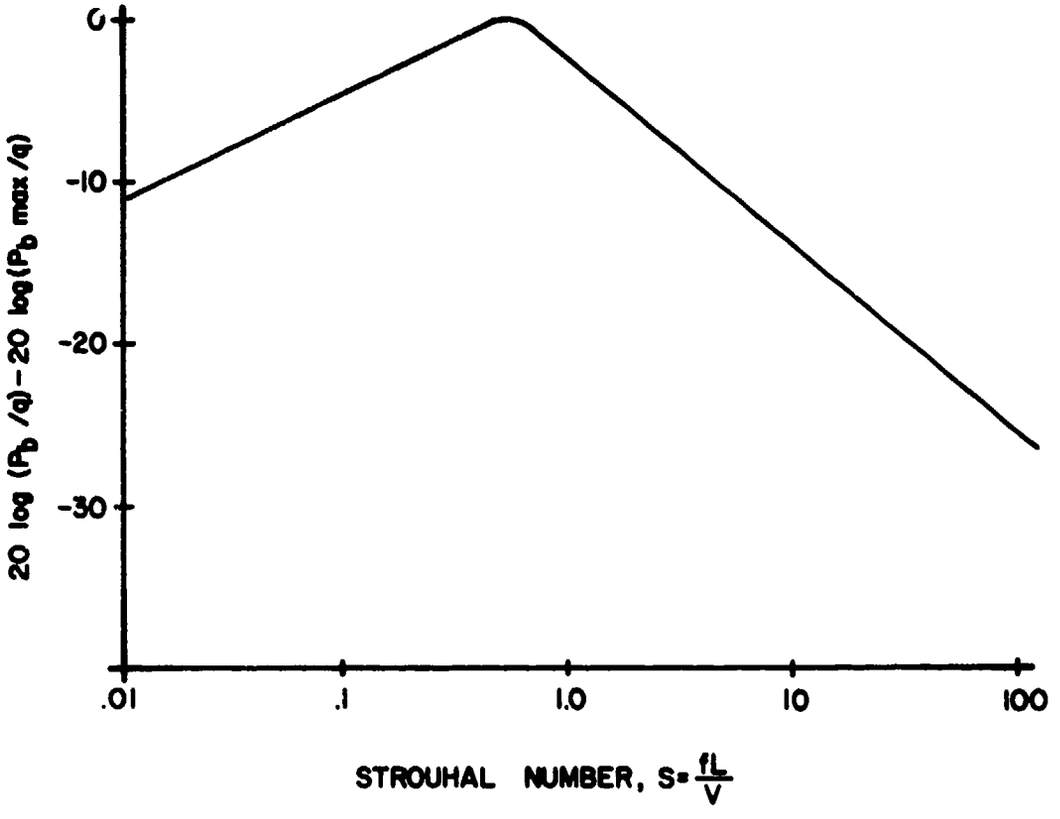

FIGURE 40 ONE-THIRD OCTAVE BROADBAND LEVEL VERSUS STROUHAL NUMBER

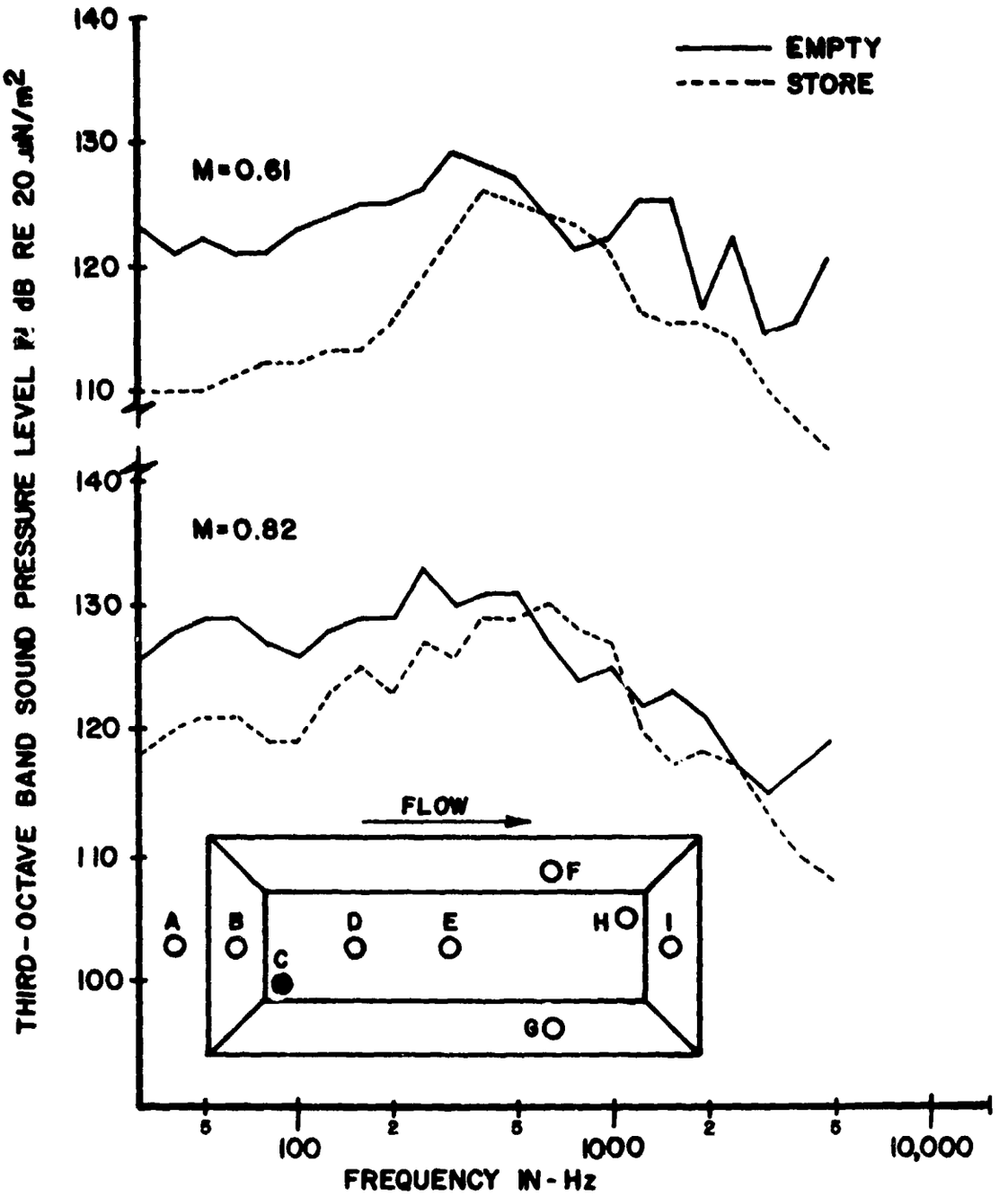

FIGURE 41 COMPARISON OF ONE-THIRD OCTAVE BAND SOUND PRESSURE LEVEL SPECTRA FROM THE L/D = 7 EMPTY AND STORE CONFIGURATION FOR AN ALTITUDE OF 30,000 FEET

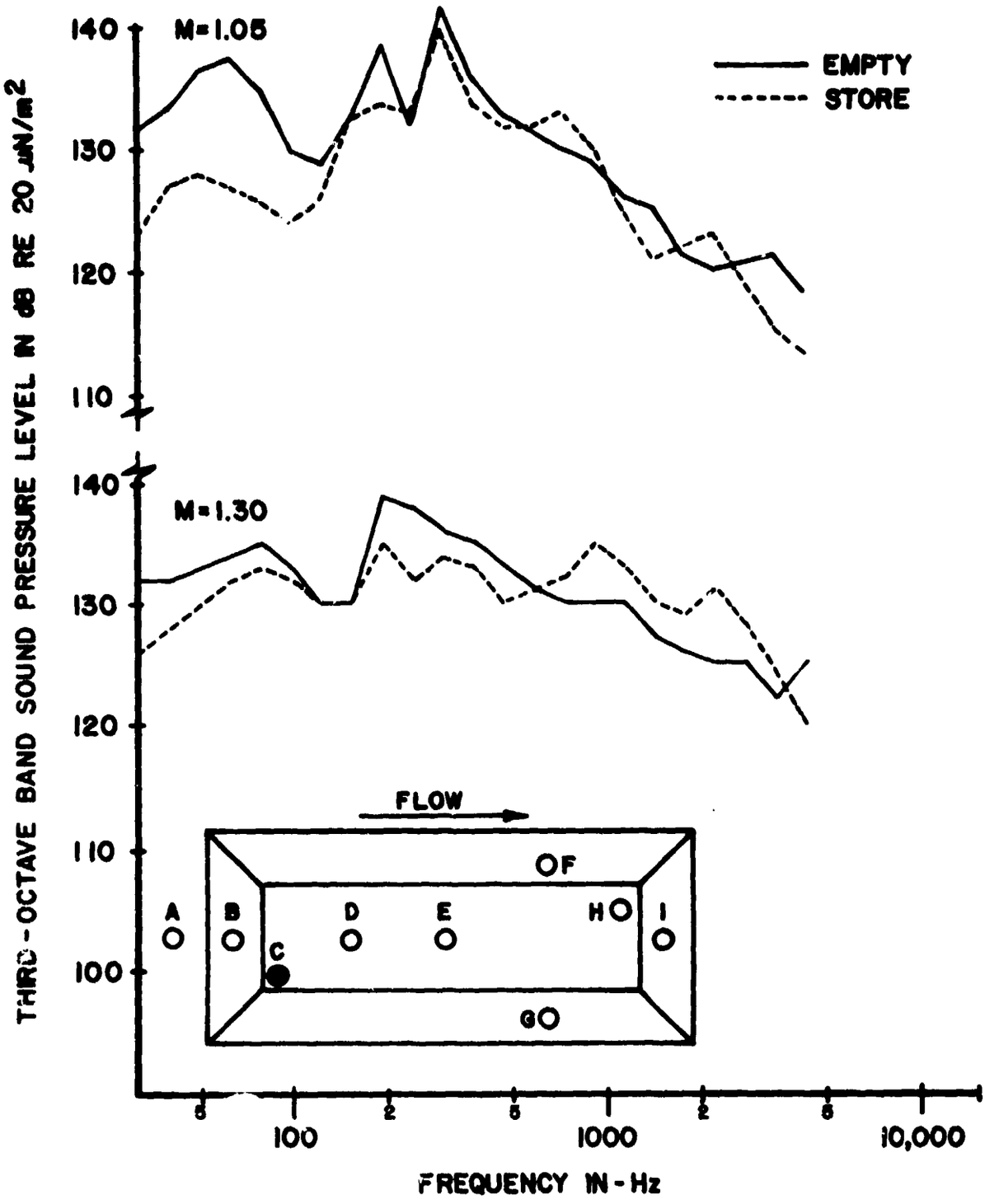

FIGURE 42 COMPARISON OF ONE-THIRD OCTAVE BAND SOUND PRESSURE LEVEL SPECTRA FROM THE L/D = 7 EMPTY AND STORE CONFIGURATION FOR AN ALTITUDE OF 30,000 FEET

for several Mach numbers. A major effect of store insertion is seen to be a reduction in the amplitude of the low frequencies.

The reduction in low frequencies appears to decrease with increased Mach number. The effect of the store on the resonant peaks is difficult to distinguish at the Mach numbers which were flight tested. These effects become more apparent at higher Mach numbers (Figure 42) and generally result in a decrease of 3 - 4 dB in the first three resonant peaks.

It was concluded in Ref 4 that the location of the store, with regard to store-shear layer interaction, was the determining factor as to the magnitude of reduction that would be realized. If the store does not interact with the shear layer, little reduction will occur. Also, it was observed that if the store is not wide enough to effectively fill the cavity mouth area the undisturbed portion of the shear layer is still capable of exciting cavity resonances. The wind tunnel data of Ref 4 showed that one store (2 inches wide in a 7 inch wide cavity opening) at Mach 0.8 resulted in only a 3 dB reduction in the peak fluctuating pressures while a two store configuration resulted in approximately 16 dB reduction. The flight tested store was 4 inches wide giving an area closure ratio between the referenced one and two configurations. In general, for the flight test Mach numbers the reduction in the level of the first three resonant frequencies was between those found in Ref 4. However, sufficient data are not available to generalize the effects of the store-in-cavity configuration. This can be clearly seen by careful examination of the data presented in Figure 46 of Ref 4, considering both Mach number and store effects. Thus, for prediction purposes, it is recommended that the predictions for an empty configuration be applied to the cavity with a store in it. This will tend to be a conservative estimate because, as shown in Figures 41 and 42, the amplitude at the lower frequencies of interest is consistently lower for the store configuration.

SECTION III

SUMMARY AND EVALUATION OF PREDICTION SCHEME

The prediction scheme presented in this report was empirically developed and is based on flight data from Ref 12 and 14 and wind tunnel data presented in the literature. The scheme is recommended for application in the following parameter ranges:

$$2 \leq L/D \leq 7$$

$$0.5 \leq M \leq 3$$

$$0 \leq X/L \leq 1$$

The predictions that result will tend to be conservative at almost all flight conditions and cavity configurations as will be shown below. The prediction scheme is summarized in the following steps.

Step I <u>Modal Frequencies</u>

The modal, or resonant, frequencies are predicted quite well with the modified Rossiter equation:

$$f_m = \frac{V}{L} \frac{m - 0.25}{\dfrac{M}{(1 + \frac{K-1}{2} M^2)^{1/2}} + 1.75} \qquad m-1,2,3 \qquad (2)$$

The equation can be used to predict modal frequencies for m as large as desired, however, this prediction scheme only concerns itself with the first three frequencies, i.e., m = 1, 2 or 3.

Step II <u>Normalized Modal Sound Pressure Amplitudes</u>

The following expressions are used to determine the maximum normalized one-third octave band sound pressure amplitude of the first three modal frequencies. The maximum value occurs at the rear of the cavity for each frequency.

$$20 \log (P_2 \max/q) = 25 \operatorname{sech} [2(M-1)] - 3.3\ L/D - 27 \qquad (5)$$

$$20 \log (P_1 \max/q) = 20 \log (P_2 \max/q) + 1.5\ L/D - 13 \qquad (6)$$

$$20 \log (P_3 \max/q) = 20 \log (P_2 \max/q) - 13\ M + 9 \qquad (7)$$

For convenience to the user values of the "sech" function are included as Table II.

Step III <u>Longitudinal Distribution</u>

The longitudinal sound pressure distribution for the first three modes is determined by the following expression:

$$20 \log (P_m/q)_{X/L} = 20 \log (P_m \max/q) - 10 \left[1 - |\cos\alpha_m X/L| + (0.33L/D - 0.6)(1-X/L)\right] \qquad (4)$$

$$\alpha_1 = 3.5 \text{ rad}$$

$$\alpha_2 = 6.3 \text{ rad}$$

$$\alpha_3 = 10.0 \text{ rad}$$

This expression describes the standing modes that were observed in the cavities for flight and wind tunnel data.

Step IV <u>Broadband Levels</u>

The final step in the prediction scheme is to determine the broadband levels. This is accomplished with the aid of Equation 8.c

$$20 \log (P_b \max/q) = 20 \log (P_2 \max/q) + \left[3.3\ L/D - 28 + 3(1-L/D)(1-X/L)\right]\left[1.2 - 0.4M\right] \qquad (8.c)$$

and Figure 40. Equation 8.c predicts the maximum normalized one-third octave broadband level which is used to enter Figure 40 to determine the entire broadband spectrum.

The spectra that result from the prediction scheme are normalized with the free-stream dynamic pressure. It is usually desired to

TABLE II VALUES OF THE SECH FUNCTION

$$\text{SECH } x = 2/\ (e^{x} + e^{-x})$$

x	SECH x	x	SECH x
0.0	1.000		
0.1	0.995	2.1	0.241
0.2	0.980	2.2	0.219
0.3	0.957	2.3	0.199
0.4	0.925	2.4	0.180
0.5	01887	2.5	0.163
0.6	0.844	2.6	0.148
0.7	0.797	2.7	0.134
0.8	0.748	2.8	0.121
0.9	0.698	2.9	0.110
1.0	0.648	3.0	0.099
1.1	0.599	3.1	0.090
1.2	0.552	3.1	0.081
1.3	0.507	3.3	0.074
1.4	0.465	3.4	0.067
1.5	0.425	3.5	0.060
1.6	0.388	3.6	0.055
1.7	0.354	3.7	0.049
1.8	0.322	3.8	0.045
1.9	0.293	3.9	0.040
2.0	0.266	4.0	0.037

reference the levels to the standard reference of $20\mu N/m^2$. To do this the value of

$$20 \log (q/20x10^{-6})$$

must be added to the predicted levels. Figure 43 has been included to simplify this task. Simply enter the figure with an altitude and free-stream velocity and read the corresponding conversion value.

Levels resulting from the prediction scheme were compared to measured data to determine the accuracy of the predictions. Figures 44-46 show a comparison of measured and predicted one-third octave band spectra for each L/D ratio tested and various locations in the cavity. The measured data are from the flight tests and from wind tunnel tests presented in Ref 3 and 4. It is seen that the wind tunnel data are generally above the flight data. This is very evident in Figure 46. The predictions will thus tend to be below the wind tunnel data because in the derivation of the equations the flight data were weighted heavier than the wind tunnel data. In Figures 44 and 45 the predictions agree very well with both the flight and wind tunnel data where the largest variation is about 7 dB. In Figure 46 the predicted spectrum agrees fairly well with the measured spectra with the exception of the wind tunnel mode 2 pressure amplitude. At this frequency the difference between the wind tunnel data and predicted spectrum is nearly 14 dB while the remainder of the spectrum is within about 7 dB of the predicted levels.

It was desired to determine how well the prediction scheme would predict the measured data for the entire range of parameters. This was accomplished by comparing the predictions to measured data from eight references which included Mach numbers from 0.2 to 3.0 and L/D ratios from 2 to 7. Levels for the first three modes from various cavity locations were used. The results of the comparison are presented in Figure 47. Ideally, all of the points would fall on the zero line or a few dB below the line. Positive data points indicate that the prediction method under-predicted the levels while negative

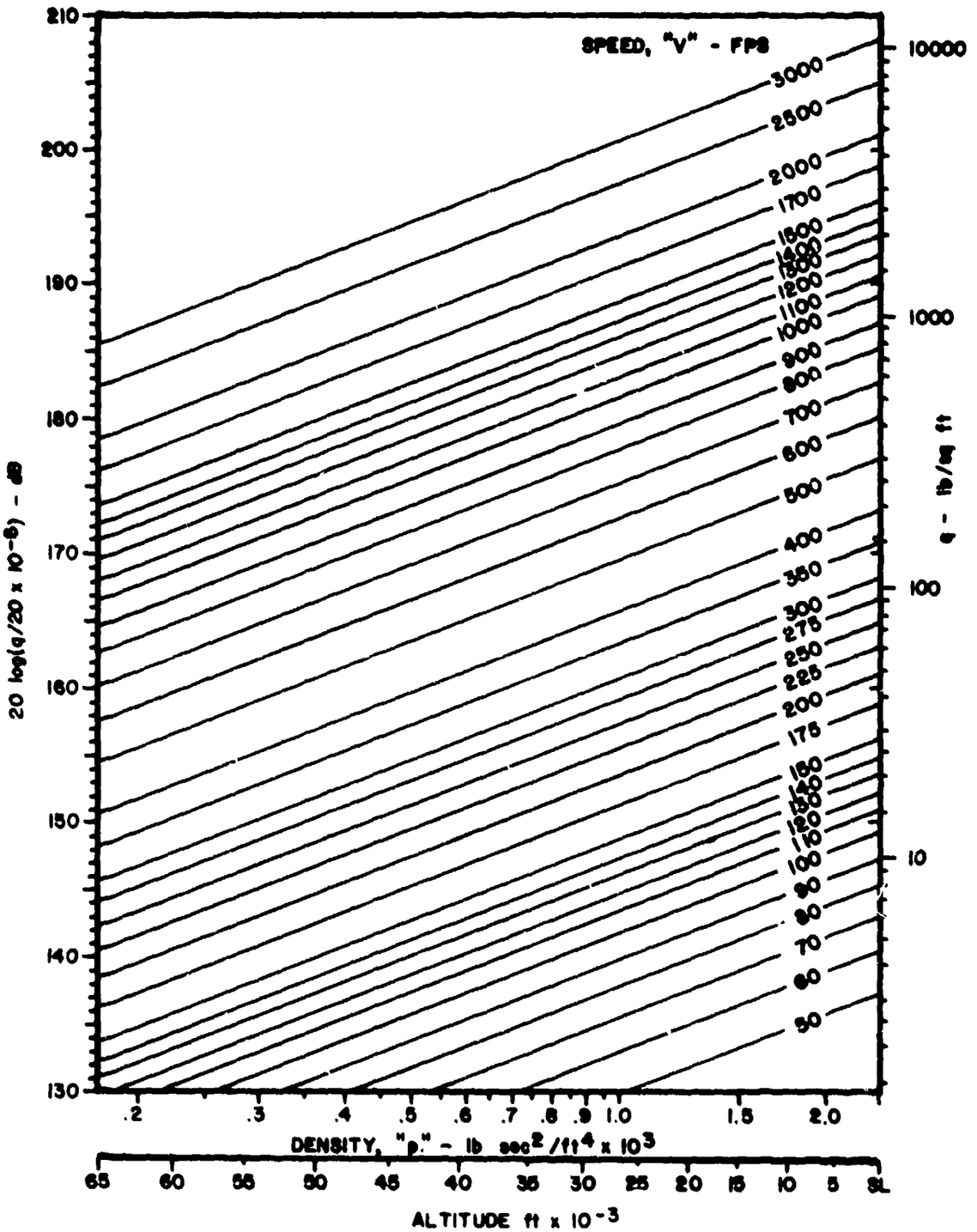

FIGURE 43 CHART FOR DETERMINING REFERENCE "q" DECIBEL LEVEL

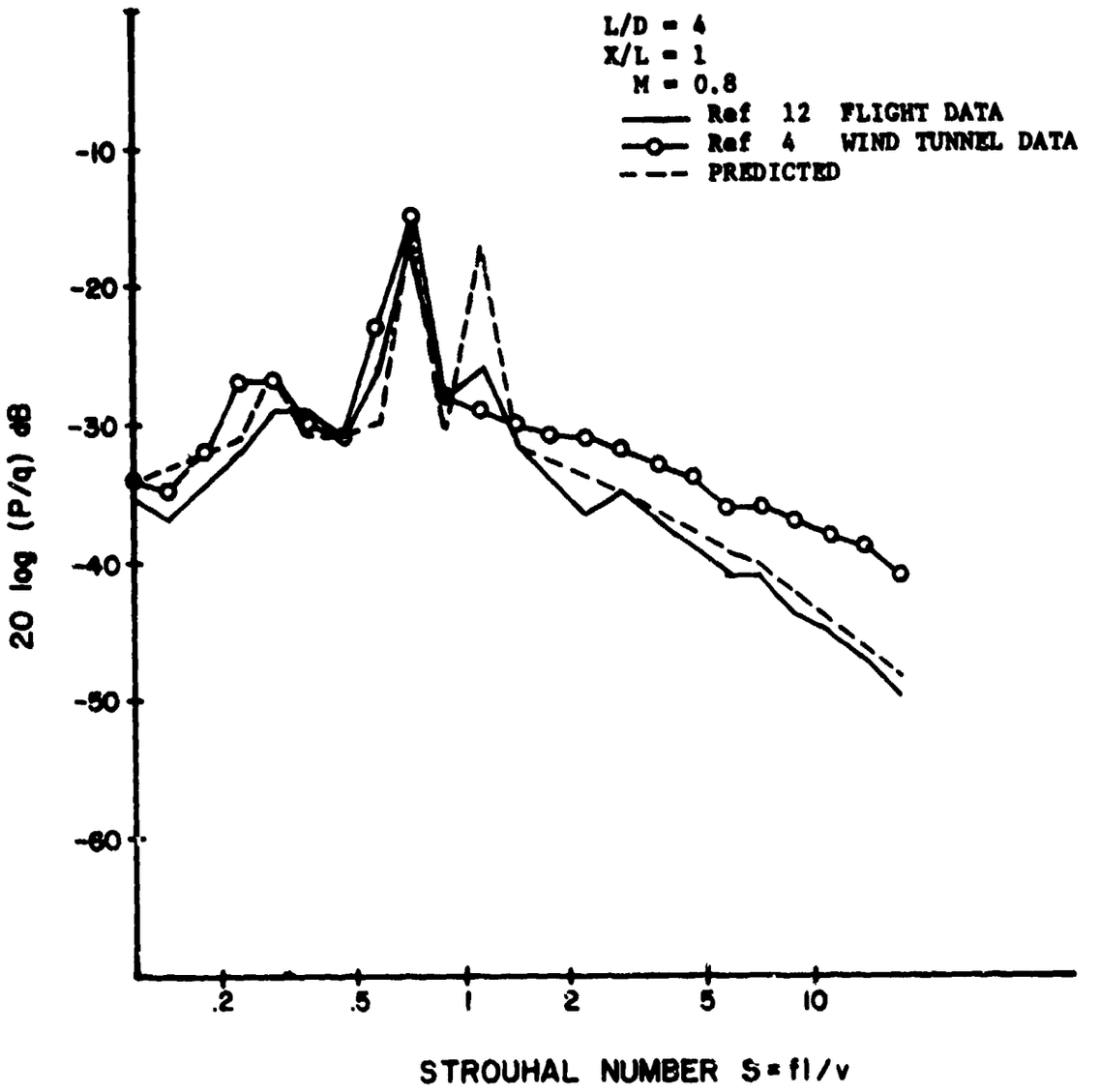

FIGURE 44 COMPARISON OF PREDICTED SPECTRUM WITH MEASURED SPECTRA

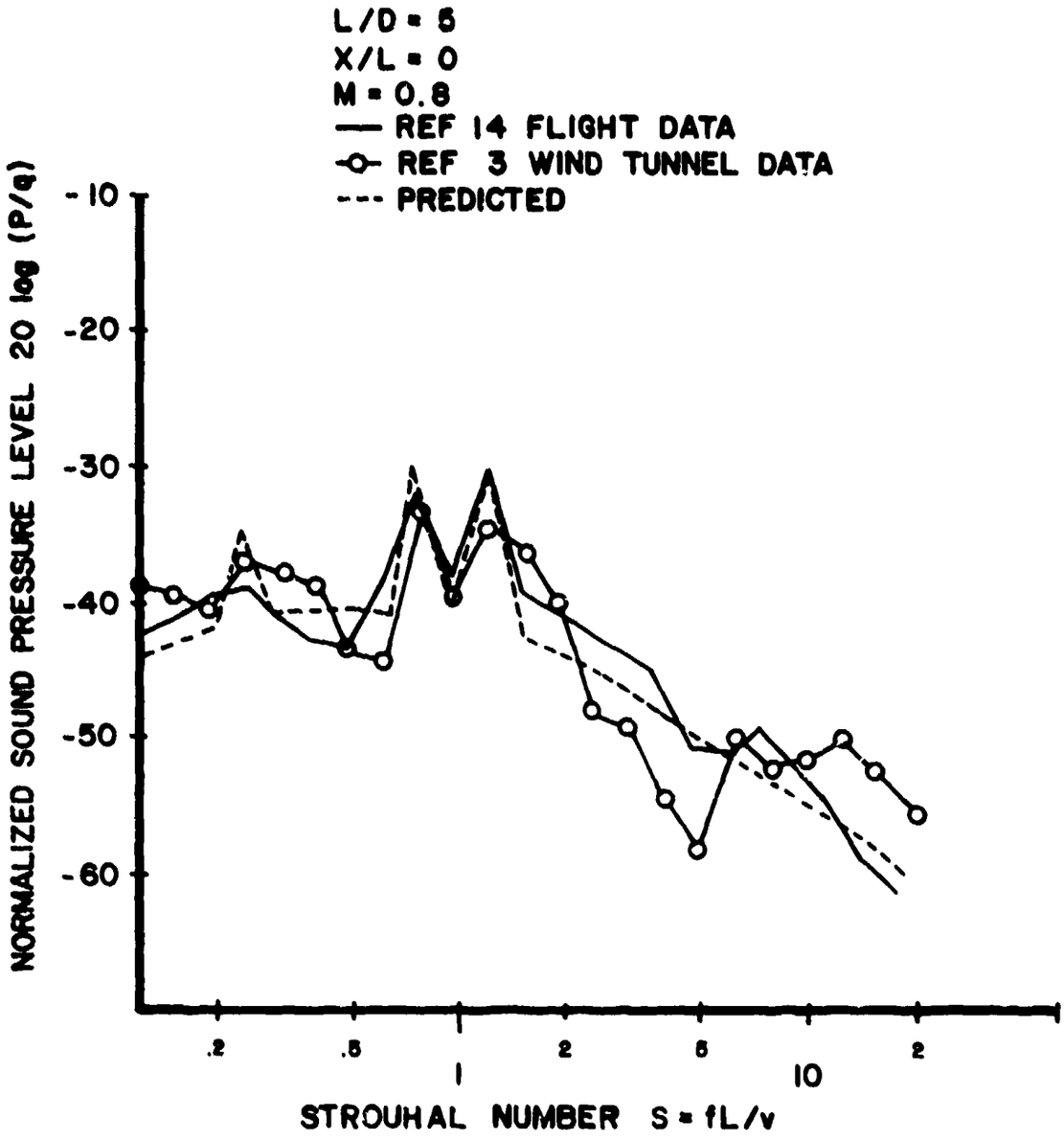

FIGURE 45 COMPARISON OF PREDICTED SPECTRUM WITH MEASURED SPECTRA

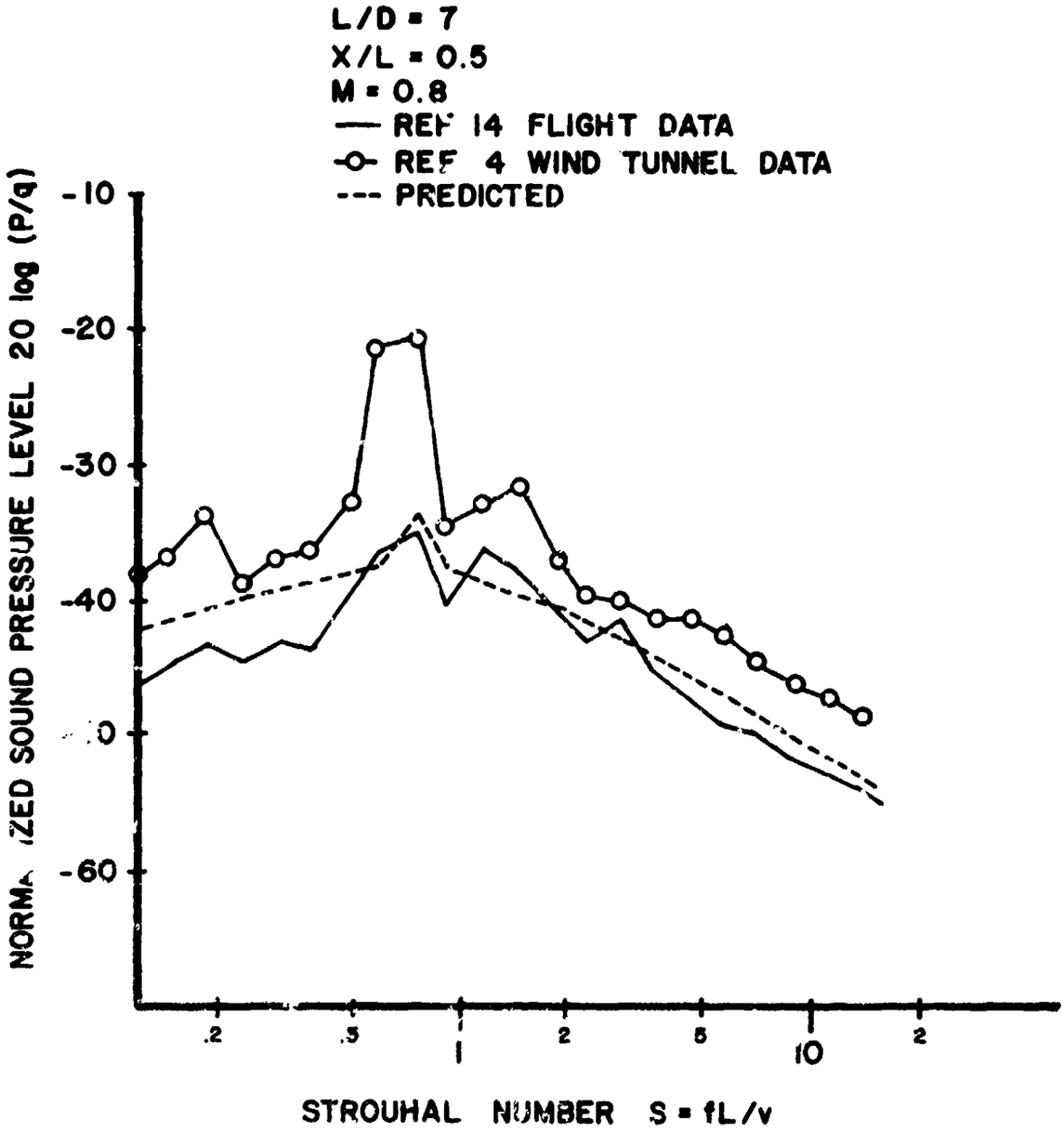

FIGURE 46 COMPARISON OF PREDICTED SPECTRUM WITH MEASURED SPECTRA

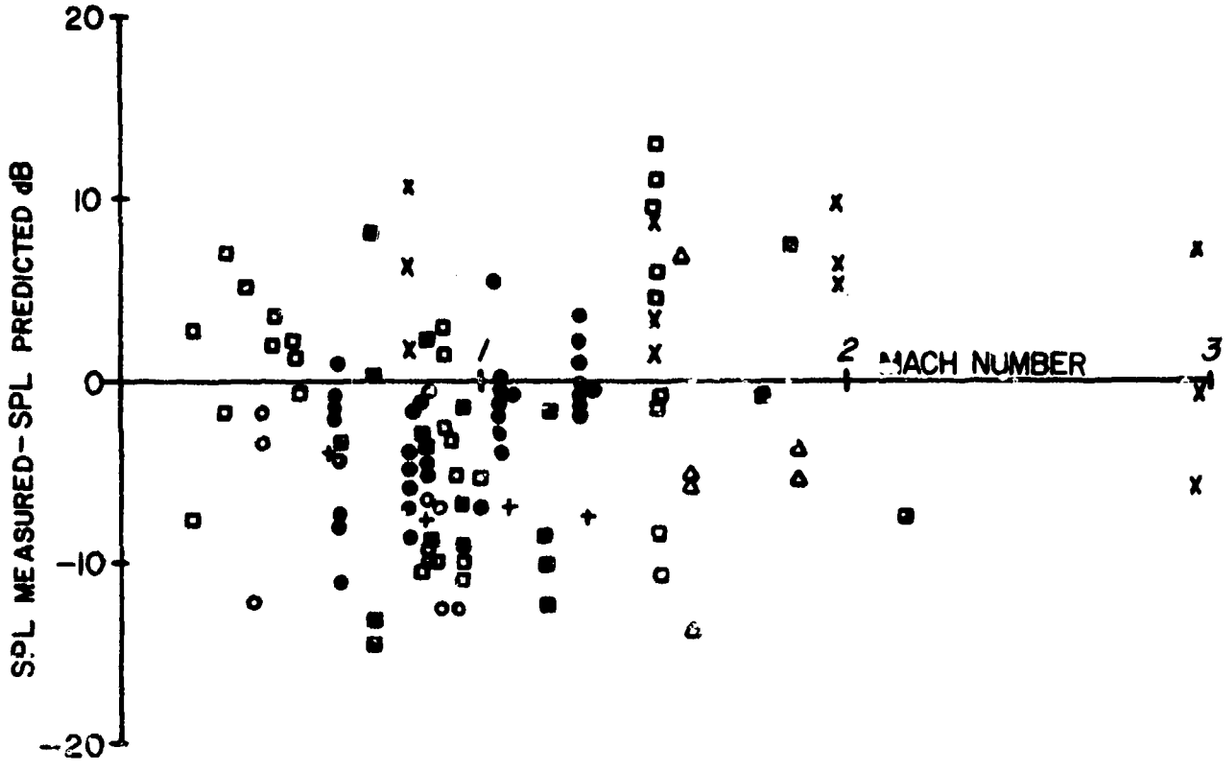

● - Flight Data
■ - Ref. 8
X - Ref. 4
+ - Unpublished F 111 Flight Data
○ - Ref. 11
□ - Ref. 3
△ - Ref. 1

FIGURE 47 COMPARISON OF PREDICTED LEVELS WITH MEASURED LEVELS

values indicate conservative predictions. Approximately 90% of the points fall within $\pm$ 10 dB of the predicted value. The prediction scheme offered in Ref 4 results in levels as much as 30 dB above the measured levels. Due to the wide range of data represented in the figure, the agreement with the predictions is considered to be good. Most of the flight data predictions are conservative while much of the wind tunnel data are above the predicted levels. The wind tunnel data were not weighted as heavily as the flight data in the development of the prediction method and thus is the primary reason for under-predicting the wind tunnel tests results.

SECTION IV

SUMMARY AND RECOMMENDATIONS

The objective of flight tests reported in Ref 12 and 14 was to verify and/or refine, with flight data, the empirical prediction scheme developed with wind tunnel results in Ref 4. From this effort many trends were observed. The observations summarized below are based primarily on the flight test results; however, wind tunnel results were considered.

1. The cavity resonant frequencies can be accurately predicted by the modified Rossiter formula.

2. The amplitude prediction methods in Ref 4 were conservative in predicting both the resonant and broadband SPL observed in actual flight tests.

3. The equations presented herein are recommended for predicting more realistic SPLs for cavity L/D ratios in the range of 2 to 7 and a Mach number in the range of 0.5 to 3.0.

4. The longitudinal variation of the rms amplitude associated with each resonant frequency can be described as ordered modes.

5. At the rear of the cavity the broadband spectrum for constant flight conditions is nearly the same for all cavity L/D ratios.

6. The maximum broadband levels increased toward the aft end of the cavity.

7. Increasing the cavity L/D ratio reduces the amplitude of the resonant frequencies.

It was revealed during the review of pertinent literature that little data exist for rectangular cavities exposed to free-stream flow for Mach numbers from 2.0 to 3.0. Verification of the current prediction method was limited in this Mach number range. It is thus recommended that additional data (preferably flight data) be obtained for this speed range and the current prediction method be evaluated with these additional data.

APPENDIX

Description of Test Configurations, Instrumentation, Procedures, and Data Reduction

1. Test Configurations

Four cavity and one flat plate configuration were flight tested. The cavities were 40 inches long, 9 inches wide and either 10 inches, 8 inches or 5.7 inches deep resulting in length-to-depth (L/D) ratios of 4, 5 and 7 respectively. They were constructed with 0.250 inch thick aluminum (6061-T6). The fourth configuration was the L/D = 7 cavity with an ogive store symmetrically mounted in it. A flat plate was fit securely over the cavity opening and flight tested for the purpose of assessing the flow conditions for which subsequent data were taken. Figure 1 illustrates each of the test configurations.

The cavities were mounted in a modified SUU-41 munitions dispenser pod. Sketches of a standard SUU-41 pod and a pod modified to accommodate the cavities are shown in Figure 2. Figure 3 is a picture of the modified pod with the L/D = 4 cavity mounted in it. The pod was mounted on the triple ejection rack (TER) of the left inboard pylon on a RF-4C aircraft. A schematic of the aircraft with the pod mounted on it is shown in Figure 4.

2. Instrumentation

The cavities were instrumented with nine microphones, one accelerometer, a thermocouple and three static pressure ports. The flat plate configuration was instrumented with a microphone, thermocouple, static pressure port, and a pressure rake. The location of the instrumentation is shown in Figures 5 and 6 with a typical microphone mounting also shown in Figure 5. The type and models of all instrumentation are presented in Figure 48.

The overall system response for the Columbia Research Model 902H crystal accelerometer was flat within $\pm$ 5 percent from 2 to 6000 Hz. The system response for the Gulton Model MVA 2100 microphones was flat within 2 dB from 5 to 6000 Hz while the Gulton

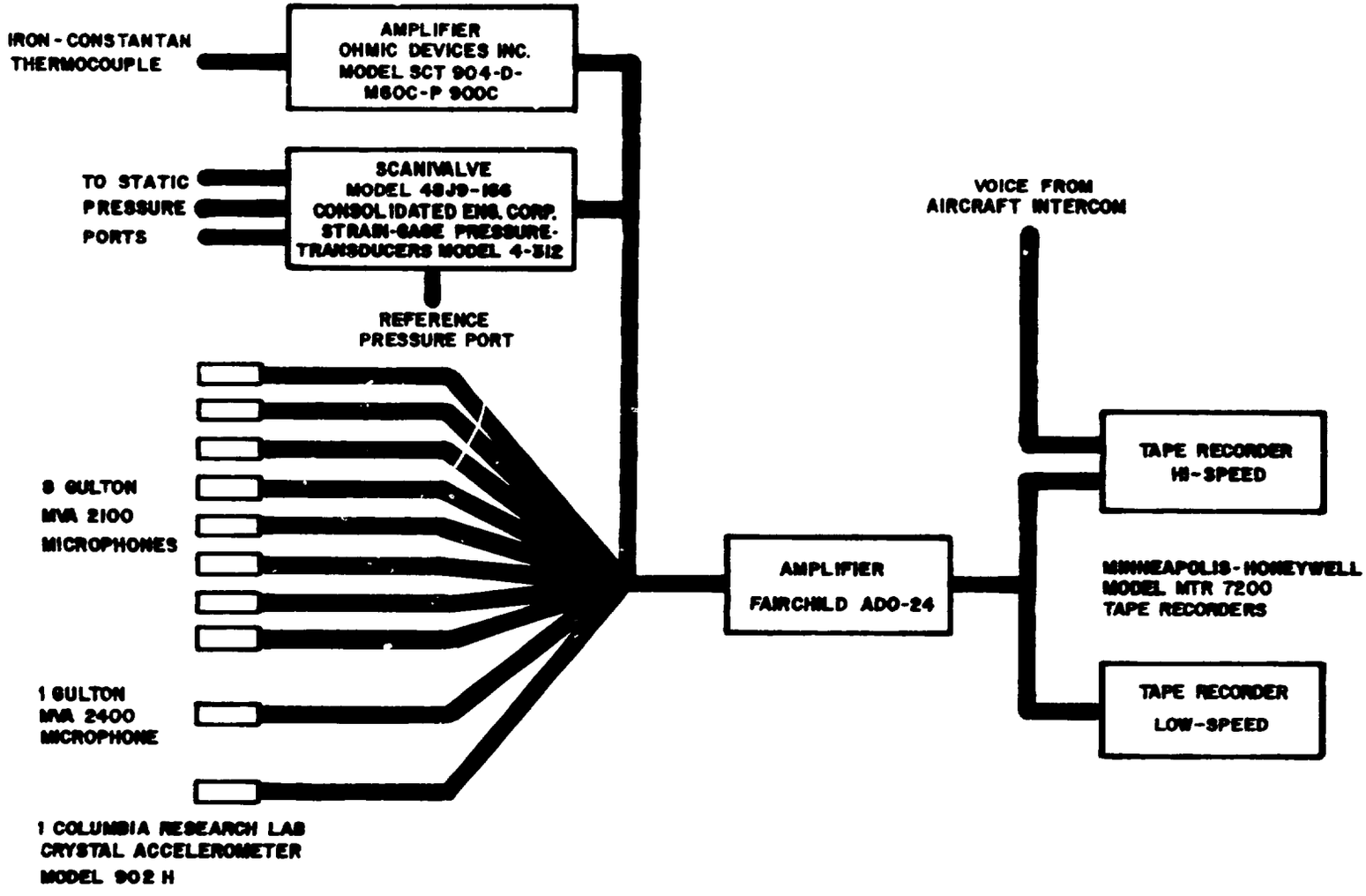

FIGURE 48 BLOCK DIAGRAM OF DATA ACQUISITION INSTRUMENTATION

Model MVA 2400 was flat within 2 dB from 2 to 6000 Hz. The system tolerance for the Iron-Constantan thermocouple was ± 4°F. The thermocouple junction was mounted flush with the rear wall using epoxy which provided electrical isolation but not thermal isolation from the wall.

The accelerometer was calibrated in the laboratory using a Bruel and Kjaer Type 1606 vibration preamplifier (± 1 g calibrator). The microphones were calibrated in the laboratory with a General Radio Type 1552-B sound level calibrator. The measurement system, once installed in the aircraft, was calibrated with an insert voltage to account for signal loss through the cables.

3. Test Procedures

The three altitudes at which the flight tests were flown are 3,000 ft, 20,000 ft, and 30,000 ft. The tests include flights for the Mach number ranges 0.61 to 0.93 for 3,000 ft and 0.61 to 1.30 for 20,000 ft, and 30,000 ft. Data were obtained at all Mach numbers between the two extremes since the aircraft was slowly accelerated from the lowest to the highest Mach number (approximately 2 to 3 minutes) with data being recorded continuously. The majority of the flights requiring speeds in excess of M = 0.9 below 30,000 ft were flown over Lake Huron with the remaining flights being flown over Washington Court House, Ohio.

4. Data Reduction

All data were continuously recorded on two fourteen channel tape recorders. The magnetic tapes recorded in-flight were played back in the laboratory on a Honeywell 7400 record-reproduce system. Overall time histories and one-third octave band analysis were performed over the frequency range of 12.5 Hz to 10,000 Hz using a General Radio 1926 multi-channel rms detector interfaced with a 2116 Hewlett-Packard digital computer. The time histories were correlated with the specific flight conditions which were recorded on a voice channel.

For selected microphone and accelerometer data, narrowband (2 Hz) analyses were performed using a Honeywell 9300 power spectral

density analyzer. The system linearity is $\pm$ 0.5 dB for a discrete frequency input. Narrowband analyses were also obtained using a Hewlett-Packard 5450 Fourier analyzer. The data reduction system used is schematically shown in Figure 49.

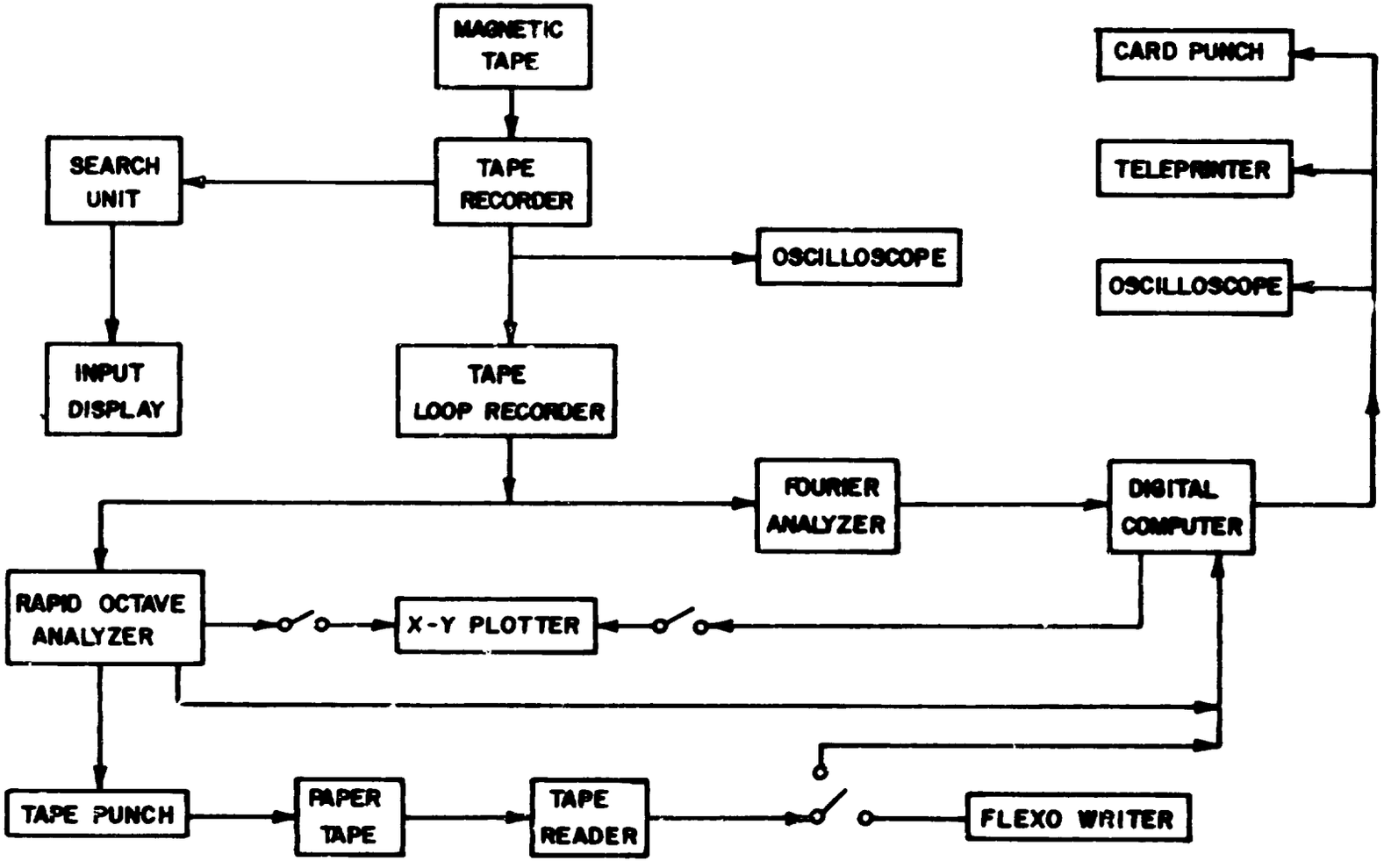

FIGURE 49 DATA REDUCTION SYSTEM

REFERENCES

1. Carr, D. L., "An Experimental Investigation of Open Cavity Pressure Oscillations," M.S. Thesis, Air Force Institute of Technology, Wright Patterson AFB, Ohio, 1974.

2. East, L. F., "Aerodynamical Induced Resonance in Rectangular Cavities," Journal of Vibration and Sound, May 1966.

3. Heller, H. H. & Bliss, D. B., "Aerodynamically Induced Pressure Oscillations in Cavities - Physical Mechanisms & Suppression Concepts," AFFDL-TR-74-133, August 1974.

4. Heller, H. H., Holmes, G. Covert, E. E., "Flow-Induced Pressure Oscillations in Shallow Cavities," AFFDL-TR-70-104, Dec 1970.

5. Krishnamurty, K., "Acoustic Radiation from Two-Dimensional Rectanguler Cutouts in Aerodynamic Surfaces", NACA Tech Note 3487, August 1955.

6. Lowson, M.V., "Prediction of Boundary Layer Pressure Fluctuations," AFFDL-TR-67-167, April 1968.

7. Maull, D. J. and East, L. F., "Three-Dimensional Flow in Cavities", Journal of Fluid Mech 16, p 620, 1963.

8. Maurer, O., "Investigation and Reduction of Open Weapon bay Pressure Oscillations in the B-1 Aircraft." AFFDL-TM-74-101-FYA, January 1974.

9. Plumblee, H. D., Gibson, J. S., and Lassiter, L. W., "A Theoretical and Experimental Investigation of the Acoustic Response of Cavities in Aerodynamic Flow", WADD-TR-61-75, 1962.

10. Roshko, A., "Some Measurements of Flow in a Rectangular Cutout," NACA Tech Note 3488, 1955.

11. Rossiter, J. E., "Wind Tunnel Experiments on the Flow Over Rectangular Cavities at Subsonic and Transonic Speeds", RAE Rep Nr 64037, R&M Nr 3438, 1966.

12. Shaw, L. L., et al, "Aero-Acoustic Environment of a Rectangular Cavity with a Length to Depth Ratio of Four", AFFDL-TM-74-19-FYA January 1974.

13. Shaw, L. L. and Smith, D.L., "Aero-Acoustic Environment of Rectangular Cavities with Length to Depth Ratios in the Range of Four to Seven", Paper presented at the 45th Shock and Vibration Symposium, October 1974.

14. Smith, D. L. et al, "Aero-Acoustic Environment of Rectangular Cavities with Length to Depth Ratios of Five and Seven", AFFDL-TM-74-79-FYA, April 1974.

☆ GOVERNMENT PRINTING OFFICE : 1975 — 657-055/34